ATOMIC MASS DIFFERENCES FOR SOME RARE EARTH ISOTOPES NEAR N = 90

By

ROY LOVITT BISHOP, B.Sc., M.Sc.

THE UNIVERSITY OF MANITOBA ELIZABETH DAFOE LIBRARY

A Thesis

Submitted to the Faculty of Graduate Studies

in Partial Fulfillment of the Requirements

for the Degree

Doctor of Philosophy

University of Manitoba

May 1969

DOCTOR OF PHILOSOPHY (1969) UNIVERSITY OF MANITOBA
Physics Winnipeg, Manitoba

TITLE: Atomic Mass Differences for Some Rare Earth Isotopes Near N = 90

AUTHOR: Roy Lovitt Bishop, B.Sc. (Acadia University)
M.Sc. (McMaster University)

SUPERVISOR: Professor H. E. Duckworth

NUMBER OF PAGES: viii, 129.

SCOPE AND CONTENTS:

A high precision voltage supply and potentiometer have been constructed to supply and measure the voltage ratio required by the new Manitoba second order mass spectrometer. The potentiometer is capable of matching the highest precision predicted for the spectrometer.

The new second order spectrometer has been completed and used to measure twenty close doublets among the rare earths between Z = 60 and 66. These new measurements have been combined with other data in order to calculate neutron separation and pairing energies. A study of the mass effect accompanying the onset of nuclear deformation near N = 90 has been made in greater detail than has heretofore been possible.

ACKNOWLEDGEMENTS

I wish to thank my supervisor, Dr. H. E. Duckworth for his guidance during the course of my studies. He is responsible both for the existence of atomic mass determinations in Canada and, through his encouragement and example, for my own participation in this field of nuclear physics.

Particular credit is due to Dr. Robert Barber. Much of what is original and valuable in this work is due directly or indirectly to his insight and suggestion. Mr. John Meredith, Mr. Grey Southon, Dr. Peter Williams and Mr. Paul Van Rookhuyzen provided valuable assistance both during the construction of the spectrometer and during the mass measurements reported here. I wish to thank all of these individuals for making our laboratory a pleasant and stimulating place to work, and for their contributions to the silly hour on Friday afternoons. I also thank Miss Sharon Drier and Miss Lynda Jones for typing this thesis.

This research was supported by the National Research Council. Scholarship assistance from the National Research Council and the University of Manitoba is gratefully acknowledged. I also thank the Executive Committee of the Board of Governors of Acadia University for granting me a leave of absence during the past three years.

Finally, I wish to thank my wife, Gertrude, for her patient understanding and support during the several years that I have been a graduate student.

CONTENTS

LIST OF FIGURES

LIST OF TABLES

FRONTISPIECE

A Mass Quintuplet

$^{150}Nd^{35}Cl_2$, $^{150}Sm^{35}Cl_2$, $^{148}Nd^{35}Cl^{37}Cl$, $^{148}Sm^{35}Cl^{37}Cl$, $^{146}Nd^{37}Cl_2$

Resolution at base $\sim$1/130,000.

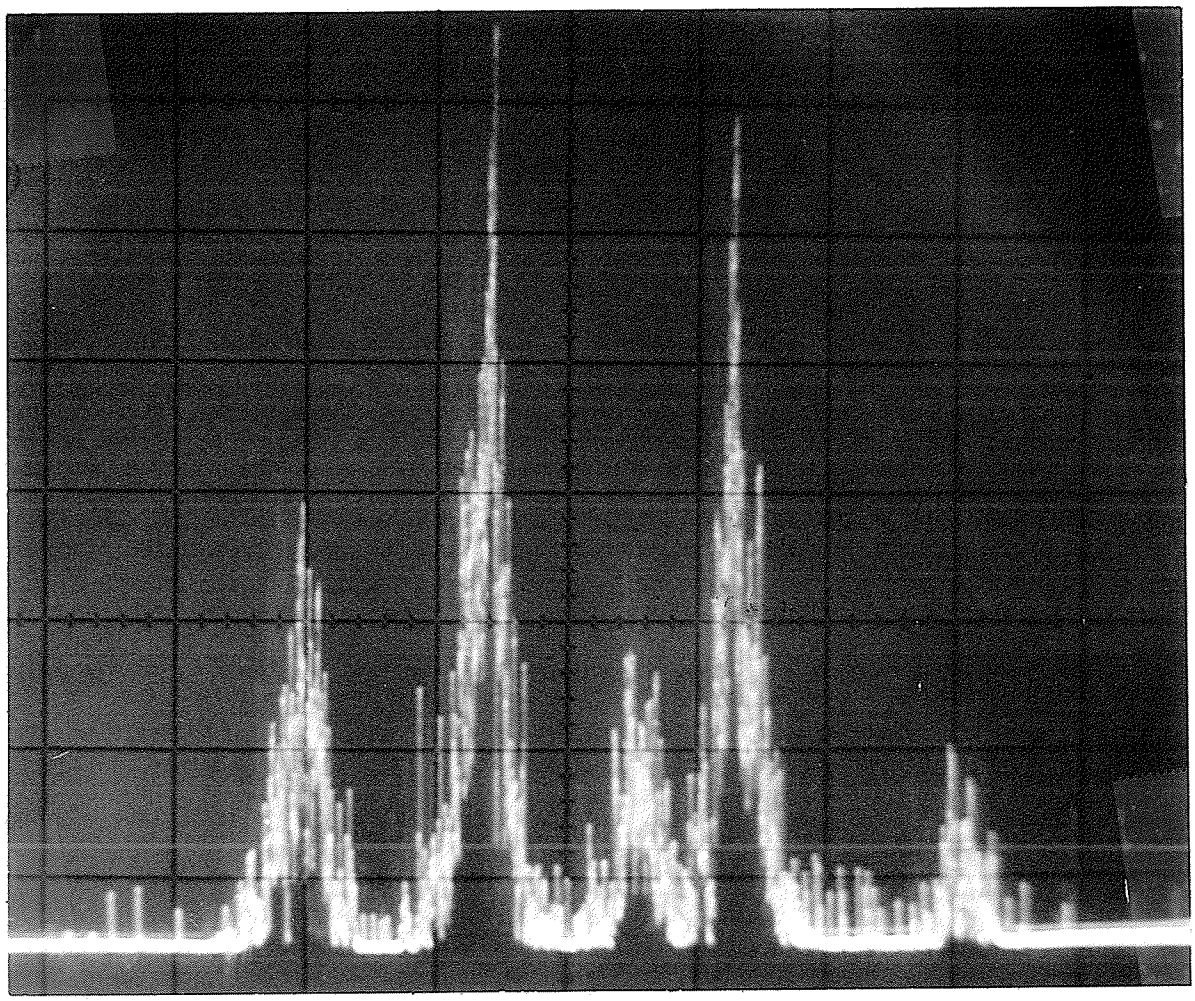

CHAPTER 1

INTRODUCTION

Mass

The concept of mass is as old as civilization; however, it was only some three centuries ago with the development of mechanics by Newton and others that quantitative definitions of mass appeared: (i) the mass of a body is a measure of the body's resistance to acceleration (inertial mass): (ii) the mass of a body is a measure of the force with which a known gravitational field acts on the body (gravitational mass). Although the two definitions are fundamentally different, experiment demonstrates that these two masses are proportional to one another to high precision ($\lesssim$ 1 part in 10^{11}, Roll, Krotkov & Dicke, 1964). (The units of the two types of mass are, by convention, chosen to be equal, thus leaving the gravitational constant to be determined experimentally.) An explanation for this extraordinary proportionality was not provided until 1916 when Einstein presented his general theory of relativity.

Eleven years earlier, in his special theory of relativity, Einstein was also responsible for the introduction of the familiar relation for mass - energy equivalence. At the present time this equivalence is one of the best confirmed results in physics.

Experiment has also consistently demonstrated that mass - energy is conserved. However, the conservation "laws" of physics are not well understood. Those conservation laws

occurring in mechanics are actually consequences of our simple symmetrical conception of space and time. In the case of mass - energy conservation, this connection appears explicitly in quantum mechanics where the assumption of time independence leads directly to such conservation (Schiff, 1955). The principle of time independence or lack of a preferred origin in time is often termed time homogeneity.

Recently the principle of time homogeneity has been examined in considerable detail (Augustynek, 1968). In particular, the possibility that it may fail on the cosmological level, that is, over long time intervals, has been considered. Additional fuel for such speculations is provided by recent discoveries indicating that the weaker an interaction is the fewer invariance principles it fulfills (Feynman, 1965). This suggests the possibility that the weakest of the four basic interactions, gravitation, which is the main interaction on the cosmological scale, may violate time homogeneity. The Brans - Dicke theory of gravitation (Dicke, 1967), considered by some theorists to be a possible alternative to Einstein's general theory, indicates that the gravitational constant (G) may slowly decrease with time due to the expansion of the universe. At present, however, the principle of time homogeneity occupies a strong position in physical theory.

In the context of this thesis, one can say that atomic masses are constants because of the homogeneity of time. With this comforting thought the mass spectroscopist can retire each night confident that the atoms in the source of his

spectrometer will have the same mass on the morrow (although other difficulties may occasionally make him a bit suspicious).

Mass Standards

The units of the fundamental quantities length and time have recently been redefined in terms of the wavelength and frequency, respectively, of certain atomic transitions. By being defined in this fashion, these units have the dual advantage of being constant with time and of being directly accessible to any suitably equipped laboratory.

The unit of atomic mass is defined as one - twelfth of the mass of a ^{12}C atom (Mattauch, 1960) (Wichers, 1962), and thus enjoys similar advantages. However, all macroscopic mass measurements are ultimately referred to a second standard, the platinum - iridium kilogram at the Bureau International des Poids et Measures at Sèvres, France. This venerable but vulnerable standard will likely be with us for several years due to its convenient size and the relative uncertainty ($\sim$ 16 ppm) in the Avogadro number (Cohen and Dumond, 1965), plus the further difficulty of assembling macroscopic quantities of known numbers of atoms.

Importance of Atomic Mass Determinations

The mass of an atom is the most important single piece of information that one can have concerning this unit of matter. An atom's mass is less than that of its constituent protons, neutrons and electrons by an amount equal to the so-called binding energy of the atom. This mass defect accounts

for the stability of an atom. A certain fraction of this energy is associated with the electrons; however, in addition to being small, the electronic binding energy varies in a gradual manner with atomic number. Hence the magnitude and behavior of the atomic binding provides information about the atomic nucleus. The magnitude of the binding energy gives information on possible nuclear reactions and disintegrations. Large scale variations with nucleon number give insights into the general nature of nuclear forces. Finer variations are related to nuclear shell structure, collective nucleon behavior, and, no doubt, to other as yet not well understood features of nuclear structure.

At this point it seems appropriate to recall that a mass spectrograph was involved in the first experimental verification of mass - energy equivalence (Bainbridge, 1933). The precision of this determination was 3%. More recently mass spectroscopic work has again been compared with reaction data to give a check with a precision of 64 ppm, an improvement of nearly three orders of magnitude (Wapstra, 1967).

Methods of Atomic Mass Determination

Alpha decay data provide the bulk of atomic mass information for atoms heavier than bismuth. A measurement of the alpha particle energy allows one to calculate the mass difference between the parent and daughter atoms. Since the magnetic analysers used for precise determinations of this energy are usually calibrated with the ^{210}Po alpha particle whose energy (5304.5 keV) has an uncertainty of 0.5 keV

(Wapstra, 1964), the resulting mass differences can only approach this accuracy.

Beta decay data are another source of atomic mass differences. The information required to link the isobars involved is contained in the beta spectra end - points and often in the energies of correlated gamma rays. The large iron - free two dimensional, magnetic spectrometer at Chalk River is the most accurate instrument for such measurements. Uncertainties of the order of 0.1 keV have been attained; however, the precision of much beta decay data, particularly those of short lived nuclei, is considerably worse. Also, many radioactive materials decay by electron capture, for which the total decay energy is difficult to ascertain experimentally.

Nuclear reaction data are a third source of atomic mass information. Many induced reactions involving charged particles (p, d, t, ^{3}He, α, ^{16}O, etc.), neutrons and photons have been studied. Accuracies approaching 1 keV or less have been attained for some reactions such as (n,γ) and (p,α). The recent development of the lithium - drifted germanium detector and its associated electronics has played an important part in the increased accuracy of gamma ray data (Heath, 1967), while improvements in charged particle accelerators are providing reaction Q values of comparable precision (Staub, 1967).

The fourth and final source of precise atomic mass data is the mass spectroscopic technique which is based on the deflection of ionized atoms in electric and magnetic fields. A detailed description of this topic will be given later (Chapters 2 and 3); however, some basic differences between it

and the above three sources of mass data should be pointed out.

Reaction and disintegration measurements are the only source of mass data for atoms not lying in the beta stability valley of the nuclear mass surface. For example, techniques have recently been developed for examining alpha unstable nuclei far from this valley (Macfarlane, 1967). By comparison, the mass spectroscopic method is usually restricted to the stable nuclei.

The mass spectroscopic method is capable of establishing the mass of any atom to high precision, whereas the above methods are restricted to determinations of mass differences inasmuch as one can proceed in steps of only a few mass units at a time from the ^{12}C standard. By means of the doublet technique and by using a secondary standard such as a hydrocarbon fragment, absolute masses can be established for virtually any atom by means of a mass spectrometer. This feature has a marginal advantage as far as nuclear structure study is concerned however, since it is the shape of the mass surface rather than its precise position which is of particular interest.

Although the mass spectroscopic technique is a brute force one in the sense that entire atoms or molecules are examined, the precision achieved is competitive with the best reaction and decay measurements. In the latter measurements the energies examined are typically of the order of 1 MeV. This coupled with a precision of one part in 10^3 or 10^4 results in possible errors of the order of 1 to 0.1 keV. In mass spectroscopic measurements the masses examined are of the order of

100u or 10^5 MeV. However with precisions of one part in 10^8 or 10^9 comparable accuracy can be attained.

CHAPTER 2

THE DEVELOPMENT OF MASS SPECTROSCOPY

Early Work

Ionized atoms or "positive - rays" were discovered by Goldstein in 1886. The first mass spectroscope was the positive - ray parabola apparatus used by J. J. Thompson in 1912. This instrument originally had a resolution of about 20. With it Thompson established the identity of the positive - ray particles and found strong evidence for the existence of isotopes.

F. W. Aston continued Thompson's investigations by completing construction in 1919 of an instrument which possessed velocity focussing and a resolution of about 130. His first experiments verified the existence of isotopes and during the next decade and a half he carried out an intensive, systematic investigation of isotopes and their masses.

A. J. Dempster was the first to exploit the direction focussing property of the 180° magnetic field. With a mass spectrometer of this design he made a study of the isotopes of several metals during the early 1920's.

A Dempster instrument modified by the addition of a Wien velocity filter was used by K. T. Bainbridge in 1933 to make a number of valuable mass determinations.

With Herzog's presentation of the general focussing equations in 1934 the number and variety of mass spectroscopes began to increase. Double focussing instruments also began to appear in this period, the first few being constructed by Dempster at Chicago, Bainbridge and Jordan at Harvard, and

Mattauch and Herzog in Vienna. In the intervening years instruments of this type have supplied most of our information concerning atomic masses. A more detailed account of the pioneering work in mass spectroscopy is given by Duckworth (1958).

The doublet technique was and still is the standard method by which atomic masses are determined. Ions having nearly the same charge to mass ratio can be compared with relative ease. In the case of the early instruments, which employed photographic detection, the dispersion of the spectroscope needed to be accurately known only over a small region. In the case of modern instruments, which employ electrical detection, relatively close doublets are also advantageous. The reasons for this will become apparent in Chapters 3 and 5.

Electrical Detection

For many years most mass spectroscopes designed for precision mass determinations used photographic detection. That is, in Aston's terminology, they were mass spectrographs. This method of detection has several disadvantages: instrument alignment is slow and difficult; proper plate exposure and development is necessary to insure the location of the center of gravity of asymmetrical spectral lines; an energy difference between doublet members is difficult to detect; and the dispersion of the spectrograph must be accurately known. In large instruments the dispersion law may never be properly known owing to the difficulty of obtaining uniform and reproducible magnetic field. Furthermore, under typical conditions, a spectral line can be located to only about $1/50^{th}$ of its width.

Electrical detection of positive ions has been used for some time; however, it was not until the early part of the last decade that this form of detection was adapted to high precision mass determinations (Nier and Roberts, 1951; Smith and Damm, 1953, 1956; Quisenberry, Scolman and Nier, 1956).

With electrical detection, a fixed collector slit is used so that a double focus is required for only one mass at a time. In addition, one of the electric or magnetic deflecting fields traversed by the ions is varied in a periodic fashion so that the various ion beams in the vicinity of the collector slit are swept across it. The collector signal may be displayed on an oscilloscope which also supplies the sweep for the ions. Thus each mass reaching the collector slit appears as a "peak" on the oscilloscope display (frontispiece).

If on alternate sweeps, the electric fields traversed by the ions are all altered by the same specific fractional amount, ions of one mass can be made to arrive at the collector slit at the same point on the oscilloscope sweep as ions of another mass did on the previous sweep. (Figure 1). When this is achieved and provided the ions receive the same energy within the source of the spectrometer, the two ion groups follow identical paths through the spectrometer. Hence the dispersion of the magnetic analyser does not need to be known. Also, since the main magnetic field is not altered during the process, differential hysteresis effects are of no consequence. The electric fields, of course, can be cycled reproducibly to high precision.

FIGURE 1

$^{161}Dy^{35}Cl_2$, $^{159}Tb^{35}Cl^{37}Cl$, $^{157}Gd^{37}Cl_2$

Resolution at base ~ 1/120,000

The electric fields in the spectrometer have been increased by 1 part in 51,000 during the lower trace.

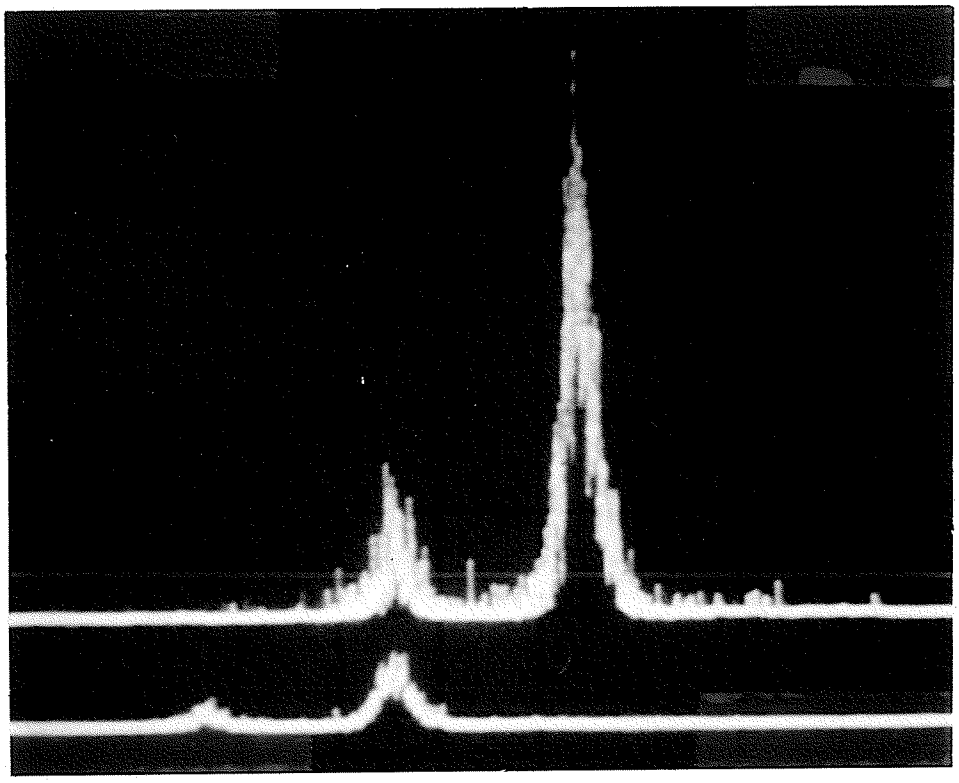

The mass difference between the two ion groups is simply related to the mass of one of the groups and to the fractional change in the electric fields required to make the two peaks coincide. This relation will be examined quantitatively in Chapter 3.

The precision of measurements made by this technique depends both on the resolution of the spectrometer, and on the precision with which one peak can be made to coincide with the other. Let m be the mass of either ion group of a doublet, and w be the base width (in mass units) of the peak corresponding to these ions. The resolution of the spectrometer is defined as $R = w/m$. If the peaks can be matched to a certain fraction f of their width, the uncertainty of the match is $\delta m = fw = fRm$, and the precision of the spectrometer is defined as:

$$\delta m/m = fR. \qquad (2\text{-}1)$$

As mentioned above, for photographic detection f is approximately 1/50. Early work using electrical detection and the peak matching method made use of the remarkable ability of the human eye to judge coincidence of the peaks. In this case $f \sim 1/1000$ can be achieved, a great improvement over the photographic method.

Recently electronic techniques have been employed to aid in the determination of coincidence (Benson and Johnson, 1966; Macdougall, 1966; Stevens and Moreland, 1967; Bainbridge and Dewdney, 1967). The technique used in our laboratory is similar to that used by Johnson and Stevens. A qualitative description is given below and specific details appear in Chapter 4.

The collector signal is sent to a signal averager which is synchronized with the oscilloscope display and ion sweep. For each sweep the averager sorts the signal with respect to time into 1024 channels, digitizes the average signal appearing at each channel, and stores the values in its magnetic core memory. The sweeps are stored alternately in an add mode and then a subtract mode. Hence if the signals corresponding to the two ion masses are adjusted for equal amplitudes, a small mismatch in the relative peak positions will appear as an S-shaped error signal, while the matched condition produces a null in the visual display of the memory contents. (Figures 2, 3).

The chief advantage of the above technique is the efficient use made of the information provided by the spectrometer. The visual technique is capable of "storing" information for time intervals of the order of one second, whereas the simpler but more specialized signal averager is typically used to accumulate information for 15 seconds or longer. Since the signal to noise ratio grows as $t/\sqrt{t} = \sqrt{t}$ where t is the time information is gathered, an improvement of about $\sqrt{15} \sim 4$ can be realized in the matching precision. A secondary advantage of this technique is that it is a null method and thus the experimenter's decision regarding the matched condition should be less subjective than in the older visual method.

At the present time a program is being devised in this laboratory so that the information gathered by the signal averager can be rapidly and impartially analyzed by a large

FIGURE 2

Signal averager display after sampling the peaks shown in Figure 1 for about 20 seconds. Mismatch ~ 1% of a peak width.

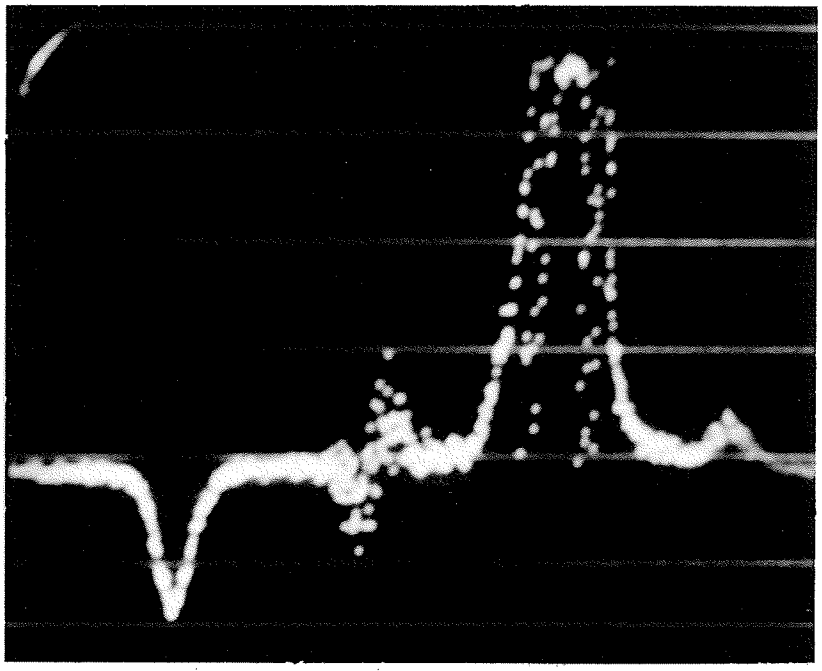

FIGURE 3

Signal averager display after sampling the peaks shown in Figure 1 for about 10 seconds. Null signal.

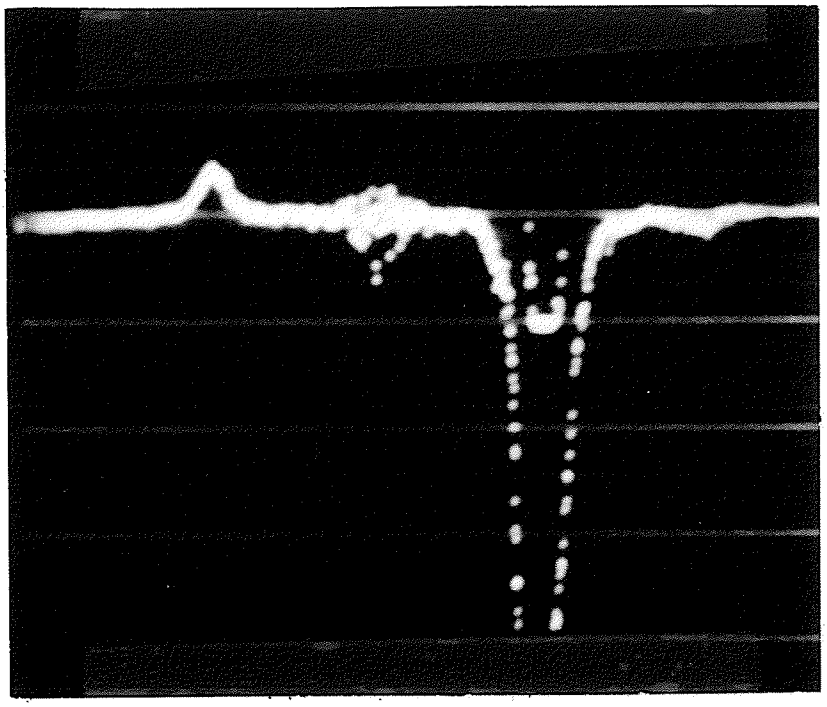

computer. It is hoped that the precision achieved to date can be maintained or even improved upon while greatly reducing the time required to establish a mass difference.

High Resolution Spectroscopes

At the present time there are ten mass spectroscopes capable of high precision measurements. Four of these are in the United States, one is in West Germany, two in Japan, one in Russia, and two in Canada. Table 1 is a summary of some of the pertinent features of these instruments. Those at the University of Minnesota and the University of Manitoba have been the most prolific producers of precise data. The existence of an intermediate direction focus, which allows the energy spread of the ions to be examined, is probably an important reason for the effectiveness of these three spectrometers. The references following the locations of the instruments refer to papers in which more detailed descriptions can be found.

Two basic types of mass spectroscopes have evolved during the last few decades. The older of these, the deflection-type instrument, is the more common and has been applied to a variety of tasks. It is based on the deflection of ions in electric and magnetic fields. All but one of the spectroscopes in Table 1 are of this type.

The other type involves a measurement of either the time for ions in a monoenergetic beam to traverse a known distance, or the cyclotron frequency of an ion circulating in a uniform magnetic field. Such instruments have made a significant contribution to mass spectroscopy in general, and to

mass determinations in particular. The latter contribution has resulted from the refinement of the cyclotron resonance spectrometer since 1945. Smith's new radio frequency spectrometer, an improved version of his mass synchrometer (Smith and Damm, 1956), is unique in that it is the only time of flight instrument capable of high precision mass measurements. Hence data from this spectrometer will be of particular interest.

The remainder of this thesis will be restricted to deflection type instruments.

TABLE 1

HIGH RESOLUTION MASS SPECTROSCOPES

	Measuring Technique	Focussing (See p.25)	Intermediate Focus?	Approximate Working Resolution^{-1}
MINNESOTA (Johnson et al., 1967)	P.M.* with averager	1st order and α^2	Yes	45,000 (+)
ARGONNE (Stevens et al., 1967)	P.M. with averager & computer	1st order and α^2	No	250,000
HARVARD (Bainbridge et al., 1957)	P.M. with lock-in amplifier	1st order and α^2	No	100,000 (+)
PRINCETON (Smith, 1967)	P.M.	---**	No	100,000
MAINZ (Hintenberger et al., 1960)	P.M.	1st order and α^2	No	100,000
OSAKA I (Ogata et al. 1967)	P.M. with differentiation	1st order	Yes	60,000
OSAKA II (Matsuda et al., 1967)	P.M.	1st & 2nd order	No	250,000
USSR (Demirkhanov et al., 1965)	Photographic	1st order	Yes	80,000
MANITOBA I (Duckworth et al., 1963)	P.M. with averager	1st order	Yes	100,000
MANITOBA II (Barber et al., 1967)	P.M. with averager	1st & 2nd order	Yes	150,000

* P.M. = Peak Matching

** A cyclotron resonance spectrometer

CHAPTER 3

ION OPTICS

Introduction

Although the gravitational interaction is generally used for the determination of the mass of a macroscopic body, the electromagnetic interaction is more convenient for atomic mass determinations. An atomic or molecular ion of mass m and charge q moving with a velocity $\vec{v}$ in an electromagnetic field experiences a force $\vec{F}$ which can be written in two parts, one velocity independent and the other velocity dependent:

$$\vec{F} = q\vec{E} + q\vec{v}\wedge\vec{B} \qquad (3\text{-}1)$$

This relation defines the electric field $\vec{E}$ and the magnetic field $\vec{B}$ at the ion's position in space and time.

In a mass spectroscope an ion encounters both electric and magnetic fields. Although co-spatial field arrangements have been used, the consecutive arrangement, in which the ion experiences first electric fields and then magnetic fields, is more common.

Electric Analysers

Two forms of electric field are usually employed. The simpler of the two is homogeneous and of small spatial extent. It is used to accelerate ions from thermal velocities to a much larger velocity v given by:

$$mc^2 (\gamma - 1) = qV_A \qquad (3\text{-}2)$$

$$\gamma \equiv (1 - v^2/c^2)^{-1/2}$$

where V_A is the total electric potential difference through which the ion is accelerated. Since only the velocity or energy of an ion is determined by such a field, at least one other operation must be performed in order to find m.

Some spectroscopes combine the above field with a magnetic field to determine m; however, the resolution of such instruments is seriously limited by the energy spread of the ions. This spread is, of course, due to the manner in which the ions are produced. Spectroscopes based on this arrangement of fields can focus ions having a small spread in direction and hence are called direction focussing or, more usually, single focussing instruments.

In high resolution spectroscopes the ions, after their initial acceleration, are passed through a second electric field which is established between the plates of a capacitor. Such plates usually have singly curved surfaces (i.e. they are cylindrical); however, spherical electrodes are sometimes used. If the radii of curvature of the surfaces of the electrodes are $(r_e + k)$ and $(r_e - k)$ respectively, the path of an ion travelling normally to the field at radius r_e is given by:

$$m \not{\delta} \frac{v^2}{r_e} = q\left|\vec{E}\right| \cong q \frac{V}{2k} \qquad (3\text{-}3)$$

where the outer and inner plates have electric potentials + V/2 and - V/2 respectively. An exact solution of this electrostatic field follows easily from Maxwell's equations and the validity of the approximation in equation (3-3) can be determined. For the spectrometer used in this investigation

(r_e = 100 cm = 100 k), both the surface of zero potential and a field of V/2k are within 50μ of the $r = r_e$ surface.

Electric analysers based on equation (3-3) determine, in the non - relativistic approximation, the kinetic energy of an ion. Thus, as before, another operation is required before m can be determined. However there is now an energy or velocity dispersion. It is possible to combine this type of electric analyser with a magnetic analyser so that the velocity dispersions cancel while direction focussing and mass dispersion are achieved by the combination. Such an arrangement is called double focussing. Figure 4 shows the double focussing properties of the spectrometer used in this investigation. The scale normal to the ion beam is greatly exaggerated for clarity. The shaded beams represent two different velocity groups of ions of the same mass, each with a continuous spread in direction. The location of the final focus of ions of a lighter mass is also indicated. Under typical operating conditions several masses having a small continuous spread in both direction and velocity are present.

Magnetic Analysers

The motion of an ion travelling normally to a magnetic field $\vec{B}$ is described by

$$m \frac{v^2}{r_m} = q\left|\vec{v} \wedge \vec{B}\right| = qvB \qquad (3\text{-}4)$$

where r_m is the instantaneous radius of curvature of the trajectory. Thus a magnetic field is a momentum analyser, or if an ion's velocity or energy is predetermined (as above), a mass analyser.

FIGURE 4

The direction focussing, velocity focussing and mass dispersing properties of the Manitoba second order mass spectrometer.

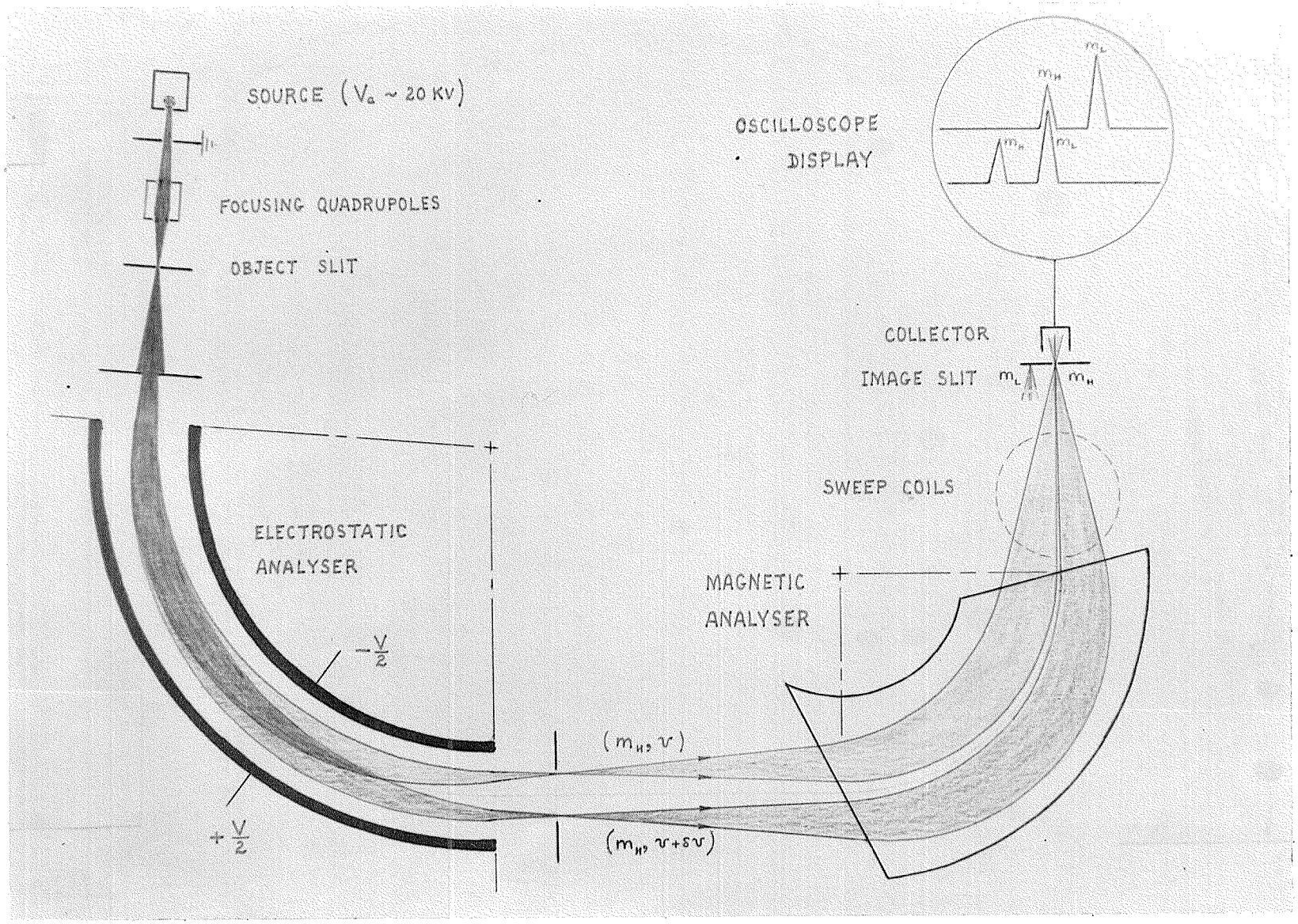
SOURCE ($V_a \sim 20$ KV)
FOCUSING QUADRUPOLES
OBJECT SLIT
OSCILLOSCOPE DISPLAY
m_L
m_H
m_H
m_L
COLLECTOR
IMAGE SLIT m_L m_H
SWEEP COILS
ELECTROSTATIC ANALYSER
MAGNETIC ANALYSER
$-\frac{V}{2}$
$+\frac{V}{2}$
(m_H, v)
$(m_H, v+\delta v)$

Non - uniform magnetic fields are employed in betatrons, isochronous cyclotrons, synchrotrons, and in certain types of beta spectrometers; however, nearly all magnetic analysers used in mass spectroscopes have a homogeneous field. Among the high resolution instruments in Table 1, the only exception is the new Japanese spectrometer (Osaka II). This employs two magnetic analysers. The first has a 1/r field and provides only mass dispersion. The second is homogeneous and provides direction focussing.

Although the experimenter's viewpoint concerning ion optics is usually presented, it is interesting to consider an ion's viewpoint. At any time an inertial reference frame can be chosen in which an ion is instantaneously at rest. Hence by equation (3-1), as far as the ion is concerned, all fields it experiences in a mass spectroscope are purely electric, although these electric fields are not the same as those in the laboratory frame. The significant point is, of course, that the "physics" is the same with respect to any inertial frame of reference.

The Mass - Voltage Relation

Electrical detection and the peak matching technique were qualitatively described in Chapter 2. The masses of the ions involved will now be related to the electric potentials in a quantitative fashion. A non - relativistic treatment will be given because under typical conditions (for example: $m \sim 100\ u$, $V_A \sim 20$ kV) relativistic corrections are of the order of $1/10^7$, while for a mass doublet the differential relativistic correction is a factor of $m/\Delta m$ smaller.

The requirement of identical trajectories applied to equation (3-4) gives:

$$mv = \text{constant} \tag{3-5}$$

Equation (3-2):

$$\frac{1}{2} mv^2 = qV_A \tag{3-6}$$

$$v = \left(\frac{2qV_A}{m}\right)^{1/2} \tag{3-7}$$

Combining (3-5) and (3-7):

$$mV_A = \text{constant} \tag{3-8}$$

From (3-3) and (3-6):

$$r_e q\left|\vec{E}\right| = 2qV_A = 2q\left|\vec{E}_A\right| s \tag{3-9}$$

Thus in general:

$$m\left|\vec{E}\right| = \text{constant} \tag{3-10}$$

This condition for identical paths has been given by Aston (1922), Swann (1931), and Bleakney (1936).

Because of the velocity focussing property of double focussing spectrometers, the location of the final focus for ions of a particular mass is insensitive to modest changes in the accelerating voltage at the source. In fact it is this behavior which is used to verify the attainment of a double focus. However, the lateral position of the final focus is very sensitive to the voltage V applied to the plates of the electric analyser. Equation (3-10) can be written

$$mV = \text{constant} \tag{3-11}$$

One of the variations available in the experimental procedure for measuring a mass doublet is that the lighter member can be matched to the heavier, or vice versa. In the

former case the electric fields in the spectrometer must all be raised. This increases the radius of curvature of the lighter ions in the magnetic analyser to equal that of the heavier ions before the change. Equation (3-11) gives:

$$(m_L + \Delta m)V = m_L\ (V + \Delta V)$$
$$\frac{\Delta m}{m_L} = \frac{\Delta V}{V} \qquad (3\text{-}12)$$

where $\Delta m \equiv m_H - m_L$ and ΔV is the necessary change in the voltage applied to the cylindrical electric analyser. In the latter case the electric fields must be decreased:

$$(m_H - \Delta m)V = m_H\ (V - \Delta V)$$
$$\frac{\Delta m}{m_H} = \frac{\Delta V}{V} \qquad (3\text{-}13)$$

The uncertainty in the mass of either member is usually negligible with respect to both the matching precision ($\delta m/\Delta m$), and the accuracy to which $\Delta V/V$ can be determined. The determination of $\Delta V/V$ will be considered in detail in Chapter 5.

First and Second Order Focussing

The beam of ions produced by the source of a mass spectroscope possesses a small, unavoidable spread in both direction and energy. The direction spread is measured by the half angle α, and the energy spread by the relative velocity spread $\beta \equiv \Delta v/v$. α and β are typically of the order of 10^{-3} or less for high resolution spectroscopes.

Herzog (1934) was the first to derive the general focussing equations for radial electric and homogeneous magnetic fields. Herzog's theory is a first order theory in the sense that all terms of higher than first order in α and β are

neglected. Hence instruments based on this theory are designed so that α and β are as small as possible. In addition to providing expressions for the velocity dispersion and location of the direction focus of electric and magnetic fields separately, Herzog's theory shows quantitatively that such fields can be combined to provide direction and velocity focussing ("double focussing") together with mass dispersion. In other words, the location of the final image is, to first order, independent of both α and β. The main points of Herzog's theory have been frequently reviewed. (e.g. Duckworth, 1958; Barber, 1962).

Hintenberger and König (1957) have developed the corresponding second order relations. In their notation the image aberrations for an electric analyser and a magnetic analyser in tandem are given by

$$y_B = r_m[B_1\alpha + B_2\beta + B_{11}\alpha^2 + B_{12}\alpha\beta + B_{22}\beta^2 + \text{higher order terms}] \quad (3\text{-}14$$

where y_B is the displacement of the ion path from the central path ($\alpha = \beta = 0$) measured in the deflection plane and normal to the central path, and B_1, B_2, etc. are functions of the instrument geometry. This expression is for a principal (object) slit of infinitesimal width. A first order double focus exists when $B_1 = B_2 = 0$. When all five coefficients are zero complete second order double focussing is attained.

Hintenberger and König (1959) have computed solutions of the five equations $B_1 = B_2 = B_{11} = B_{12} = B_{22} = 0$ and give the design parameters of several spectrometers possessing complete second order double focussing.

CHAPTER 4

THE NEW SECOND ORDER SPECTROMETER (MANITOBA II)

Geometry and Slit System

The spectrometer used in this investigation is number 8 in Table I of the 1959 paper by Hintenberger and König. Figure 5 shows the basic design and layout of the instrument. This design was chosen because the ion paths in field free regions are short, the deflection angles are reasonable, and the magnetic field boundaries are straight. All of these features are advantageous both for ease of construction and for convenience of operation. Also, an intermediate direction focus is formed between the two analysers. This permits the electric analyser to be used as an energy analyser with a resolution of about one electron-volt. As pointed out in Chapter 2, this feature is invaluable for insuring that chemically dissimilar ion groups have received the same energy within the source and hence follow the same path through the spectrometer. The scale of the spectrometer is determined by r_e which was chosen to be one meter.

A description of the spectrometer is given by Barber et al. (1967); however, since this instrument was the main tool for this investigation, a detailed description is included here.

Herzog's theory gives magnifications of -0.87 and -0.57 for the electric and magnetic analysers respectively. The overall magnification is thus +0.50. The dispersion is $0.53\,\Delta m/m \equiv 0.53\,\delta$ meters, or 5.3 mm for a 1% mass difference.

FIGURE 5

The geometry of the Manitoba second order spectrometer (Manitoba II)

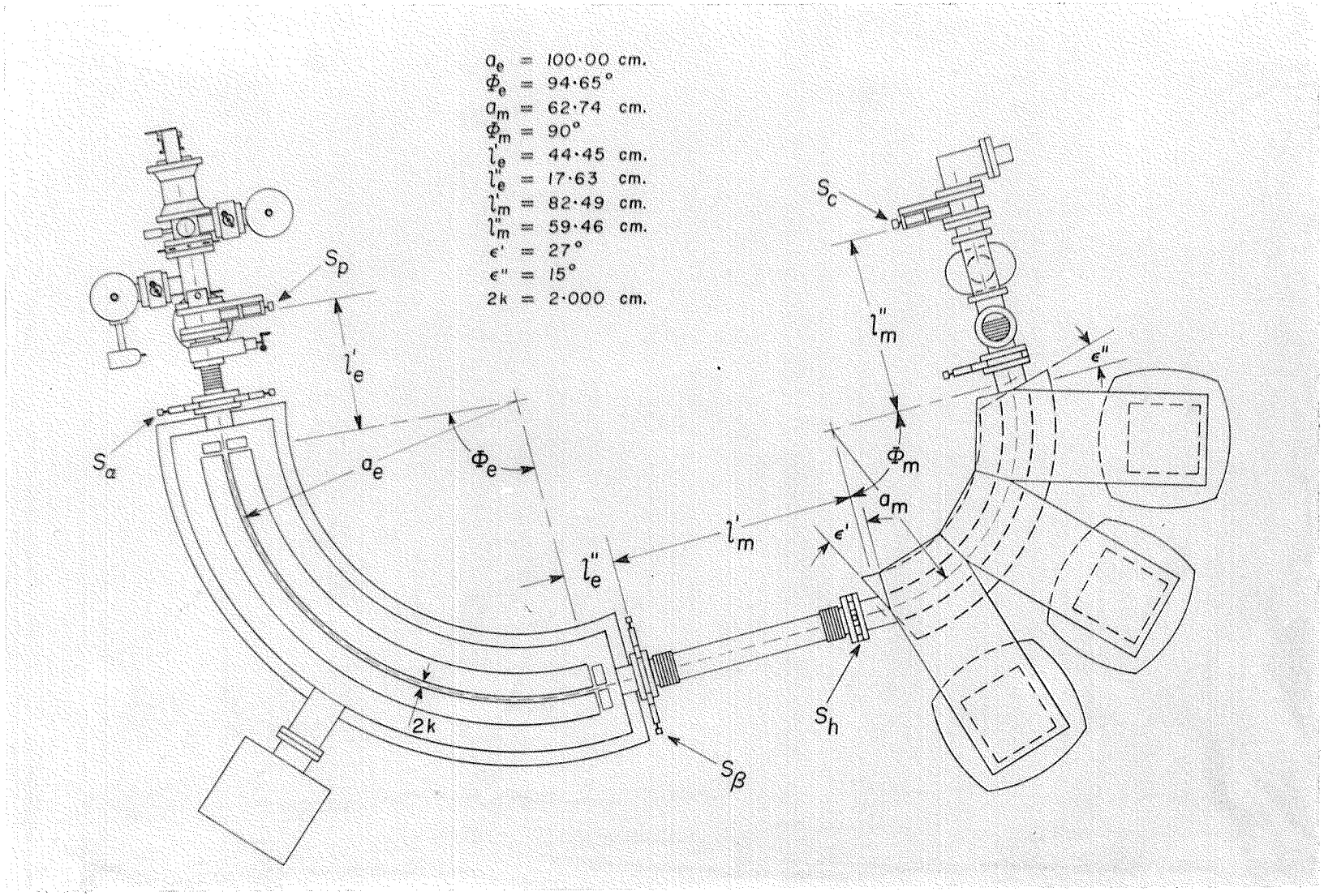
a_e = 100·00 cm.
Φ_e = 94·65°
a_m = 62·74 cm.
Φ_m = 90°
l'_e = 44·45 cm.
l''_e = 17·63 cm.
l'_m = 82·49 cm.
l''_m = 59·46 cm.
ϵ' = 27°
ϵ'' = 15°
2k = 2·000 cm.
S_p
S_α
S_c
S_h
S_β
l'_e
l''_e
l''_m
l'_m
a_e
a_m
Φ_e
Φ_m
ϵ'
ϵ''
2k

The resolution at the base of the peaks is $S_p/0.53$ where S_p is the principal (object) slit width expressed in meters. For a resolution of 1/200,000, $S_p = 2.6\mu$ and the collector slit width $S_c = 0.50\ S_p = 1.3\mu$.

The principal and collector slits are variable in width and in orientation about an axis defined by the central ion path. The chamfers of the slit jaws make an angle of 45° with respect to this axis. The jaws are made of hardened tool steel. They are designed to overlap by about 100μ so that the slits can be closed without damaging their edges.

The principal slit is typically subjected to an ion current of the order of 10^{-5} A. With an accelerating potential of about 20,000 volts, some 0.2 watts are dissipated in the vicinity of the slit edges. After a couple of weeks of this bombardment, the resulting deterioration in resolution and peak shape necessitates retouching of the slit edges. This is accomplished with a flat plate glass tool and #900 alundum abrasive mixed with a bit of water. The quality of the individual slit edges is then checked visually against a plate glass reference flat. The alignment of the reassembled slit is checked visually by viewing the slit against a bright background. Much less frequently the collector slit receives the same treatment.

The angular spread (2α) accepted by the spectrometer is determined by the slit S_α. It is usually set at 1.2 mm to give $\alpha \sim 2 \times 10^{-3}$. S_β is located at the intermediate direction focus and thus determines the energy range of the ions accepted

by the magnetic analyser. It is typically set at 3 mm corresponding to $\beta \sim \pm 8 \times 10^{-4}$. S_h limits the height of the beam entering the magnetic analyser. It is usually set at $\sim$ 2 mm.

Vacuum System

The entire vacuum enclosure is made of 304 stainless steel. Metal gaskets are used throughout except in the valves and on the source side of the principal slit where Viton "O" rings are used. The spectrometer is divided into two regions for pumping purposes. The region on the source side of the principal slit is evacuated by two oil diffusion pumps. These have an untrapped speed of 100 liters/second, are equipped with water-cooled baffles and liquid nitrogen traps, and are backed by a conventional rotary mechanical pump. A system of valves enables the source region to be opened to the atmosphere and be pumped down again to below 10^{-6} torr in less than ten minutes. This arrangement is very convenient when routine source maintenance is required.

The remainder of the spectrometer is evacuated by two ion pumps. A 140 liter/second pump is located on the electric analyser and a 50 liter/second pump is located between the magnet and the collector. The pressure in this region is usually $\sim 10^{-7}$ torr or better.

Ion Source

A diagram of the ion source is shown in Figure 6. The basic design is similar to source number 7.1 on page 646 of the compendium on Ionenphysik and other topics by Von Ardenne (1962). It differs from the conventional mass

FIGURE 6

The Ion Source

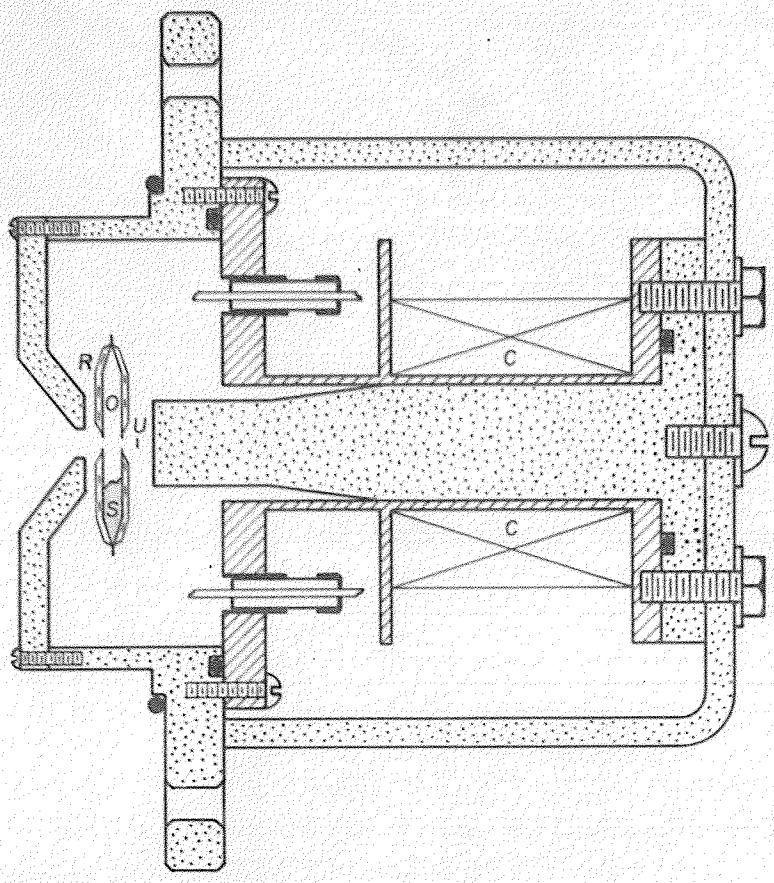

BRASS

IRON

S SAMPLE
O OVEN (stainless steel)
U Re FILAMENT (coated with LaB_6)
R W RIBBON HEATER & BN INSULATION
C Cu WINDINGS FOR $\vec{B}$
E 5 cm.

spectroscopic electron bombardment source in that the ions are drawn out parallel to the ionizing electron beam instead of at 90^{o} to this beam. An improvement of one or two orders of magnitude in ion current ($i \sim 10^{-5}$ A) has been achieved by this technique. The energy spread is of the order of only one electron-volt. L. G. Smith (1967) uses a similar source with his cyclotron resonance spectrometer.

In this investigation ions were obtained from rare earth chlorides. These compounds are solids which must be heated to several hundred degrees Centigrade before their vapor pressure is sufficient for the production of an adequate ion beam. As indicated in Figure 6 this was done in a stainless steel oven. The oven is closed except for two small holes through which the ionizing electron beam enters and from which ions are drawn by the penetration of the main accelerating field. The copper windings and the iron pole pieces provide an axial magnetic field which guides the electron beam through the oven. The potentials of the electron filament, oven, and source case are adjusted to cause the electrons to oscillate back and forth through the ionization region.

When a fresh sample is placed in the oven it must be baked out for a minute or so at a low heat under vacuum. Initially this procedure was difficult since at some critical temperature the sample flies apart until most of it is sprayed out of the oven. This inconvenience was avoided by placing a small metal clip over the oven apertures during the baking out process.

When the source is in operation a small blue plasma cloud is often visible just inside the front aperature of the

oven. Occasionally the pressure in the source region becomes high enough so that the ion beam appears as a fine blue line traversing the high voltage accelerating gap; however, doublet measurements are carried out at somewhat lower pressures in order to minimize the energy spread in the ion beam.

The source potential is provided by a commercial high voltage power supply (Universal Voltronics Corp., Model BRE 30-2, 30 kV, 2 mA). This supply typically has a short term stability of better than 0.5 volt, and is stable to within a few volts over several minutes.

After acceleration the ion beam passes through two electric quadrupole lenses which are arranged one after the other (Whineray, 1966). This arrangement produces a line image at the principal slit and allows the ion beam to be displaced and/or deflected in both horizontal and vertical directions. The circuit which provides the quadrupole potentials is described by Meredith (1969).

Figure 7 shows the entire source arm. The location of the principal slit, et cetera, can be determined by a comparison with Figure 5. The source arm is positioned with respect to the electric analyser by the "x-y-θ" table located directly below the principal slit. A single ball bearing rolling between hardened steel plates provides the main support for the source arm. The source arm and table rest on an eight inch "I" beam which is bolted to the electric analyser base. Thus the entire source assembly can be moved with the electric analyser as a unit.

FIGURE 7

The Source Arm

NOTE: Since Figures 7, 9, 11, 14, 15 and 22 contain considerable detail, they are presented as stereo pairs. These may be viewed with or without optical aid. In the latter case the observer has simply to keep the optic axes of his eyes parallel (as when looking at a distant object) while focussing on the photographs. The brain involuntarily causes the optic axes to intersect at the object being observed; however, with practice this program can be changed.

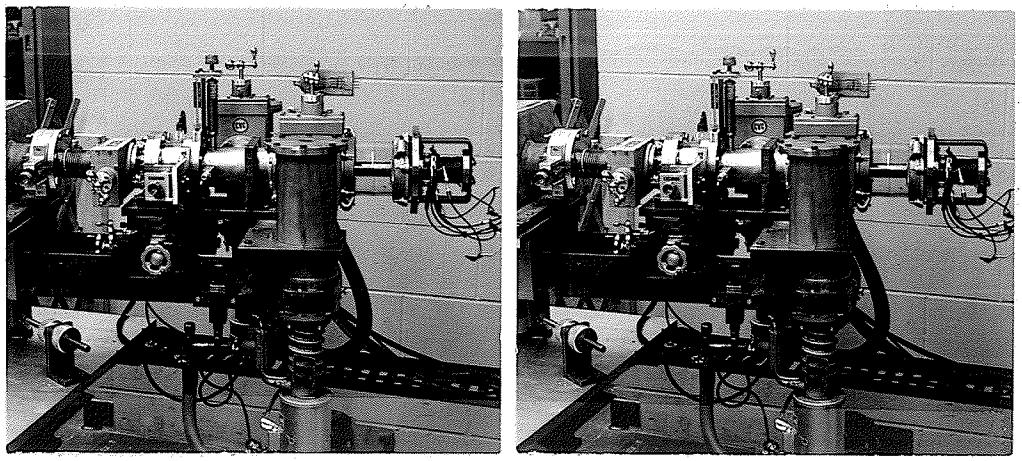

Electric Analyser

The geometry of the electric analyser appears in Figure 5. Figure 8 is a view of the interior of the analyser. The two cylindrical plates are made of gold plated Armco iron. The one meter mean radius of curvature is accurate to 3μ. The plates are positioned relative to the inner edge of the stainless steel base plate by means of a locating screw on each of the five inner mounts. Each plate is 17.8 cm high and rests on five quartz blocks. The 2 cm gap is determined by five pairs of quartz spacers which are ground to an accuracy of 3μ. The top spacer of each pair is visible in Figure 8. The outer plate is pressed against the spacers and inner plate by an inconel spring arrangement located on the outer mounts. The electric field is terminated at the physical boundaries of the analyser plates by grounded blocks which are located in accordance with Herzog's theory (1935).

The electric analyser with its cover in place is visible in the view of the entire spectrometer shown in Figure 9. The vacuum seal between the cover and the base plate is made by a gold wire.

The analyser and source arm are supported by three ball bearings located approximately along the tangents to the ion path at the entrance and exit to the field. These balls roll between horizontal, hardened steel plates. With this arrangement the analyser and source assembly, which weigh about 1.1 tons, can be easily swung as a unit about a pivot which is located directly below the intermediate direction focus. This adjustment is one of the variables used to achieve a double focus.

FIGURE 8

The Interior of the Electric Analyser

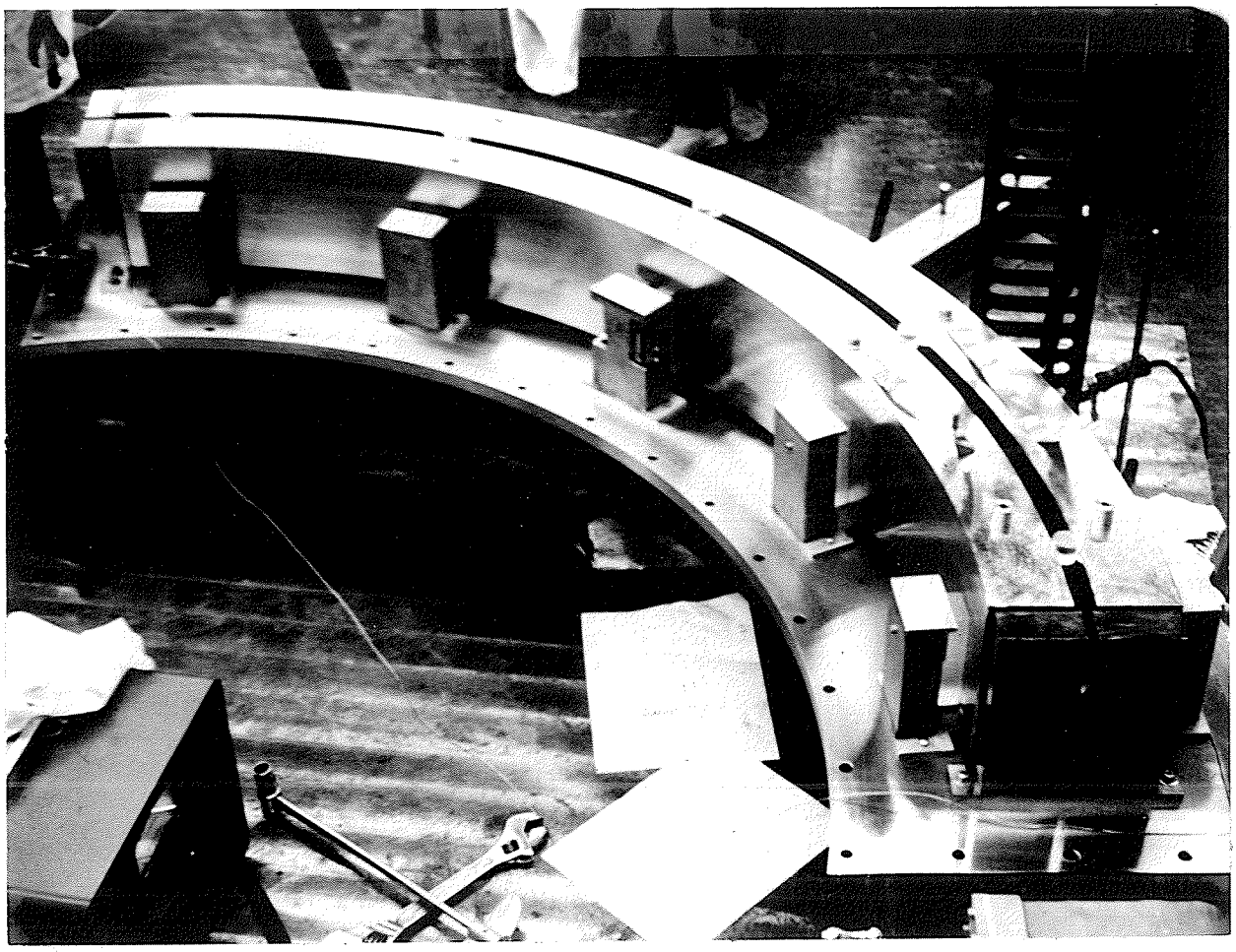

FIGURE 9

The Second Order Spectrometer

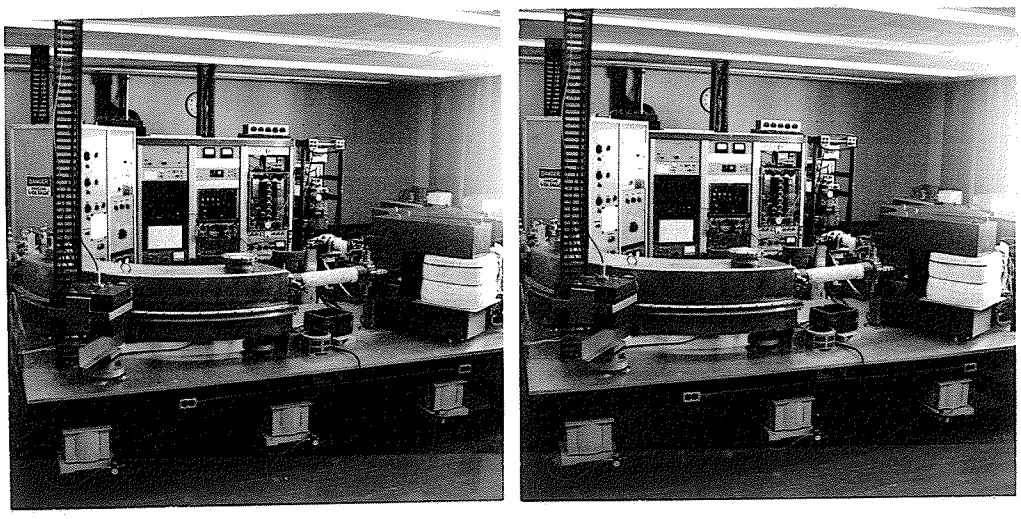

The voltage on the analyser plates is provided by a series of ten 97.2 volt mercury batteries (Eveready #E302462). The electrical circuitry associated with these batteries is described in detail in Chapter 5.

Magnetic Analyser

The geometry of the magnetic analyser appears in Figure 5. A view of the 5 ton magnet is shown in the right hand side of Figure 9. The pole pieces are single blocks of Armco iron and are separated by 1" inconel spacers. Above and below the pole pieces are 3 mm shimming gaps. Aluminum spacers provide mechanical support in these gaps. In addition to allowing for small adjustments of the field (part of the yoke immediately above the upper gap can be tilted slightly), these two gaps provide a very uniform field between the pole pieces. For any field in the range 0.3 - 0.8 W/m^2 the uniformity is about 1 part in 5000 to within about one gap width of the boundary.

The magnet yoke is made in three "C" sectors. Each sector has two water-cooled exciting coils. The six coils are connected in parallel electrically and in three parallel branches of two coils each for cooling. As indicated in Figure 10, the magnet current is stabilized with respect to a zener regulated voltage supply. The transistorized current regulator maintains the magnetic field constant to 1 ppm or better for 15 s or longer. A detailed circuit diagram of this supply is given by Meredith (1969).

FIGURE 10

Block Diagram of all Circuits

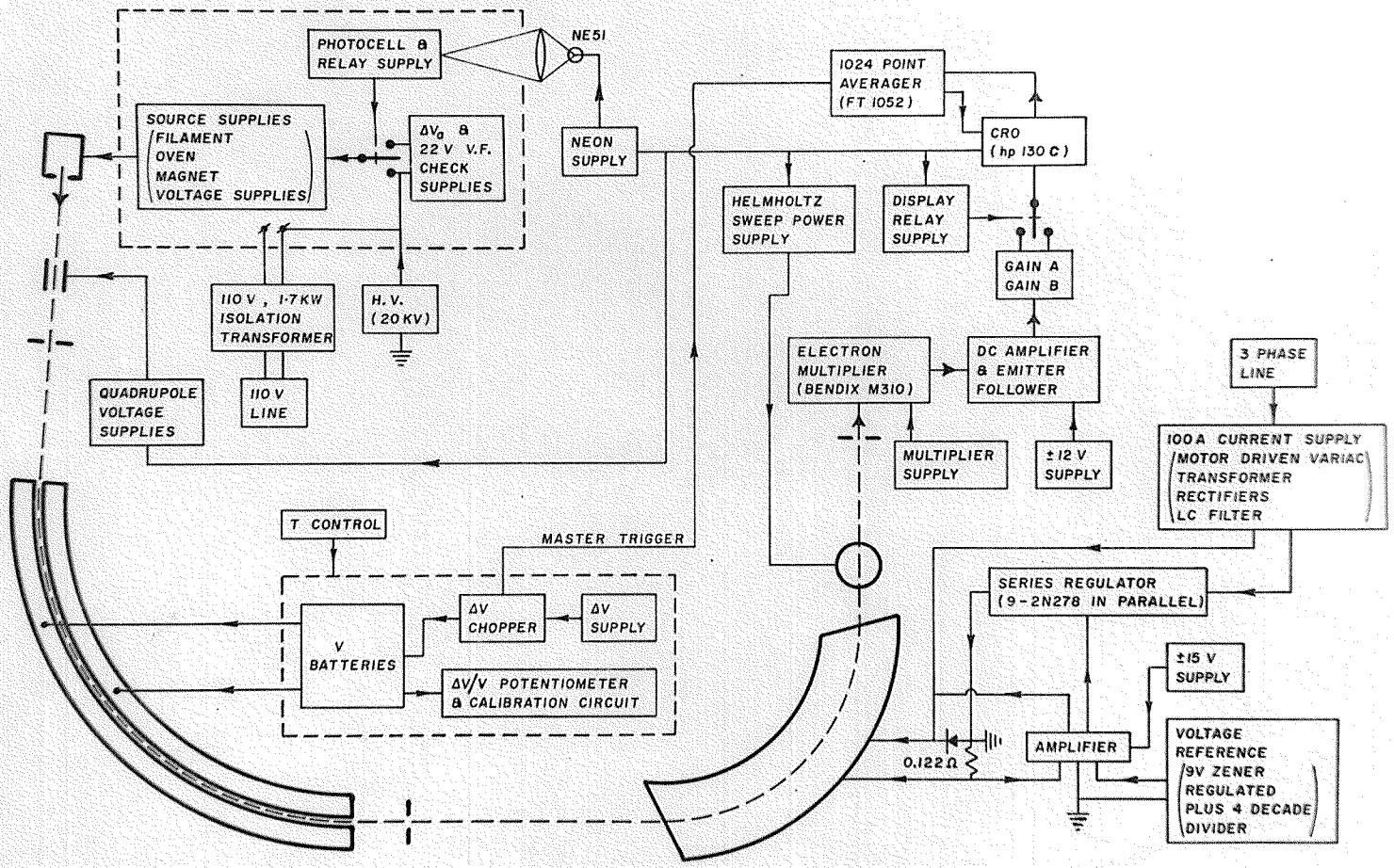
PHOTOCELL & RELAY SUPPLY
NE51
SOURCE SUPPLIES (FILAMENT OVEN MAGNET VOLTAGE SUPPLIES)
ΔV0 & 22 V V.F. CHECK SUPPLIES
NEON SUPPLY
1024 POINT AVERAGER (FT 1052)
CRO (hp 130 C)
HELMHOLTZ SWEEP POWER SUPPLY
DISPLAY RELAY SUPPLY
GAIN A GAIN B
110 V, 1·7 KW ISOLATION TRANSFORMER
H.V. (20 KV)
ELECTRON MULTIPLIER (BENDIX M310)
DC AMPLIFIER & EMITTER FOLLOWER
3 PHASE LINE
QUADRUPOLE VOLTAGE SUPPLIES
110 V LINE
MULTIPLIER SUPPLY
±12 V SUPPLY
100 A CURRENT SUPPLY (MOTOR DRIVEN VARIAC TRANSFORMER RECTIFIERS LC FILTER)
T CONTROL
MASTER TRIGGER
SERIES REGULATOR (9-2N278 IN PARALLEL)
ΔV CHOPPER
ΔV SUPPLY
V BATTERIES
ΔV/V POTENTIOMETER & CALIBRATION CIRCUIT
±15 V SUPPLY
AMPLIFIER
0.122 Ω
VOLTAGE REFERENCE (9V ZENER REGULATED PLUS 4 DECADE DIVIDER)

Ion Detection

The detector arm of the spectrometer appears in Figures 5 and 11. The arm is supported by a stainless steel frame which is attached to the spectrometer table. A brass and perspex frame supports the Helmholtz coils located between the magnetic analyser and collector slit. These coils are driven by a sawtooth current at a frequency of about 19 c/s. The resulting magnetic field sweeps the ion beam across the collector slit. All ions passing through this slit are detected by a low noise, high gain, magnetic electron multiplier. Under typical conditions the ion current arriving here is $\sim$ 1-10 fA. A block diagram of the detection circuitry appears in Figure 10.

The location of the collector slit in a plane normal to the ion beam is controlled by screw drives. Adjustments along the ion beam are also possible.

In addition to the final collector, the ion beam can be monitored by an electrometer at four intermediate points. The first probe is located on the source arm between the quadrupole lens and principal slit. An ion current of 1-10 μA can be collected here under usual conditions. The second available probe is the outer plate of the electric analyser. A third collector is positioned between the analysers at the intermediate direction focus. The final probe is located just beyond the exit of the magnetic analyser. Usually only the interanalyser probe is called upon when starting up the spectrometer.

FIGURE 11

The Detector Arm

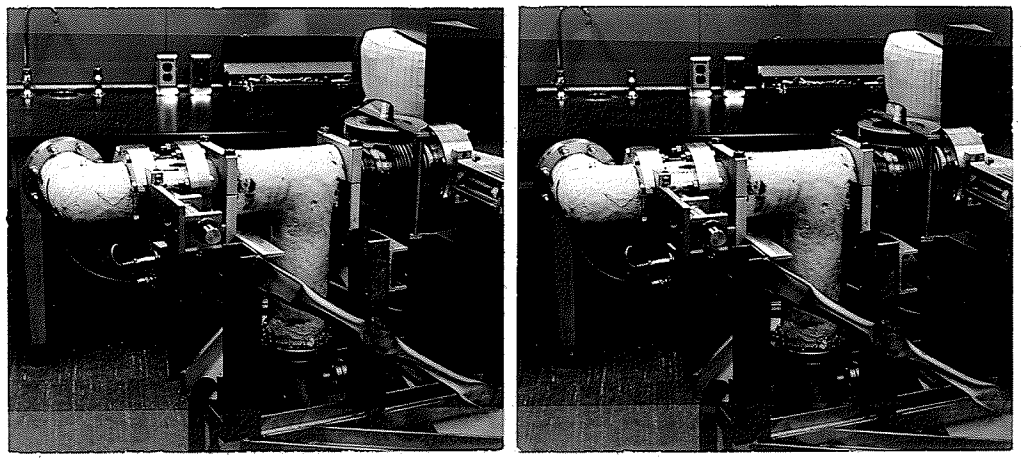

Spectrometer Support

The entire spectrometer rests on a 1.7 ton steel table. The top of this table is a 5' x 12' x 1" steel slab which is machined flat on its top side and is welded to a lattice of 8 inch "I" beams on its bottom side. Initially this slab was supported by eight steel legs standing in a channel iron frame which, in turn, rested on the laboratory floor. With this arrangement the spectrometer was consistently affected by external vibrations. The main effect of such disturbances was to cause the source and collector arms to vibrate at frequencies of the order of 20-40 c/s. This motion caused the peaks on the display oscilloscope to oscillate sideways at a beat frequency of the arm vibrations and sweep rate. The amplitude of this disturbance varied from the threshold of detectability ($\sim 1/20^{th}$ peak width) to a peak width or more. In the former case the net effect was a slight loss in the effective resolution, while in the latter case no useful measurements could be taken. Sources of vibration ranged from persons walking within 20 feet of the spectrometer to construction work within a mile radius.

The vibration problem was completely eliminated by replacing the rigid legs by eight pneumatic mounts (model KAM -2 -3, Kinetic Air Mounts, Consolidated Kinetics Corp., Columbus, Ohio). Each mount contains a pressure regulator and a rubber bellows which will support 2 tons when inflated to a pressure of 100 psi. A 224 ft^3 cylinder of nitrogen will operate the system for over a month. In the event of a pressure failure, the spectrometer settles about 1/2" onto steel supports. Three of the mounts are visible in Figure 9.

With the pneumatic mounts the spectrometer has a highly damped natural frequency of about 1 c/s. The isolation efficiency for disturbances of the order of 30 c/s is over 99%.

When standing beside the spectrometer, I find it a bit fascinating that its 8 ton mass is being supported by an excess of molecules striking it from beneath.

Focussing

The focussing properties of the spectrometer were investigated by Barber (1965) before construction began. A computer program was devised to determine the effect of various nonuniformities in the field of the magnetic analyser on the widths and positions of the direction and velocity foci. It was found that the widths are not appreciably altered although the foci may be moved by differing amounts from the theoretical position of the double focus. Also, the foci can be brought together by a suitable small change in the field, although this may not occur at the theoretical position of the double focus. Since the second order aberrations are not extremely sensitive to geometry, it was concluded that once a first order double focus is found, a second order double focus also exists.

The first step in achieving a double focus is to apply a 22 volt square wave to the source at one - half the frequency of the display oscilloscope sweep (Figure 10). The electric analyser is then swung slowly through a few degrees about its pivot at the energy defining slit.

Lack of velocity focussing results in a peak being displaced with respect to itself on alternate sweeps, while a direction focus is characterized by a distinct sharpening of the peaks. The magnetic field necessary to bring the ions to the same point on the oscilloscope display is a maximum for a certain position of the electric analyser. If a direction focus occurs at this position, it indicates that the electric analyser is direction focussing correctly. Usually both the velocity and direction foci occur near this angle and only a small change in l_e' (to move the direction focus) or a lateral movement of the collector slit (to move the velocity focus) is sufficient to achieve a double focus.

Other adjustments include the several controls on the source conditions and quadrupole voltages. These are set mainly for optimum ion intensity. The widths of the principal and collector slits are adjusted for a suitable compromise between resolution and peak intensity. The resolution and peak shape are also very sensitive to the tilts of these two slits. Occasionally a small but distinct improvement in focussing results if the history of the magnetic field is erased. This is accomplished by decreasing the field to zero.

As mentioned at the beginning of this Chapter, chemically dissimilar ion groups may not follow the same path through the instrument. To check this the accelerating voltage is adjusted until the ion beams are partially cut off by one jaw of the energy defining slit. If the corresponding peaks on the oscilloscope display decrease together, the two ion groups are following the same path. By applying an "artificial"

energy difference by means of the square wave modulation on the source, energy differences of less than 1 eV have been detected by this technique.

The presence of stray 60 c/s magnetic fields often causes the ion peaks to vibrate with a subsequent loss in resolution. Such fields are conpensated for by a coil placed near the interanalyser tube (Figure 9). With the Helmholtz sweep removed and the display oscilloscope operating at 60 c/s, the main magnetic field is adjusted to sit on the side of a peak. The amplitude and phase of the compensating field is then adjusted to cancel the 60 c/s ripple appearing on the display oscilloscope.

Although the focussing technique described above is always used when required, a multitude of obscure adjustments and corrections have been performed over the past couple of years to keep the spectrometer operating. Problems have ranged from the embarrassing one of trying to find the ion beam, to more subtle problems such as the cause of occasional random shifts in peak positions. However, if the experimenter persists to the point of getting the instrument operating correctly, this particular spectrometer is usually quite docile and even cooperative for some time thereafter.

Measuring Technique

Figure 10 is a block diagram of most of the electrical circuits associated with the spectrometer. Only the circuits connected with the vacuum system are omitted. The large arrowheads indicate the path of the ion signal.

The essential features of the peak matching technique were described in Chapter 2. As noted in Chapter 3, the lighter member of a doublet can be matched to the heavier one, or vice versa. Also, the sawtooth sweep on the Helmholtz coils can be reversed. In addition, the larger member of a doublet can be attenuated by sending it through either the "Gain A" circuit or the "Gain B" circuit. These three alternatives can be combined in eight different ways. In order to avoid errors arising from the operator's judgement of the matched condition, all eight combinations are used, with the average of the eight ΔV settings representing the value of one "run".

According to equations (3-12) and (3-13), it is incorrect to average all eight ΔV values since, assuming V to be constant, the four settings obtained when matching the lighter member to the heavier ("ΔV add") will be somewhat larger than the other four settings obtained when matching the heavier member to the lighter ("ΔV subtract"). However for close doublets an average of the eight setting is valid:

Let ΔV_+ represent the average of the four ΔV settings obtained when matching the lighter to the heavier, and ΔV_- be defined in the reverse fashion. Let $\overline{\Delta V}$ be the average of all eight settings, and $\bar{m}$ be the average of m_L and m_H. Then according to equations (3-12) and (3-13):

$$\Delta m = (\bar{m} - \frac{\Delta m}{2})\frac{\Delta V_+}{V} \qquad (4\text{-}1)$$

$$\Delta m = (\bar{m} + \frac{\Delta m}{2})\frac{\Delta V_-}{V} \qquad (4\text{-}2)$$

Add: $$2\Delta m = \bar{m}\left(\frac{\Delta V_+ + \Delta V_-}{V}\right) + \frac{\Delta m}{2}\left(\frac{\Delta V_- - \Delta V_+}{V}\right)$$

$$\Delta m = \bar{m}\,\frac{\overline{\Delta V}}{V} + \frac{\Delta m}{4}\left(\frac{\Delta V_- - \Delta V_+}{V}\right) \qquad (4\text{-}3)$$

But: $$\left(\frac{\Delta V_- - \Delta V_+}{V}\right) = \left(\frac{\Delta m}{m_H} - \frac{\Delta m}{m_L}\right) \cong -\left(\frac{\Delta m}{\bar{m}}\right)^2$$

Hence: $$\bar{m}\,\frac{\overline{\Delta V}}{V} \cong \Delta m\left[1 + \frac{1}{4}\left(\frac{\Delta m}{\bar{m}}\right)^2\right] \qquad (4\text{-}4)$$

To determine whether or not this correction is significant, the precision of the spectrometer must be considered. Equation (2-1) can be written:

$$\frac{\delta m}{\Delta m} = \left(\frac{m}{\Delta m}\right) fR \qquad (4\text{-}5)$$

The best performance expected of the spectrometer was chosen to correspond to $f \sim 1/10^4$ and $R = 1/250{,}000$. Thus the matching precision given by equation (4-5) is:

$$\frac{\delta m}{\Delta m} = \frac{0.4}{10^9}\left(\frac{m}{\Delta m}\right) \qquad (4\text{-}6)$$

If we require that the correction to Δm in equation (4-4) be at least an order of magnitude less than the matching precision, then:

$$\frac{1}{4}\left(\frac{\Delta m}{m}\right)^2 \leq \frac{0.4}{10^{10}}\left(\frac{m}{\Delta m}\right)$$

$$\frac{\Delta m}{m} \leq \frac{1}{1840}$$

Hence for doublets closer than about 1/2000, the eight settings of ΔV may be averaged and the expression:

$$\Delta m = \bar{m}\,\frac{\overline{\Delta V}}{V} \qquad (4\text{-}7)$$

used to calculate Δm.

This procedure was used for the mass measurements reported in this thesis (Chapter 6). The average of approximately 20 runs is the final value quoted for each doublet measurement. In an attempt to eliminate any systematic errors, these runs were distributed among three or more operators, and were performed over a minimum period of three days. In addition the spectrometer was readjusted before each run. The uncertainty assigned to each doublet measurement is the standard deviation of the mean. As will be shown in Chapter 5, the $\Delta V/V$ potentiometer usually contributes negligible error.

For doublets wider than about 1/2000, the ΔV settings must be considered in groups of four and equations (3-12) and (3-13) used to calculate Δm. In practice this slight complication is overshadowed by the necessity of making a substantial change in the magnetic field when going from the "ΔV add" to the "ΔV subtract" arrangement. For doublets involving a one or two mass unit jump, the change in the field is such that the spectrometer must often be readjusted. Hence the concept of a run as defined above loses its meaning. In such cases an equal number of "add runs" and "subtract runs" should be taken to determine the value of a doublet.

To date no wide doublets have been measured as the present quadrupole voltage supplies are not designed to follow equation (3-10). A few preliminary measurements have been done on the doublet $^{156}Gd^{35}Cl^{37}Cl$ - $^{156}Gd^{35}Cl_2$; however, since the static voltages on the quadrupoles affect the peaks being matched by different amounts, the ion groups follow different

paths and the measurements are not reliable. These preliminary values for $^{37}Cl - ^{35}Cl$ differ with the accepted value by 1 ppm to 53 ppm. However, in addition to verifying that the $\Delta V/V$ potentiometer is accurate to at least this sort of precision, these results also indicate that for the close doublets examined in this work, the present quadrupole supply is more than adequate.

CHAPTER 5

THE MEASUREMENT OF $\Delta V/V$

Precision Required

As mentioned above, the voltage V applied to the electric analyser is supplied by ten 97.2 volt mercury batteries. If this voltage is combined with the optimum matching precision provided by the spectrometer (equation 4-6), we obtain:

$$\frac{\delta m}{\Delta m} = \frac{0.4}{10^9} \frac{m}{\Delta m}$$

$$= \frac{0.4}{10^9} \frac{V}{\Delta V}$$

$$= \frac{0.39 \times 10^{-6}}{\Delta V} \qquad (5\text{-}1)$$

According to equations (3-12) and (3-13), Δm appears experimentally as the ratio $\Delta V/V$ (the uncertainties on m_L and m_H are usually negligible). If ΔV and V are measured separately on the same potentiometer, the limit on the accuracy to which $\Delta V/V$ can be determined all occurs in the measurement of ΔV, since $\Delta V \ll V$. Hence according to equation (5-1), the potentiometer must be accurate to $\pm 0.39\ \mu V$ if it is to match the precision of the spectrometer.

The V Circuit

Mercury batteries were chosen to supply V because of their excellent stability. The highest voltage battery commercially available is supplied by Union Carbide (Eveready). It is composed of 72, 1.35 volt cells in

series for a total of 97.2 volts. This size was selected as a reasonable compromise between convenience in measuring V (more measurements would be required if batteries of lower voltage were used) and the complexity of the potentiometer circuit (the present circuit would have to be more complex and contain higher resistances in order to measure voltages above 100 volts and still satisfy equation (5-1)).

The choice of $V = 10 \times 97.2$ volts represents a compromise between both the size of the absolute uncertainty allowed on ΔV and the relative energy spread of the ions on one hand, and the required magnitudes of both the accelerating voltage and magnetic field on the other.

Although mercury batteries are very stable, their temperature coefficient is not negligible. If, for example, a person's hand is placed within one centimeter of one of the V batteries for a second or two, a noticeable shift in its voltage occurs on the measuring potentiometer. For this reason the V batteries together with the ΔV circuit and $\Delta V/V$ potentiometer are located in a temperature controlled "perspex" box (Figure 12). The control is provided by a thermistor sensor and a silicon controlled rectifier power supply (Honeywell R7187A) which drives a nichrome wire heater (200 watts maximum). An interference filter (Cornell-Dubilier #1F-18) reduces pickup from the SCR switching to a negligible level. A small fan driven by a synchronous electric clock motor circulates the air within the box, and a container of silica gel absorbs any water vapor.

FIGURE 12

The $\Delta V/V$ Potentiometer, V and ΔV Circuits, and Temperature Controlled Box.

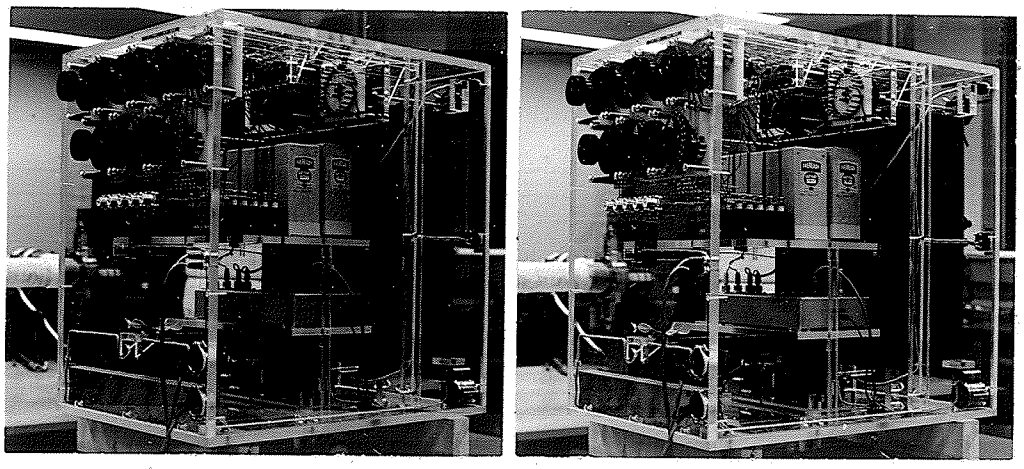

A diagram of the V circuit appears in the lower right of Figure 13. The electrical connections between the ends of the battery chain and the plates of the electric analyser are composed of several metals and are about 4 C^{o} warmer at the battery end than at the analyser end. However the two leads are nearly identical and junctions between dissimilar metals are at the same temperature in one lead as in the other ($\Delta T \leq 0.1$ C^{o}). Hence the net thermal and contact voltages will be equal and the only effect will be a negligible shift in the position of the surface of zero potential between the analyser plates. In any case, an asymmetric lead potential would affect only V (as ΔV is added to V), and the absolute accuracy to which V must be known is a factor of $m/\Delta m$ less stringent than that of ΔV.

The surfaces of the electric analyser plates must also be electrically identical. The gold plate and clean vacuum system (ion pumps and metal gaskets) were both chosen with this requirement in mind.

The ΔV Circuit

A diagram of the circuit which supplies ΔV appears in Figure 14. This circuit produces a square wave which has $\lesssim 50$ μV of pickup. The relay units are adjusted to break-before-make.

The ΔV relay is a "low thermal chopper". The contacts are gold blocks and are operated by a camshaft-pushrod arrangement which, in turn, is driven by a synchronous motor and O-ring belt (Figure 15). This design is

FIGURE 13

The $\Delta V/V$ Potentiometer and V Circuit

The potentiometer circuit (left-hand side of the figure) consists of a 100KΩ voltage divider (VDR) attached to a series resistance of 2.5MΩ and is driven by the 100 volt power supply. The series resistance is broken into nine sections in order to facilitate its calibration against the input resistance of the VDR.

The V batteries are measured across the entire potentiometer (Switches B and C are set to look at battery #6 in Figure 13) while ΔV is measured across only the VDR (R_1 or R_1 plus R_2 are included for large ΔV's). The chain of twelve 10KΩ resistors (DMR) is used to establish known ratios which are then used to calibrate the settings of the VDR.

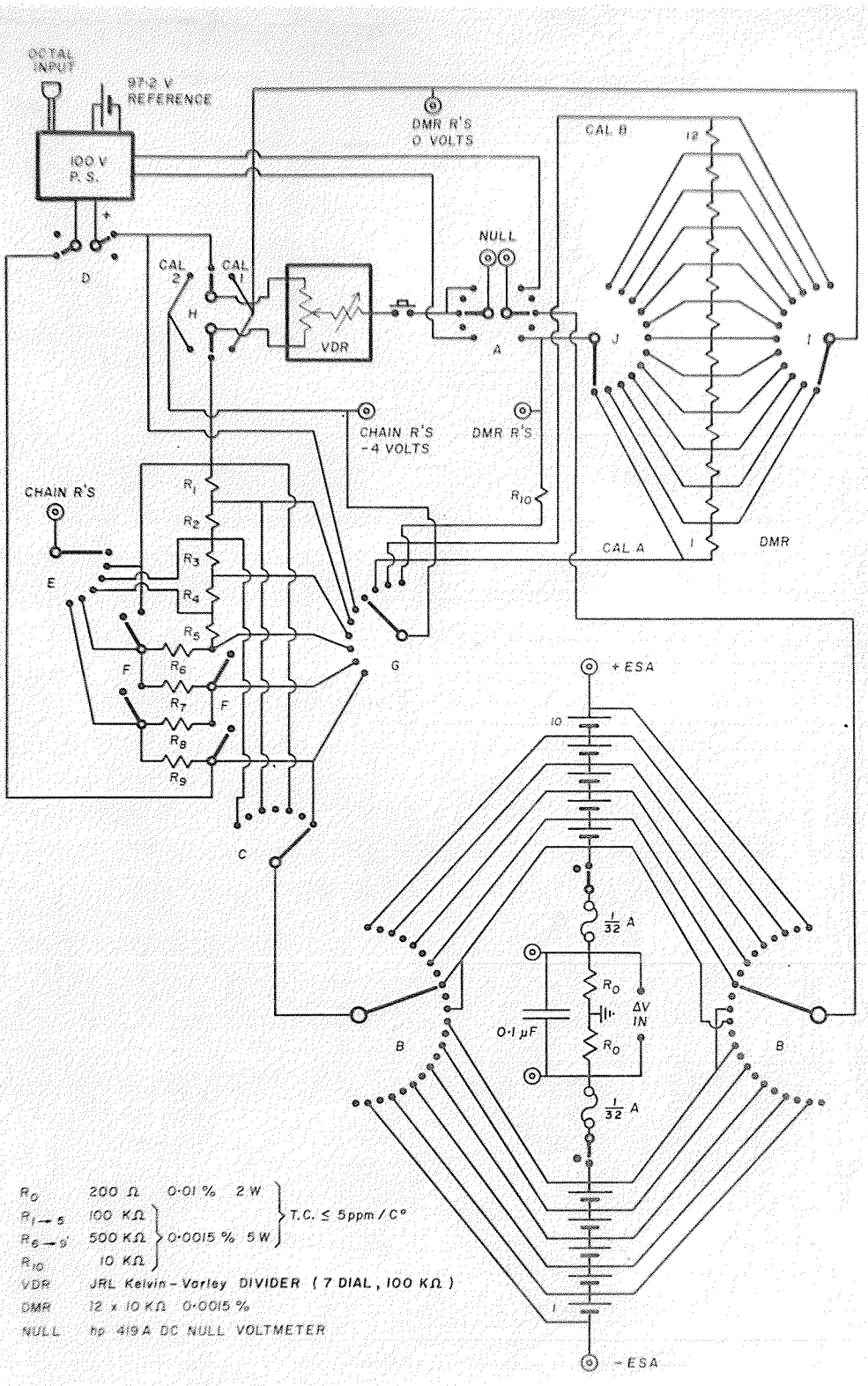

R_0	200 Ω	0·01 % 2 W	T.C. ≤ 5ppm / C°
$R_{1 \rightarrow 5}$	100 KΩ	0·0015 % 5 W	
$R_{6 \rightarrow 9}$	500 KΩ		
R_{10}	10 KΩ		
VDR	JRL Kelvin-Varley DIVIDER (7 DIAL , 100 KΩ)		
DMR	12 x 10 KΩ 0·0015 %		
NULL	hp 419A DC NULL VOLTMETER		

FIGURE 14

The ΔV and Trigger Circuits

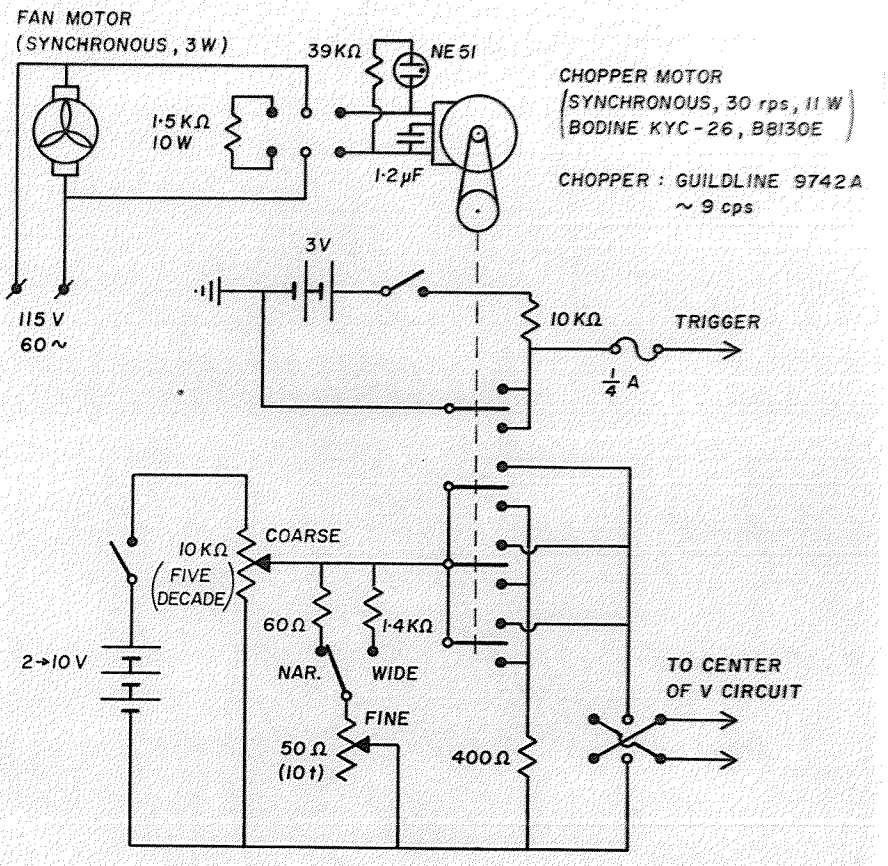
FAN MOTOR
(SYNCHRONOUS, 3 W)
39 KΩ
NE 51
1·5 KΩ
10 W
1·2 μF
CHOPPER MOTOR
(SYNCHRONOUS, 30 rps, 11 W
BODINE KYC-26, B8130E)
CHOPPER : GUILDLINE 9742A
~ 9 cps
3V
115 V
60 ~
10 KΩ
TRIGGER
¼ A
10 KΩ
(FIVE DECADE)
COARSE
60 Ω
1·4 KΩ
NAR.
WIDE
FINE
2→10 V
50 Ω
(10 t)
400 Ω
TO CENTER
OF V CIRCUIT
ALL COMPONENTS & WIRING SHIELDED

FIGURE 15

The ΔV Chopper

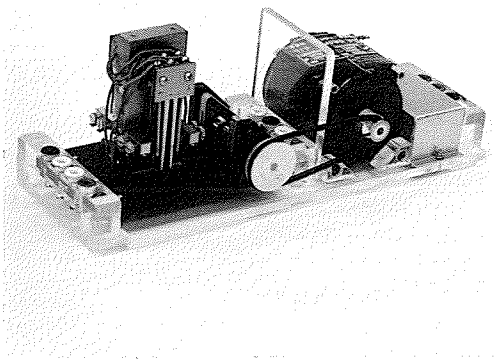

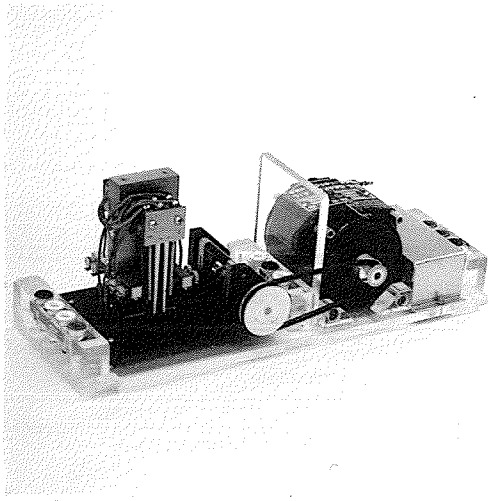

superior to a solenoid driven, mercury wetted relay as it is less susceptible to pickup, temperature changes, and static-dynamic differences in contact resistances. In addition the O-ring belt, although not an elegant drive, has the advantage that the resulting frequency of ΔV and the master trigger cannot be equal to or a harmonic of the frequency of any source of pickup such as the 60 c/s line. Hence any pickup on ΔV and the detection circuitry occurs at a rejection frequency and will tend to average to zero.

The chopper frequency is limited by the 1024 channel signal averager which requires a minimum time of 50 μs per address. Hence the sweep period is slightly more than 50 ms, and the chopper must operate no faster than about 9 c/s (the trigger frequency is twice that of the ΔV square wave).

As indicated in Figure 13, ΔV is developed across two 200Ω resistors (the 400Ω resistor in Figure 14 insures that the load seen by the ΔV circuit will be the same whether or not the chopper is operating). Equation (5-1) and an analysis of the ΔV circuit indicates that variations (δR) in the resistance of the chopper contacts must satisfy:

$$\frac{\delta R}{400\Omega} \sim \frac{\delta(\Delta V)}{\Delta V} \leq \frac{0.39 \times 10^{-6}}{\Delta V} = \frac{0.4}{10^9} \frac{m}{\Delta m} \qquad (5\text{-}2)$$

The parallel arrangement of three chopper units (Figure 14) has $\delta R \lesssim 50\mu\Omega$ which corresponds to $m/\Delta m \gtrsim 300$. However, many ΔV settings are involved in a doublet measurement and the variations δR will tend to cancel. Thus measurements on

doublets somewhat wider than 1/300 will not be adversely affected.

During the construction of the ΔV circuit several sources of serious pickup were found and eliminated by one means or another. The most interesting of these was a rather large, short voltage pulse which appeared about every two seconds. In addition to appearing on the ΔV output, it also supplied an extra trigger pulse which, of course, threw the detection circuitry out of phase with ΔV. The trouble was finally traced to the chopper drive. The O-ring belt and camshaft were acting as a miniature Van de Graaff generator. The camshaft was grounded.

The $\Delta V/V$ Potentiometer

A diagram of the $\Delta V/V$ potentiometer appears on the left hand side of Figure 13. The main component is the 7 decade, 100KΩ voltage divider (VDR). This is the best voltage divider currently available and is guaranteed to be accurate to one step in the sixth dial. With calibration the accuracy approaches one step in the seventh dial.

If the potentiometer is to match the precision of the spectrometer, one step in the seventh dial must correspond to 0.39 μV (equation 5-1). Thus a potential of 3.9 volts must be applied to the VDR. Since the potentiometer must measure batteries having a nominal value of 97.2 volts, the VDR must have a resistance of:

$$\sim 100\text{K}\Omega \times \frac{97.2 - \frac{3.9}{2}}{3.9} = 2.44\text{M}\Omega$$

in series with it. The value of this resistance must be accurately known in terms of the resistance of the VDR.

It is difficult to establish the absolute value of a resistance to better than about 1 part in 10^5; however, with a high resolution Wheatstone bridge nominally equal resistances in the range of $10^3\Omega$ to $10^7\Omega$ can be compared to 1 part in 10^7. During such a comparison three or more of the high value dials on the bridge are not altered with the result that shifts in the remaining dials are significant. This well known technique is called the substitution method.

Resistances which are substantially different can be compared with the same precision provided one of the two is very nearly n^2 times as large as the other and can be split into n equal parts which are then connected in parallel ($n = 1, 2, 3, \ldots$). The parallel arrangement is nearly equal to the other resistance and thus the substitution method can be used.

Let R be the mean value of a set of n nominally equal resistors whose actual values are R_i, and $r_i = R_i - R$. The series resistance is:

$$R_S = nR$$

The parallel resistance is:

$$\frac{1}{R_p} = \sum_i \frac{1}{R_i} = \frac{1}{R} \sum_i \frac{1}{1 + r_i/R}$$

$$= \frac{1}{R} \sum_i \left[1 - \frac{r_i}{R} + \left(\frac{r_i}{R}\right)^2 - \ldots\right]$$

$$= \frac{1}{R} \left[n + \sum_i \left(\frac{r_i}{R}\right)^2 - \ldots\right]$$

since $\sum_i r_i = 0$. Hence:

$$\frac{R_s}{R_p} \cong n^2 \left[1 + \frac{1}{n} \sum_i \left(\frac{r_i}{R}\right)^2\right] \qquad (5\text{-}3)$$

The minimum series resistance of 2.44 MΩ is fortuitously close to 5^2 times the resistance of the VDR. Thus the resistance in series with the divider was chosen to be 2.5 MΩ and, as indicated in Figure 13, switch F provides either a series or parallel configuration of the five 0.5 MΩ resistors. One of these five is composed of five 0.1 MΩ resistors. This feature allows both for the measurement of wide doublets (described below) and for an alternate method of calibration (described in the next section). The five 0.5 MΩ resistors deviate on the average about 7 parts in 10^6 from their mean value. Equation (5-3) gives:

$$\frac{R_s}{R_p} = 25 \left[1 + 0.6 \times 10^{-10}\right] \cong 25 \qquad (5\text{-}4)$$

According to Union Carbide, mercury batteries decrease in emf at a rate of approximately 6 parts in 10^7 per hour at 25°C. As it would not be convenient to measure V more often than about once per hour, this drift sets a rough upper limit on the width of doublets that can be measured. If the drift is to be equal to or less than the matching precision, equation (4-6) gives $m/\Delta m \gtrsim 1500$. However, as indicated in Figure 13, the 100 volt power supply is referred to a 97.2 volt mercury battery. This battery is identical to the V batteries and all eleven batteries are located side by side in the temperature

controlled box (Figure 12). Hence to a first approximation the potentiometer and the V batteries drift together. The improvement should be considerable since each battery is composed of 72 cells and variations in the ageing rates will tend to average out. In practice the value of V as measured by the potentiometer is typically steady to within 1 part in 10^6 over several weeks, an improvement of two to three orders of magnitude over the absolute ageing rate. A second major advantage of this arrangement is that the effects of any temperature fluctuations will also tend to cancel.

A diagram of the 100 volt potentiometer supply appears in Figure 16. The portion of the circuit to the left of the dashed line is located outside of the temperature controlled box in order to minimize pickup. Regulation with respect to the 97.2 volt mercury battery is provided by the operational amplifier and series transistor. The amplifier samples the voltage difference between the reference battery and the center of the 2KΩ, 100KΩ divider chain. The trim potentiometer is adjusted for a difference signal $\lesssim 1\ \mu V$. The output voltage typically follows the reference battery to a few parts in 10^8 over several days.

As mentioned above, the V batteries are measured across the 2.5 MΩ chain plus a certain fraction of the VDR. In Figure 13 switches A, B, C, D, F, and H are set to measure battery number 6. For $m/\Delta m = V/\Delta V \geq 972/3.9 = 250$, ΔV is measured across part of the VDR (Switch C is moved two positions to the left). For $250 \geq m/\Delta m \geq 125$, ΔV is measured

FIGURE 16

The 100 V Potentiometer Supply

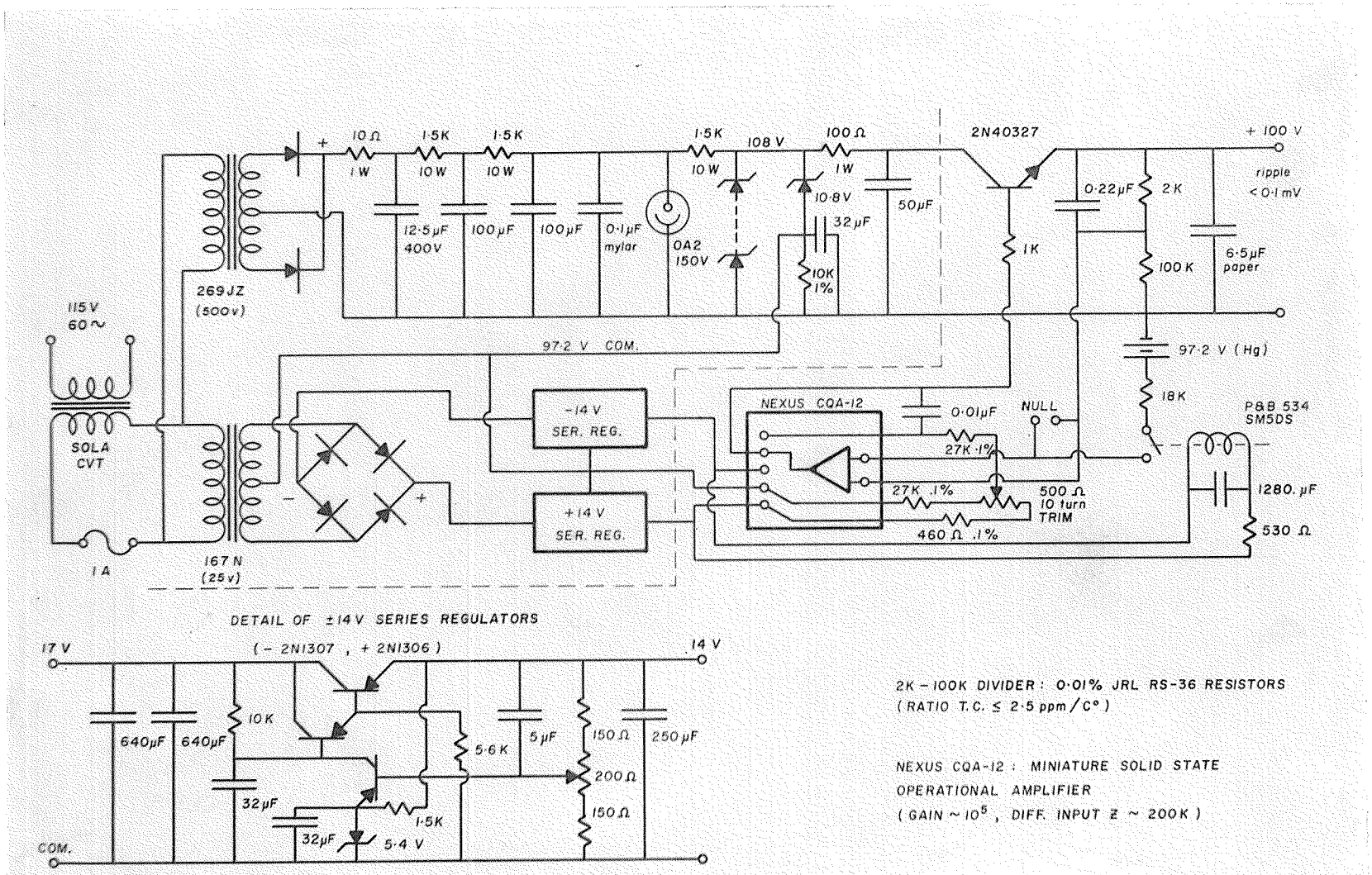

DETAIL OF ±14 V SERIES REGULATORS

2K – 100K DIVIDER : 0·01% JRL RS-36 RESISTORS
(RATIO T.C. ≤ 2·5 ppm / C°)

NEXUS CQA-12 : MINIATURE SOLID STATE
OPERATIONAL AMPLIFIER
(GAIN ~ 10^5 , DIFF. INPUT Z ~ 200K)

across R_1 plus part of the VDR. For $125 \geq m/\Delta m \geq 83$, R_2 is included.

The VDR circuit is shown in Figure 17. (The equivalent circuit is shown in Figure 13). The input resistance R_n of the VDR varies significantly with the position n of its first dial. It is experimentally convenient to measure the difference $\Delta R = R_n - R_5$. The ratio $\Delta R/R_5$ is plotted in Figure 18. The input resistance can be written as:

$$R_n = R_5 (1 + d_{n5}) \tag{5-5}$$

In like manner the resistance of the parallel configuration of the 2.5 MΩ resistor chain may be written as:

$$R_p = R_5 (1 + c) \tag{5-6}$$

and by equation (5-4):

$$R_s = 25 \; R_5 (1 + c) \tag{5-7}$$

Similarly:

$$\begin{aligned} R_1 &= R_5 (1 + c_1) \\ R_2 &= R_5 (1 + c_2) \end{aligned} \tag{5-8}$$

The power supply which drives the potentiometer is a constant voltage source V_s. The current through the potentiometer is:

$$\begin{aligned} i_n &= \frac{V_s}{R_s + R_n} \\ &= \frac{V_s}{R_5[25(1+c) + 1 + d_{n5}]} \end{aligned} \tag{5-9}$$

According to Figure 17, the largest value of $|d_{n5}|$ is $\sim 7 \times 10^{-7}$ (The circuit is usually operated near 25°C.).

FIGURE 17

The Voltage Divider (VDR) Circuit

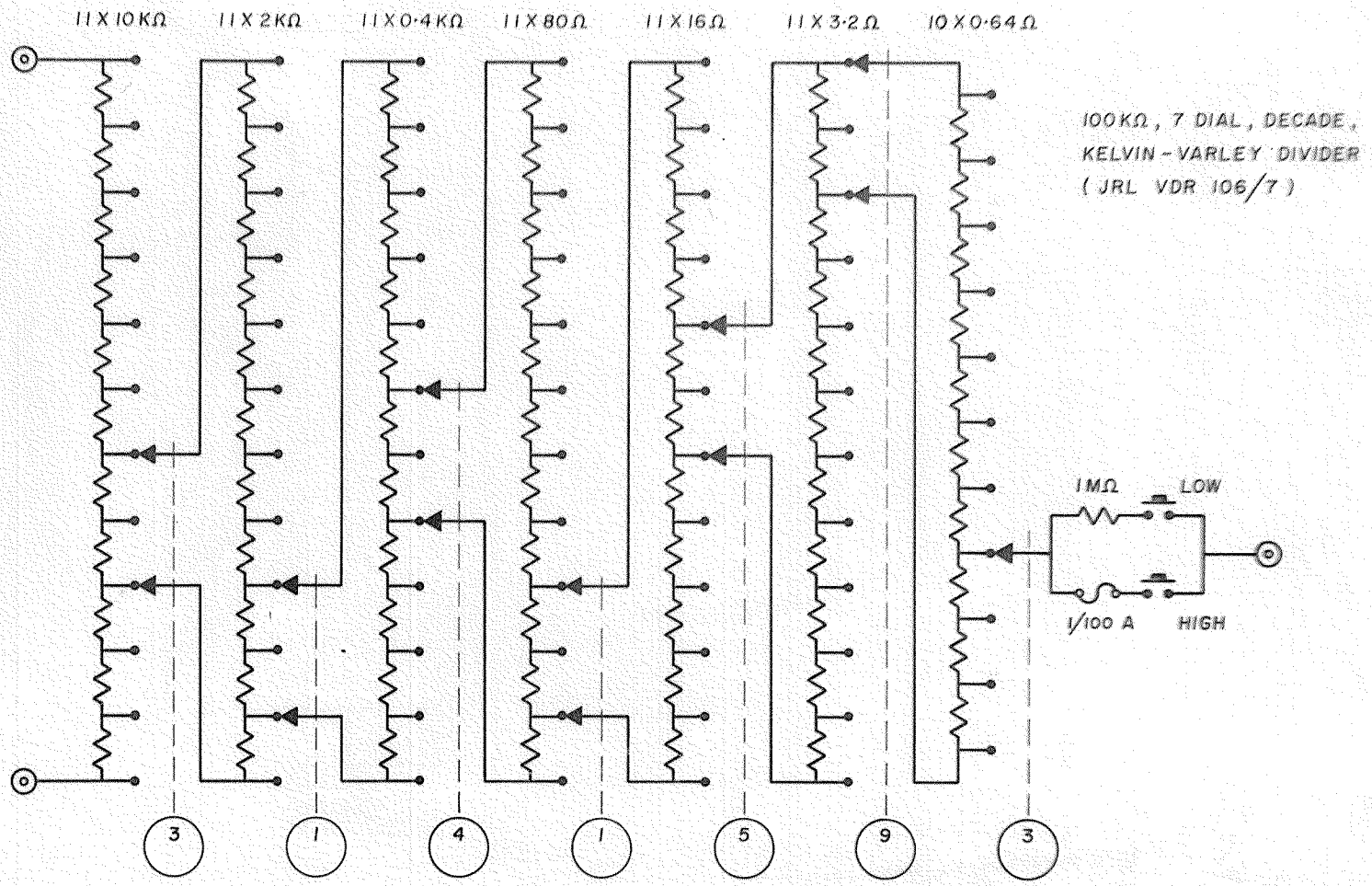

100 KΩ, 7 DIAL, DECADE,
KELVIN-VARLEY DIVIDER
(JRL VDR 106/7)

FIGURE 18

Variation of the VDR Input Resistance
with the Position of the First Dial

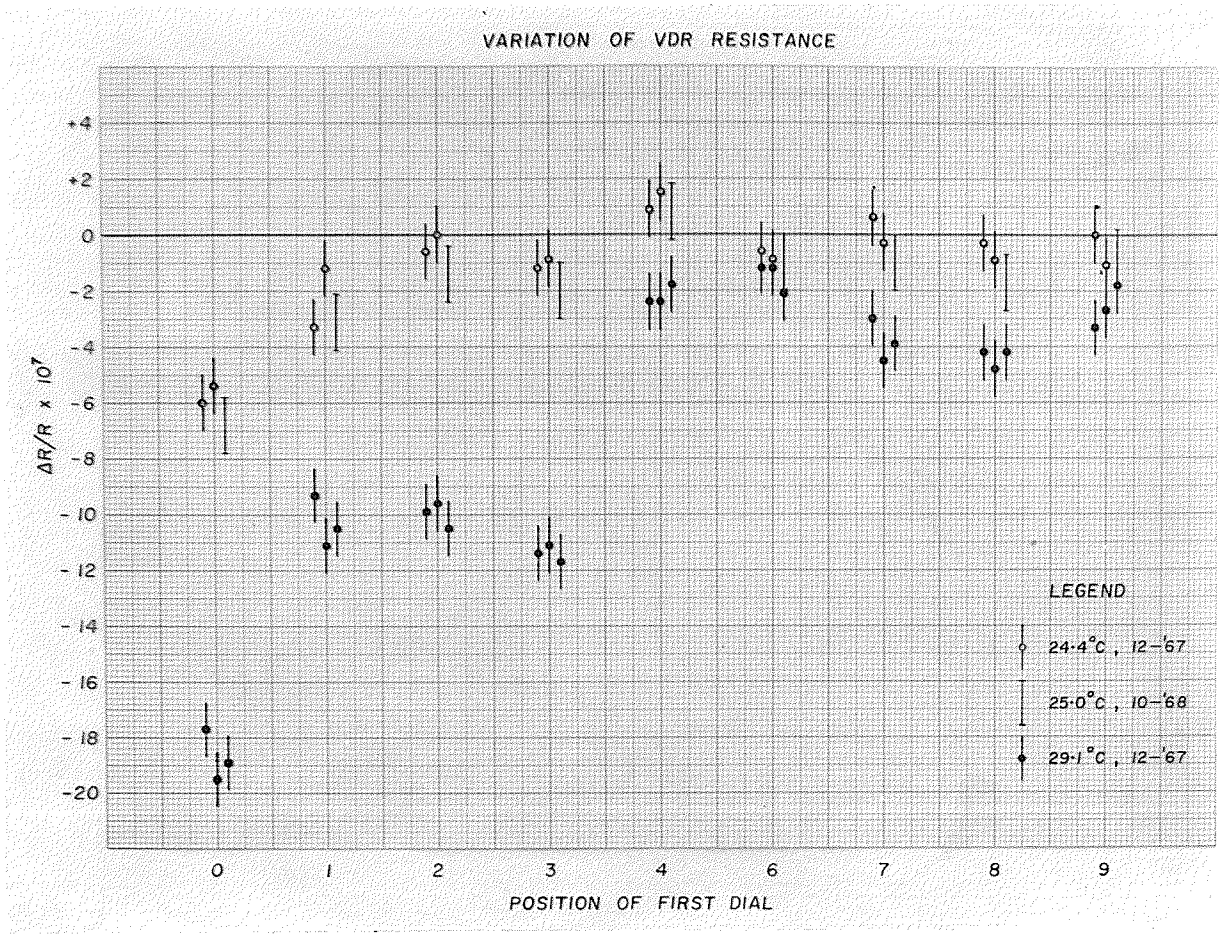
VARIATION OF VDR RESISTANCE
+4
+2
0
-2
-4
-6
-8
-10
-12
-14
-16
-18
-20
ΔR/R x 10⁴
0
1
2
3
4
6
7
8
9
POSITION OF FIRST DIAL
LEGEND
24·4°C, 12–'67
25·0°C, 10–'68
29·1°C, 12–'67

However, since the VDR composes only $1/25^{th}$ of the load, the effect on i_n is only about 3 parts in 10^8 as indicated in the above equation. Variations of this magnitude and smaller are negligible since the calibrations of the VDR and of the 2.5 MΩ chain are, at best, good to only 1 part in 10^7. Hence the current does not significantly depend on the position of the first dial of the VDR ($i_n = i$).

Let $r_{\Delta V}$ be the indicated VDR ratio for a particular setting of ΔV. For a "run" the mean of these settings corrected for the calibration of the VDR may be written as $\overline{r}'_{\Delta V}$. Similarly the VDR settings for each of the ten V batteries may be written r_j ($j = 1, 2, .., 10$). As is shown below, the calibration of the VDR does not affect the r_j.

The value of ΔV for a run on a doublet with $m/\Delta m \geq 250$ is:

$$\overline{\Delta V} = i\, \overline{r}'_{\Delta V}\ R_5\ (1 + d_{n5}) \qquad (5\text{-}10)$$

The voltage of the j^{th} battery of the V circuit is:

$$(V/10)_j = i[25\ R_5(1+c) + r_j\ R_5(1 + d_{n_j 5})] \qquad (5\text{-}11)$$

As in the case of equation (5-9), the correction $d_{n_j 5}$ is negligible with respect to the uncertainty of 1 part in 10^7 in $25(1+c)$. Hence:

$$\frac{\overline{\Delta V}}{V} = \frac{\overline{r}'_{\Delta V}\ (1 + d_{n5})}{250(1+c) + \sum_{j=1}^{10} r_j} \qquad (5\text{-}12)$$

For $m/\Delta m = V/\Delta V \geq 972/0.39 = 2500$, the first dial of the VDR is set at zero when measuring ΔV and $d_{n5} = d_{05} = -7 \times 10^{-7}$ (at 25°C). If this correction is to be a factor of

3 or more smaller than the matching precision, then by equation (4-6):

$$7 \times 10^{-7} \leq \frac{1}{3} \times \frac{0.4}{10^9} \frac{m}{\Delta m}$$

Thus for $m/\Delta m \gtrsim 5000$, d_{n5} in equation (5-12) can be neglected.

It is easy to show that for $250 \geq m/\Delta m \geq 125$, when R_1 must be included to measure ΔV, $(1+c_1)$ is added to the numerator of equation (5-12). Similarly for $125 \geq m/\Delta m \geq 83$, $(2+c_1+c_2)$ must be added.

According to equation (5-1) and the potentiometer design, the $r_{\Delta V}$ settings must be made to one step in the seventh dial of the VDR. The precision of the r_j settings must be such that the relative precision of the $(V/10)_j$ values equals or exceeds the matching precision (equation 4-6). For example, if $m/\Delta m = 10{,}000$, the $(V/10)_j$ values must be known to $\lesssim \pm 0.4$ mV which corresponds to one step in the fourth dial of the VDR for the r_j settings. For $m/\Delta m = 250$, the precision required on the r_j is 2.5 steps in the sixth dial. For wider doublets the uncertainty on c ($\pm 1 \times 10^{-7}$ at best) becomes the limiting factor and additional precision on the r_j is unnecessary. This supports the comment made earlier that the calibration of the VDR, which involves corrections to the seventh dial, does not affect the r_j.

Similar arguments indicate that the absolute uncertainties on c and d_{n5} must be appreciably less than the matching precision multiplied by unity. The absolute uncertainties on c_1 and c_2 should be $\lesssim 1 \times 10^{-7}$.

Calibration of the $\Delta V/V$ Potentiometer

In this section and the next a description is given of the calibration and design of the potentiometer circuit. This is done in considerable detail for two reasons. Firstly, the performance of the potentiometer critically depends on many details of the circuit design and on the use of correct methods of calibration. Secondly, a detailed account will be of valuable assistance to those who will be using the potentiometer.

The calibration of the potentiometer is carried out in two stages. (a) The first stage is the comparison of the 2.5 MΩ resistance chain against the input resistance of the VDR. This can be carried out by two independent methods. Associated with this calibration is the determination of the small variation of the input resistance of the VDR with the positions of its first dial. (b) The second stage is the determination of the VDR ratio settings to a precision of one or two steps in its seventh dial. The DMR resistor chain, which can be measured by two independent methods, provides several ratios accurate to better than $\pm 1 \times 10^{-7}$. These ratios are examined with the VDR to obtain corrections to the nominal VDR settings. Four different circuit arrangements are available for this VDR-DMR comparison.

(i) The 2.5 MΩ Resistor Chain

A six decade Wheatstone bridge (Tinsley, Type 4970) is employed for this calibration. The balance condition is detected with the nullmeter mentioned in Figure 13. With

this meter battery operated at a sensitivity of $\pm 10\ \mu V$ f.s. and about 10 volts excitation on the bridge, one can interpolate to obtain a precision approaching 5 parts in 10^8 (± 5 mΩ) for a 100KΩ resistor or 2 parts in 10^7 ($\pm 0.1\Omega$) for a 500KΩ resistor.

The resistors are measured through the inputs labelled "CHAIN R's" and are selected by the switches E and G (Figure 13). Since the substitution method is used, the resistances of the connectors between the bridge and these two switches have no effect provided they do not vary during a set of measurements. In addition the temperatures of the bridge and of all terminals must be steady. Thermal potentials in the bridge circuit can be avoided by introducing the nullmeter before the battery. The reading of the meter is taken as the zero position.

The resistance of the 2.5MΩ resistor chain can be determined with respect to the VDR by two methods. The first method makes use of switch F to place the 2.5MΩ chain in the parallel configuration. Several measurements of the resistance of the VDR (with the first dial at 5) and of R_p are then taken, alternating from one to the other in order to allow for drift. By averaging the first and third of any set of three successive measurements and comparing this with the second, several values of c are obtained (equation 5-6). The spread among these values together with the uncertainty in the original measurements gives an estimate of the uncertainty of the average value of c (usually $\pm 1 \times 10^{-7}$).

In the second method, the five 100KΩ resistors (R_1 to R_5) are each compared with the VDR. After a set of six measurements is taken, the first two or three are repeated so that any drift can be allowed for. The value of each resistor is expressed in the form $R_5 (1 + c_i)$. The sum of the five resistors is then measured and the value obtained is set equal to the sum of the individual values. The four resistors R_6 to R_9 are measured at the same time and again a couple of measurements are repeated to check for drift. The five values are expressed in the form $5R_5 (1 + c_i)$ and the sum $(25R_5(1 + c'))$ is evaluated. The possible errors on the original measurements are carried along in the usual fashion (square root of the sum of the squares) to find the uncertainty on c' (usually $\pm 3 \times 10^{-7}$). Good agreement has been found between the two methods of calibration $(|c - c'| \leq 3 \times 10^{-7})$.

(ii) Variation of the VDR Resistance

The variation of the input resistance of the VDR with the position of its first dial (equation 5-5) is measured with the Wheatstone bridge described above. The sensitivity of the nullmeter is expressed as so many mΩ per μV. With the dials of the bridge set near a balance and its key held closed, the first dial of the VDR is moved through the sequence 5, 0, 5, 1, 5, 2, ..., 9, 5. $\Delta R = R_n - R_5$ is calculated from the nullmeter deflections. With this technique the uncertainty in the ΔR values is ±10 mΩ or 1 part in 10^7 of R_5 (Figure 18).

(iii) Calibration of the VDR

The VDR circuit is shown in Figure 17. The Kelvin Varley design has the advantage that the magnitude of the resistors in successive decades decreases by a factor of only 5. Thus seven decades can be assembled with resistors that differ at most by a factor of $5^6 \sim 1.6 \times 10^4$. The relative precision to which the resistors are matched is ± 2 parts in 10^6 in the first decade and becomes worse by a factor of about 3.6 with each successive decade. Hence the absolute precision is worst in the first decade and improves by a factor of $5/3.6 \sim 1.4$ per decade. The variations in the first dial and, to a lesser extent, the second dial limit the guaranteed accuracy of the VDR to one step in the sixth dial.

Corrections to the indicated VDR ratio for the various positions of the first and second dials can be obtained by balancing the VDR against several resistance ratios which are known to $\lesssim 1 \times 10^{-7}$. The resistance ratios are selected from the series arrangement of twelve 10KΩ resistors in Figure 13 (DMR). These resistors and those in the first three decades of the VDR are enclosed in sealed, oil filled containers.

The DMR resistors can be measured by two methods. The first method involves the Tinsley Wheatstone bridge and the substitution method. The precautions mentioned in (i) apply. In addition, since the DMR resistors are relatively small (10KΩ) these measurements are quite sensitive to bad switch contacts. Although the switches are well designed

(see next section), after several months without use their contacts may show variations in resistance of several milliohms. This trouble can usually be eliminated by rotating the switch wiper several times. If this fails, the contacts must be cleaned.

The resistors are measured through the inputs labelled "DMR R's" and are selected by switches I and J. After a set of twelve measurements is taken the first two or three are repeated in order to allow for drift. A precision of ±2 mΩ can be attained.

In the second method switch H is placed at "CAL 1" and switch G is at its extreme clockwise position. A few volts are applied to the "-4 VOLTS", "0 VOLTS" terminals. Each one of the DMR resistors (R_i) in turn is placed in series with R_{10} and the pair is examined with the VDR. The usual technique of repeating a few values is used to allow for drift. If r is the VDR setting then:

$$r = \frac{R_{10}}{R_{10} + R_i} \qquad (5\text{-}13)$$

and the twelve R_i can be calculated. The VDR can be read to ±0.5 of a step in its seventh dial to give a precision of ±2 mΩ. Once again a substitution method is being used so equation (5-13) does not have to be corrected for the VDR calibration and R_{10} does not have to be accurately known; however, the success of this technique does require either $R_{10} > R_i$ or $R_{10} < R_i$ for all i so that the first and second dials of the VDR do not have to be moved. The variations among the R_i obtained by the two methods show excellent agreement.

The DMR ratios are calculated in a straight forward manner on a desk calculator to eight significant figures. Possible errors are calculated in the usual fashion and range from $\pm 2 \times 10^{-8}$ to $\pm 6 \times 10^{-8}$. The corrections which must be applied to the nominal n/7 ratios are plotted in Figure 19. The small scatter among the values at 21.9°C is due to the fact that the data were taken at 21.8°C, 22.1°C, and 21.6°C.

About 50 of the 100 possible combinations of the first two dials of the VDR can be obtained on the DMR chain by selecting ratios of the form n/N where $n < N = 12$, 11, 10, 9, and 7. The ratio can be set up starting from either end of the chain by means of the "CAL A" and "CAL B" positions of switch G. N and n are selected by switches I and J, respectively. In addition to providing a variation in the wiring arrangement, each n/N with "CAL A" differs slightly from its counterpart in "CAL B" due to variations among the DMR resistors. (With "CAL B" the n/12 ratios are not available due to the lack of an extra position in switch I; however, this is of little consequence).

Another variation is provided by the "CAL 1" and "CAL 2" positions of switch H. This change flips the VDR over so that for each unique ratio n/N presented by the DMR, the ratio 1 - n/N is also available.

In practice the "CAL 1" and "CAL 2" positions are used for all ratios. The "CAL B" option is used only for the n/10 ratios in order to provide sufficient data on either side of the nominal values of these ratios. With N = 12, 11,

FIGURE 19

DMR Ratio Corrections (N=7, CAL A)

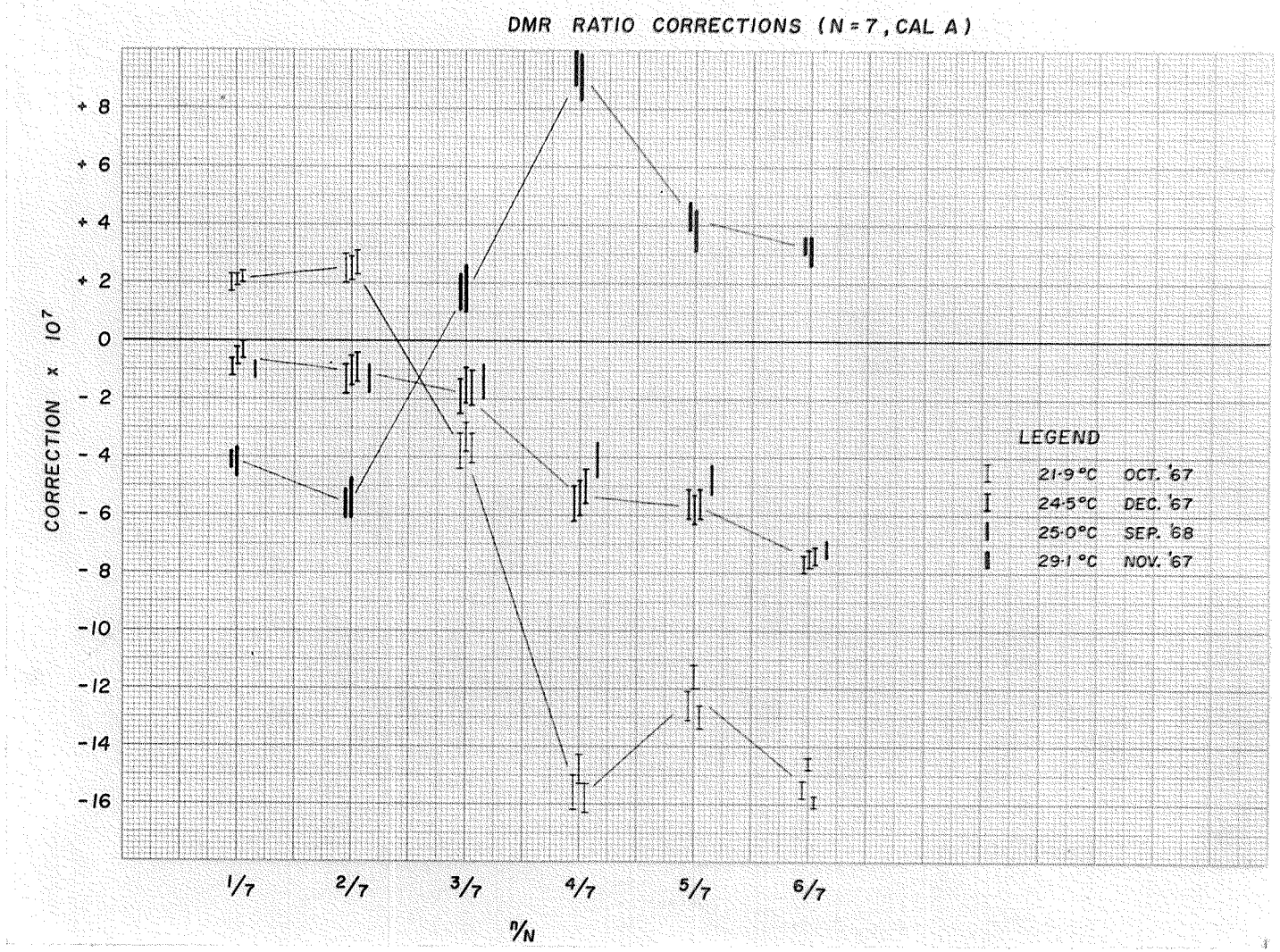
DMR RATIO CORRECTIONS (N = 7, CAL A)
CORRECTION x 10^7
+ 8
+ 6
+ 4
+ 2
0
- 2
- 4
- 6
- 8
-10
-12
-14
-16
1/7
2/7
3/7
4/7
5/7
6/7
n/N
LEGEND
21·9 °C OCT. '67
24·5 °C DEC. '67
25·0 °C SEP. '68
29·1 °C NOV. '67

10, 9, and 7, these variations provide 106 different comparisons.

For the VDR-DMR comparison 5 or 6 volts is applied to the "0 VOLTS", "-4 VOLTS" terminals. A reversing switch is used in the battery circuit in order to double the sensitivity and to eliminate thermal emf's. The VDR settings can be interpolated to ±0.2 of a step in the seventh dial. Here as in most other measurements involved in the calibration of the potentiometer, the operator must bring to bear a fair amount of care and patience. Most measurements are sensitive to any motion within 10 feet or so of the apparatus and are best carried out on weekends. This particularly applies to measurements which must be done in an uninterrupted sequence in order to allow for drift. The VDR-DMR comparison as outlined above requires about twelve hours exclusive of the calibration of the DMR, calculation of ratios, preparation of tables, and analysis of the data.

The average of the required corrections is then computed to 0.1 step in the seventh dial for each of the 50 or so settings of the first and second dials of the VDR. Possible errors are carried along and usually range from about ±0.3 to ±0.8 in the seventh dial.

These data can be reduced to a set of 20 corrections, one for each of the positions of the first dial and the second dial of the VDR. The first step is to calculate the average of all corrections with the first dial at 0. This procedure is repeated for the other nine

positions of this dial. These averages are assigned to the respective first dial positions.

In the second step the first dial corrections are applied to all VDR settings that have the second dial at 0. These predictions are compared with the corrections found experimentally and the average of the differences is assigned as the correction required on the 0 position of the second dial. This procedure is repeated for each of the other nine positions of the second dial.

The third step is to use the preliminary dial corrections found in steps one and two to calculate corrections for the various combinations of the first two dials for which corrections were obtained experimentally. Differences δ between the predicted and experimental values are calculated. $\Sigma\,\delta$ and $\Sigma|\delta|$ are recorded as a measure of how successful the predictions were.

In the fourth step $\Sigma\delta$ is evaluated for each of the positions of the first dial. Adjustments are then made to the first dial corrections so that each of the ten $\Sigma\delta$ together with the total $\Sigma\delta$ tend to zero.

Steps two, three and possibly four are then repeated. At some point in this procedure, any changes in the dial corrections become negligible. Hence a best set of corrections is obtained.

The VDR has been calibrated at four temperatures (Figures 20 and 21). The 1967 values were calculated to one step in the seventh dial, and, as indicated, the lines

FIGURE 20

VDR Ratio Corrections for the Various Positions of the First Dial

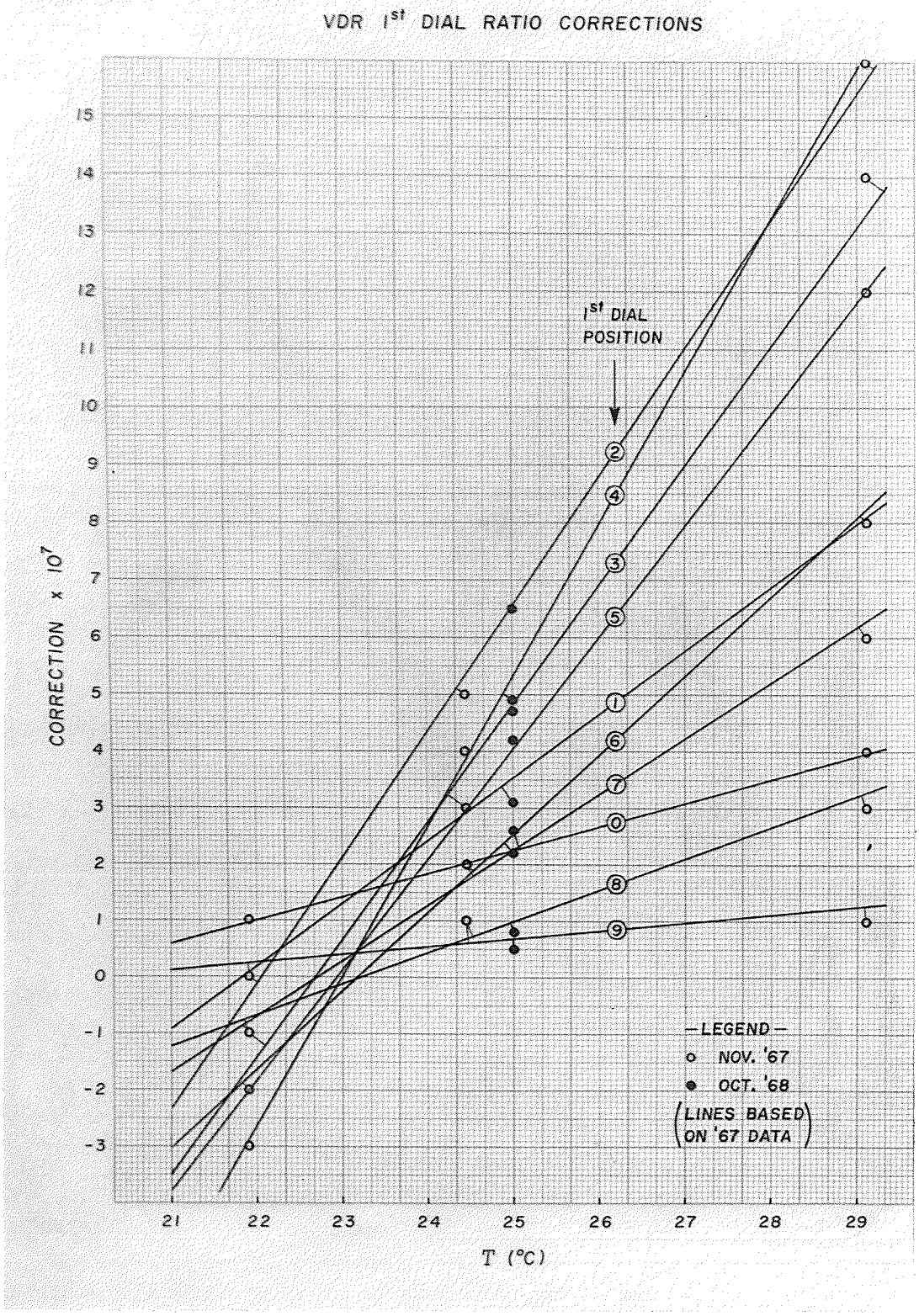
VDR 1st DIAL RATIO CORRECTIONS
CORRECTION x 10^7
T (°C)
1st DIAL POSITION
2
4
3
5
1
6
7
0
8
9
—LEGEND—
NOV. '67
OCT. '68
(LINES BASED ON '67 DATA)
15
14
13
12
11
10
9
8
7
6
5
4
3
2
1
0
-1
-2
-3
21
22
23
24
25
26
27
28
29

FIGURE 21

VDR Ratio Corrections for the Various Positions of the Second Dial

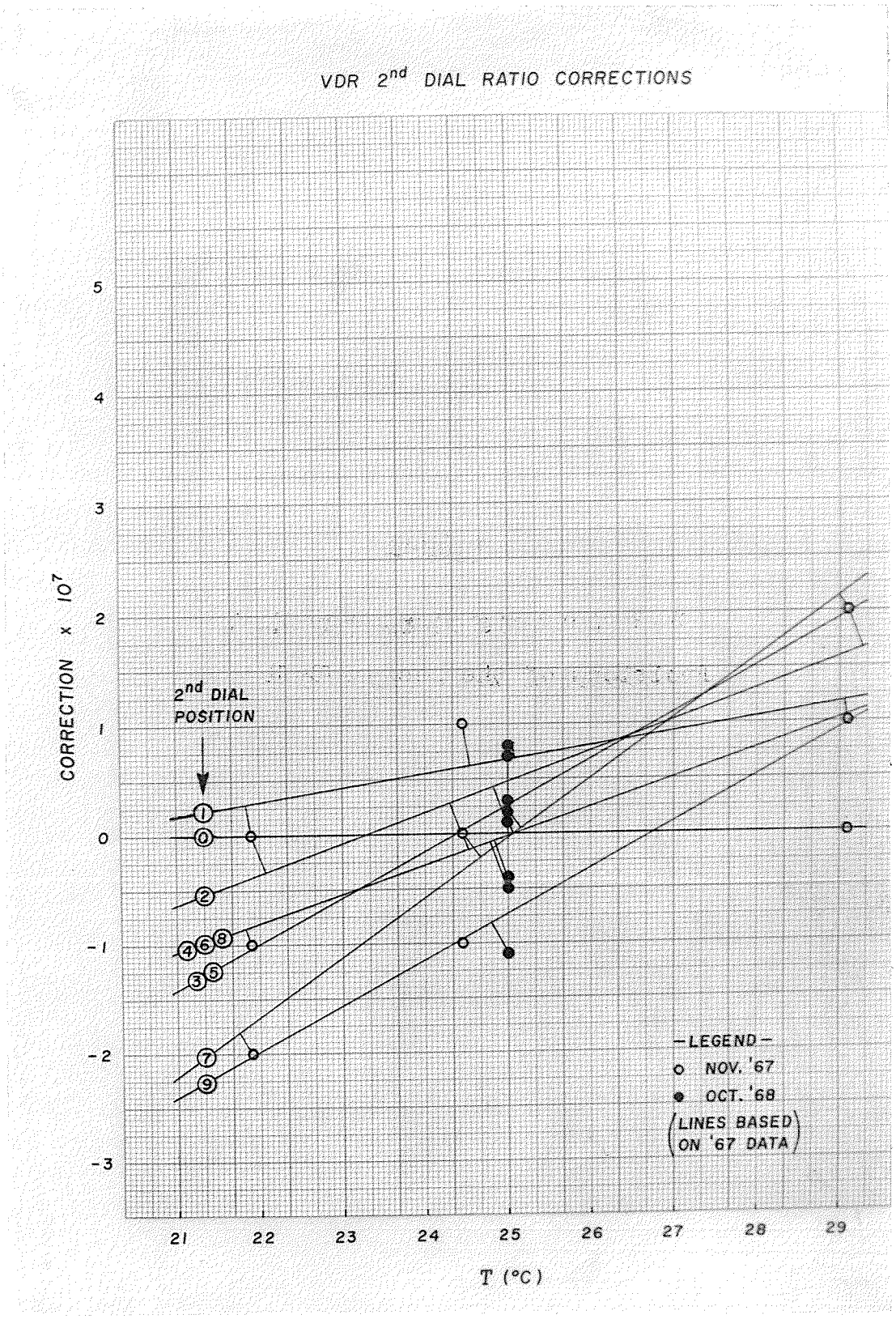
VDR 2nd DIAL RATIO CORRECTIONS
CORRECTION x 10⁷
5
4
3
2
1
0
-1
-2
-3
2nd DIAL POSITION
1
0
2
4
6
8
3
5
7
9
21
22
23
24
25
26
27
28
29
T (°C)
—LEGEND—
NOV. '67
OCT. '68
(LINES BASED ON '67 DATA)

are based on these data. The 1968 values were calculated to the nearest tenth of a step in the seventh dial as described above. For the 1968 data, the average of the absolute values of the differences between the predicted and experimental corrections for the various (49) combinations of the first two dials is 0.23 step in the seventh dial. The differences form a roughly Gaussian distribution between extreme values of ±0.6 step. Considering this result together with the uncertainties on all measurements, corrected ratios should be good to one step in the seventh dial of the VDR.

Three features of Figure 20 are of interest. The first is that the VDR resistors were obviously adjusted for optimum performance near 23°C. Secondly, as one would expect for a Kelvin Varley circuit, the intermediate dial positions have the largest corrections. Last but not least is the excellent agreement between data taken nearly one year apart.

Since the dial positions to which some of the points in Figure 21 belong are not obvious, the October 1968 corrections (25.0°C) are given below.

TABLE 2 — VDR DIAL CORRECTIONS (25.0°C)

Dial Position	0	1	2	3	4	5	6	7	8	9
Dial 1 Correction	2.6	3.1	6.5	4.7	4.9	4.2	2.2	2.2	0.8	0.5
Dial 2 Correction	0.7	0.8	0.1	0.3	-0.4	0.3	0.1	0.2	-0.5	-1.1

Circuit Design

(i) Switches

Switches A through J (Figure 13) are type 9610 "Dual Contact" switches produced by Guildline Instruments Ltd. The wiper of each switch is in the form of a narrow "X" with either side composed of eight individually sprung leaves. The force within these leaves holds one end of wiper against dual contacts at the center pole and the other end against similar contacts at the various switch positions. This design ensures a highly reproducible contact resistance. The ends of the leaves make a small angle with respect to the direction of wipe to provide a self cleaning feature. All switch conductors are copper and are of substantial design. Thermal emf's generated in the switch are $\lesssim 0.01\ \mu V$ and, with clean contacts, variations in contact resistance are $\lesssim 0.1\ m\Omega$.

The switch contacts are mounted on a sheet (4" × 4" × 1/2") of insulator. A 500 V battery and electrometer was used to examine the quality of the insulator supplied with the switches. The resistance between pairs of contacts was found to vary from about $0.7 \times 10^{12}\Omega$ to $5 \times 10^{12}\Omega$. Since the potentiometer circuit contains resistances of the order of $10^4\Omega$ to $10^6\Omega$ and as the errors due to circuit design are to be $\lesssim 1$ part in 10^8, insulation resistances of the order of $10^{12}\Omega$ are too low.

All switches with the exception of B and H were rebuilt using "delrin", a waxy opaque white plastic, in

place of the dark brown insulator which was originally supplied. The new insulation resistances are about $4 \times 10^{14}\Omega$. Resistances of the order of $10^{12}\Omega$ are quite adequate for switch B which is attached to the V batteries. Switch H was in an earlier shipment from Guildline and although not mounted on delrin, its insulation is nearly as good.

The resistances of common insulators such as those used on wires and for circuit boards varies from about $10^{9}\Omega$ to $10^{11}\Omega$. Resistances of the order of $10^{12}\Omega$ and higher are quite sensitive to humidity and surface films. In the case of delrin, resistances of the order of $10^{15}\Omega$ can be achieved if the final cleaning of the surfaces is done with distilled water (breathe on the surface) followed by rubbing with a clean cloth. The measurement of such resistances requires some obvious precautions in the arrangement of the battery-electrometer circuit. In addition the indicated resistance often increases with a time constant of several minutes due to dielectric absorption or polarization.

(ii) Wiring

Most of the leads appearing in Figure 13 are gauge #14 annealed bare copper wire which has a resistance of 1 mΩ/12 cm. The leads from the VDR to switch H, and from the center positions of this switch to switches E and G are gauge #6, 7 strand, annealed bare copper wire which has a resistance of 1 mΩ/77 cm. Nearly all leads are supported in air by their own rigidity and that of the con-

nections at their ends. The majority of connections are secured with Kester low thermal emf solder (30% Sn, 70% Cd) using #1544 resin flux. All measurements of resistance in the milliohm range were made using a four terminal ammeter-voltmeter technique. The nullmeter mentioned earlier was used to measure the voltage drops.

A view of a portion of the circuit of Figure 13 appears in Figure 22. The 100 V supply is at the lower left, the DMR box is in the center rear, and the 25R chain appears at the top and slightly right of center.

The resistances of several leads in Figure 13 are not critical. These include the leads from the 100 V supply, the leads in the V circuit including those attached to switches A, B and C, and a few others.

The leads attached to the DMR are adjusted in length so that they contribute negligible error when the DMR resistors are measured. When switches I and J are set to examine the various DMR resistors, the lead resistances between the poles of I and J are equal to within ± 0.15 mΩ. The resistance between the oil immersed resistors is $\gtrsim 5 \times 10^{12} \Omega$ which is adequate.

When the DMR resistors are measured by using the VDR to compare them with R_{10}, the resistance of the leads in the R_{10} branch acts simply as part of R_{10}. Similarly, the leads in the branch containing a DMR resistor can be considered as part of this resistor. Since only relative values are important, these leads have no effect on the results provided they are nearly the same from resistor

FIGURE 22

Part of the $\Delta V/V$ Potentiometer Circuit

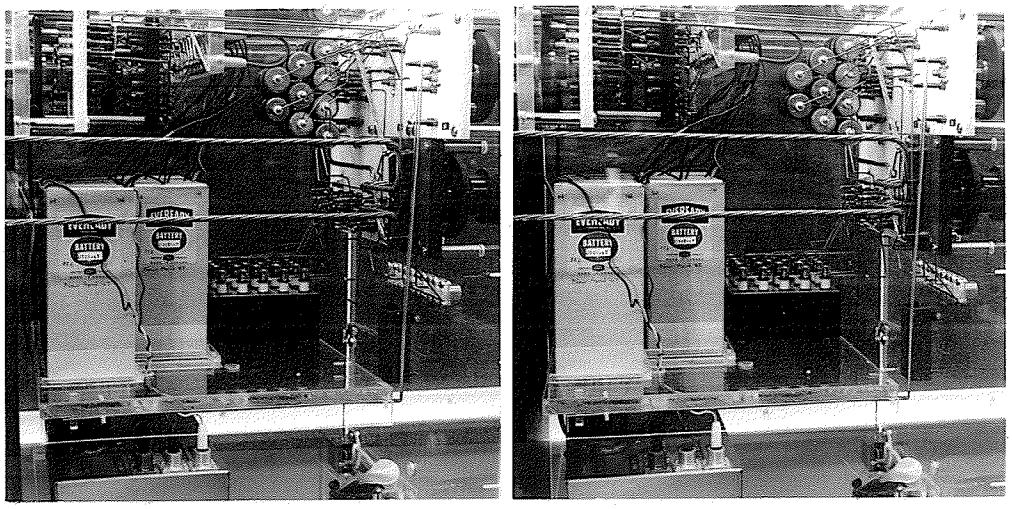

to resistor (± 0.15 mΩ as above). The few milliohms between the VDR terminals and the junctions where the exciting voltage is applied effectively compress the VDR steps by a few parts in 10^8; however, since R_{10} and the DMR resistors are nearly equal, the effect on the VDR settings is several orders of magnitude smaller again and thus is completely insignificant.

The comparison of the VDR against the DMR ratios is also unaffected by lead resistances. The resistances of each of the four leads from the "0 VOLTS" and the "- 4 VOLTS" junctions to the DMR and VDR terminals equals 3.5 ± 0.3 mΩ. The two 3.5 mΩ leads in the VDR branch apparently introduce an error approaching 0.3 step in the seventh dial at either end of the VDR; however, since the load presented by the DMR with N = 12, 11, 10, 9 or 7 is equal to that presented by the VDR to within about $\pm 30\%$, the currents in the two branches are equal to the same sort of precision and the voltage drops over the four leads are roughly the same. Hence lead induced errors in the VDR settings are $\lesssim 0.1$ step in the seventh dial.

The resistors in the 25R chain are individually enclosed in oil filled metal cylinders and have a resistor to case resistance of the order of $10^{12}\Omega$ to $10^{13}\Omega$. For this reason these resistors are suspended in air by their leads (Figure 22). The lead resistances from the "CHAIN R's" inputs to the resistors R_1 to R_9 and the VDR vary $\lesssim 1$ mΩ and hence contribute errors $\lesssim 1$ part in 10^8. In several

cases some of the leads near switch F act simply as part of the resistor chain. The resistance of the leads from the bottom of the VDR to the top of the 25R chain is ~ 1.5 m which introduces an error ~ 1 part in 10^8.

Precision Achieved

The limit of about 1 part in 10^7 on the precision of all electrical measurements connected with the determination of $\Delta V/V$ is due mainly to random fluctuations of about 0.05 μV in the nullmeter. This size of fluctuation is what is expected for the Johnson noise in the frequency range of 1 or 2 c/s for a resistor of the order of $10^5\Omega$ at room temperature. Thus the precision achieved cannot be greatly improved by minor changes such as a more sensitive nullmeter, better switches, et cetera.

Another factor which indirectly limits the overall precision to the order of 1 part in 10^7 was mentioned in the previous section. The resistors in the potentiometer circuit range from about $10^4\Omega$ to $10^6\Omega$. Hence if insulation resistances, and variations in both lead and contact resistances are to introduce errors of 1 part in 10^8 or less, they must be $\gtrsim 10^{6+8} = 10^{14}\Omega$ and $\lesssim 10^{4-8} = 10^{-4}\Omega$ respectively. Both of these extremes begin to present problems experimentally.

The performance of the potentiometer during calibration indicates that the precision required by equation (5-1) can be achieved for doublets approaching $m/\Delta m \sim 250$. For wider doublets the precision of the

potentiometer remains in the vicinity of 1 or 2 parts in 10^7 and thus falls behind equation (5-1).

Figure 23 shows the precision achieved for the mass measurements reported in the next chapter. The arrow indicates the optimum expected performance (see equation 4-6) which is a factor of 8 better than that achieved to date. Hence the $\Delta V/V$ potentiometer contributes negligible error to these measurements.

The resolution R has been about 1/125,000 and $f \sim 1/2500$ (2× and 4× respectively of the optimum expected values). One reason for this is that most of the measurements were obtained before the spectrometer was vibration mounted. In addition, during some of the early work the field of the magnetic analyser was not steady. The recent elimination of both of these problems combined, in the near future, with a computer assisted determination of the matched condition will, no doubt, result in significant improvements in both f and the effective resolution.

The first two measurements made with the new spectrometer appear in Table 3. As indicated, the second of these was obtained using the circuit described in this chapter. The excellent agreement with the other values presented indicates that the apparatus is free of serious systematic errors.

FIGURE 23

The Precision Achieved by the Spectrometer

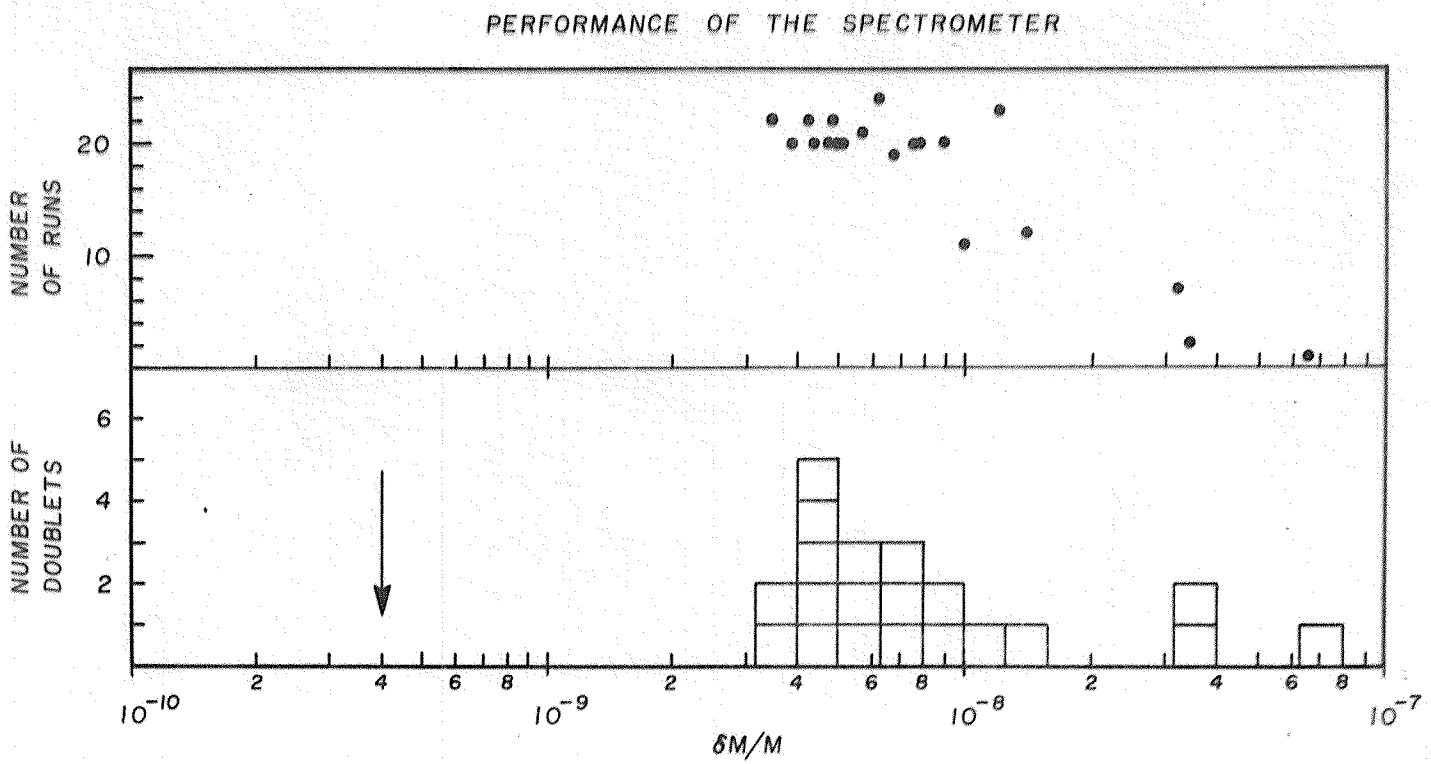
PERFORMANCE OF THE SPECTROMETER
NUMBER OF RUNS
20
10
NUMBER OF DOUBLETS
6
4
2
2
4
6
8
10^{-10}
10^{-9}
10^{-8}
10^{-7}
$\delta M/M$

TABLE 3

$^{114}Cd^{35}Cl_2$-$^{112}Cd^{35}Cl^{37}Cl$ MEASUREMENTS

Source	M (μu)
McMaster Visual (1963) (With CdCl)	3 547. $^{2.*}$
Minnesota (Damerow et al., 1963)	3 554. $^{4.}$
Aldermaston (t,p)(McLatchie, 1966)	3 548. $^{10.}$
McMaster Visual (Modified sweep & ΔV, 1965)	3 546. $^{3.}$
McMaster Signal Averager (1966)	3 547. $^{3.}$
McMaster Signal Averager & Nier ΔV/V Circuit (1966)	3 548. $^{2.}$
Manitoba Signal Averager & Potentiometer-Voltmeter (1967)	3 547.0 $^{2.3}$
Manitoba Signal Averager & New ΔV/V Circuit (1968)	3 548.2 $^{2.1}$

*The experimental uncertainties are shown as superscripts following the convention used in the Nuclear Data Sheets.

CHAPTER 6

ATOMIC MASS MEASUREMENTS

Introduction

The mass determinations reported in this Chapter involved the elements from neodymium to dysprosium (Z = 60 - 66). This region is of particular interest as it spans the transition from spherical nuclei at N = 82 to highly deformed nuclei beyond N = 92. Evidence for this transition appears in isotope shift data, in electric quadrupole moment data, in alpha decay systematics, in the beginning of well developed rotational spectra, et cetera. Mass spectroscopic evidence for the onset of nuclear deformation in the vicinity of N = 90 is also well established (Hogg and Duckworth, 1954; Johnson and Nier, 1957; Barber et al., 1964; Benson and Johnson, 1966; Demirkhanov et al., 1967).

The measurements presented here provide additional information concerning this effect and, together with mass spectroscopic results obtained three years ago at McMaster University, provide for the first time connections accurate to a few keV between all of the stable isotopes in this region. In addition the new data permit the calculation of some decay energies with improved precision and provide checks on the accuracy of several precise reaction Q values.

Most of the mass doublets measured in this work were of the form $^{A}X^{35}Cl - {}^{A-2}X^{37}Cl$. The mass defects of adjacent isotopes among the rare earths are roughly the same whereas the defects of the two stable chlorine isotopes differ by about 3 mu. Hence doublets of this type have

$m/\Delta m \sim 50{,}000$ which is made to order for the spectrometer described in Chapter 4. In addition the precision required of the $\Delta V/V$ potentiometer is only a few parts in 10^5 for such close doublets (see equation 4-6).

New Mass Differences

The twenty doublets measured in this work are presented in Table 4. The first column contains a convenient labeling system which is used below. Most values represent the mean of about 20 runs; however, doublets T, D, H, P and O involved 1, 2, 7, 11, and 12 runs respectively. The estimates of the standard deviations assigned to T and D are believed to be conservative. For the other doublets the error stated is the standard deviation of the mean. As pointed out in Chapter 5 the $\Delta V/V$ potentiometer contributes negligible error to these measurements.

Comparison of Results

The last column of Table 4 provides a comparison with work done at McMaster University. The agreement with the 1966 McMaster work is fairly good except for A. It is known that certain of the 1964 McMaster measurements were subject to a systematic error.

In Table 5 the new mass differences are compared with other mass spectrometric data. The isotopic mass differences in column two were obtained by using the value

$$^{37}Cl - {}^{35}Cl = 1\ 997\ 049.3^{0.4}\ \mu u$$

which is the average of results obtained by Benson and Johnson (1964) and Dewdney and Bainbridge (1965).

TABLE 4

NEW ATOMIC MASS DIFFERENCES (μu)
(Z = 60 - 66)

Code	Doublet	ΔM (new)	McMaster-New
A	$^{146}Nd^{35}Cl_2$-$^{144}Nd^{35}Cl^{37}Cl$	5 981.3$^{0.9}$	- 15.$^{5.}$ M6
B	$^{150}Nd^{35}Cl_2$-$^{146}Nd^{37}Cl^{37}Cl$	13 669.1$^{1.1}$	- 15.$^{10.}$ M6
C	^{144}Sm -^{144}Nd	1 911.4$^{1.1}$	40.$^{4.}$ M4
D	^{148}Nd -^{148}Sm	2 075.$^{5.}$	
E	^{150}Nd -^{150}Sm	3 616.8$^{1.0}$	15.$^{6.}$ M4
F	$^{148}Sm^{35}Cl_2$-$^{144}Sm^{37}Cl^{37}Cl$	8 719.2$^{2.6}$	- 9.$^{13.}$ B4
G	$^{152}Sm^{35}Cl_2$-$^{148}Sm^{37}Cl^{37}Cl$	10 808.1$^{1.7}$	- 6.$^{12.}$ M6
H	$^{151}Eu^{35}Cl_2$-$^{149}Sm^{35}Cl^{37}Cl$	5 612.$^{7.}$	
I	$^{154}Gd^{35}Cl_2$-$^{152}Gd^{35}Cl^{37}Cl$	4 018.5$^{2.0}$	- 2.$^{32.}$ B4
J	$^{156}Gd^{35}Cl_2$-$^{154}Gd^{35}Cl^{37}Cl$	4 203.7$^{1.4}$	2.$^{11.}$ M6
K	$^{158}Gd^{35}Cl_2$-$^{156}Gd^{35}Cl^{37}Cl$	4 925.0$^{1.3}$	4.$^{4.}$ M6
L	$^{159}Tb^{35}Cl_2$-$^{157}Gd^{35}Cl^{37}Cl$	4 332.2$^{1.1}$	
M	^{160}Gd -^{160}Dy	1 854.0$^{0.8}$	
N	$^{161}Dy^{35}Cl_2$-$^{159}Tb^{35}Cl^{37}Cl$	4 533.9$^{0.9}$	
O	$^{158}Dy^{35}Cl_2$-$^{156}Dy^{35}Cl^{37}Cl$	3 080.6$^{3.3}$	
P	$^{160}Dy^{35}Cl_2$-$^{158}Dy^{35}Cl^{37}Cl$	3 730.9$^{2.3}$	
Q	$^{162}Dy^{35}Cl_2$-$^{160}Dy^{35}Cl^{37}Cl$	4 551.0$^{1.0}$	4.$^{7.}$ B4
R	$^{163}Dy^{35}Cl_2$-$^{161}Dy^{35}Cl^{37}Cl$	4 743.5$^{1.1}$	2.$^{4.}$ W6
S	$^{164}Dy^{35}Cl_2$-$^{162}Dy^{35}Cl^{37}Cl$	5 325.2$^{0.8}$	- 4.$^{4.}$ W6
T	^{154}Sm -^{154}Gd	1 339.$^{10.}$	

B4 Barber et al. (1964)
M4 McLatchie et al. (1964b)
M6 Macdougall et al. (1966)
W6 Whineray (1966)

TABLE 5

COMPARISON WITH OTHER MASS SPECTROMETRIC DATA
(comparison with McMaster data is shown in Table 4)

Mass Difference	New (μu)	Others	Others - New
$^{146}Nd-^{144}Nd$	2 003 030.6$^{1.0}$	2 003 026.$^{3.}$	B6 - 4.6$^{4.0}$
		2 003 080.$^{20.}$	D7 49.$^{21.}$
$^{150}Nd-^{146}Nd$	4 007 767.7$^{1.4}$	4 007 761.$^{4.}$	B6 - 6.7$^{5.4}$
		4 007 740.$^{40.}$	D7 - 28.$^{41.}$
$^{144}Sm-^{144}Nd$	1 911.4$^{1.1}$	1 890.$^{80.}$	D7 - 21.$^{81.}$
$^{148}Nd-^{148}Sm$	2 075.$^{5.}$	2 120.$^{60.}$	D7 45.$^{65.}$
$^{150}Nd-^{150}Sm$	3 616.8$^{1.0}$	3 590.$^{90.}$	D7 - 27.$^{91.}$
$^{148}Sm-^{144}Sm$	4 002 817.8$^{2.7}$	4 002 940.$^{70.}$	D7 122.$^{73.}$
$^{152}Sm-^{148}Sm$	4 004 906.7$^{1.9}$	4 004 930.$^{50.}$	D7 23.$^{52.}$
$^{151}Eu-^{149}Sm$	2 002 661.$^{7.}$	2 002 630.$^{30.}$	D7 - 31.$^{37.}$
$^{154}Sm-^{154}Gd$	1 339.$^{10.}$	1 300.$^{50.}$	D7 - 39.$^{60.}$
$^{154}Gd-^{152}Gd$	2 001 067.8$^{2.0}$	2 001 104.$^{80.}$	B0 36.$^{82.}$
		2 001 410.$^{40.}$	D3 342.$^{42.}$
$^{156}Gd-^{154}Gd$	2 001 253.0$^{1.5}$	2 001 312.$^{60.}$	B0 59.$^{61.}$
		2 000 910.$^{40.}$	D3 - 343.$^{41.}$
$^{158}Gd-^{156}Gd$	2 001 974.3$^{1.4}$	2 001 994.$^{90.}$	B0 20.$^{91.}$
		2 002 260.$^{30.}$	D3 286.$^{31.}$
$^{160}Gd-^{160}Dy$	1 854.0$^{0.8}$	1 890.$^{90.}$	D3 36.$^{91.}$
$^{159}Tb-^{157}Gd$	2 001 381.5$^{1.2}$	2 001 450.$^{50.}$	D3 68.$^{51.}$
$^{161}Dy-^{159}Tb$	2 001 583.2$^{1.0}$	2 001 400.$^{50.}$	D3 - 183.$^{51.}$
$^{158}Dy-^{156}Dy$	2 000 129.9$^{3.3}$	2 000 201.$^{80.}$	B0 71.$^{83.}$
		2 000 290.$^{160.}$	D3 160.$^{163.}$
$^{160}Dy-^{158}Dy$	2 000 780.2$^{2.3}$	2 000 867.$^{80.}$	B0 87.$^{82.}$
		2 001 250.$^{130.}$	D3 470.$^{132.}$
$^{162}Dy-^{160}Dy$	2 001 600.3$^{1.1}$	2 001 574.$^{60.}$	B0 - 26.$^{61.}$
		2 001 600.$^{80.}$	D3 0.$^{81.}$
$^{163}Dy-^{161}Dy$	2 001 792.8$^{1.2}$	2 001 736.$^{60.}$	B0 - 57.$^{61.}$
		2 002 100.$^{50.}$	D3 307.$^{51.}$
$^{164}Dy-^{162}Dy$	2 002 374.5$^{0.9}$	2 002 327.$^{100.}$	B0 - 47.$^{101.}$
		2 002 510.$^{50.}$	D3 135.$^{51.}$

B0 Bhanot, Johnson and Nier (1960)
D3 Demirkhanov et al. (1963)
B6 Benson and Johnson (1966)
D7 Dermirkhanov et al. (1967)

The last two columns contain other data and a comparison with the new values. Only the two neodymium mass differences by Benson and Johnson are comparable in precision with our work. The agreement with these two values is acceptable. The new data agree well with the 1960 Minnesota work. Several of the 1963 Russian values seem to be badly in error; however there is good agreement with their later work although their uncertainties are relatively large.

Additional Data

The new results can be combined with other data to evaluate several quantities of interest. Figure 24 is a chart representing all of the nuclides in this region together with useful mass spectroscopic, decay and reaction connections. The legend is self - explanatory. The McMaster doublets indicated are listed in Table 6. The reaction data and decay data together with their provenance are listed in Tables 7, 8 and 9. Only those reaction links which enter directly into the calculation of closed loops, decays, and neutron separation energies are noted in Figure 24. Other reaction data are compared with calculated neutron separation energies in Tables 10 and 11.

Several quantities are required in order to carry out the various calculations required below. The adopted values of these quantities are:

FIGURE 24

A vs Z near N = 90

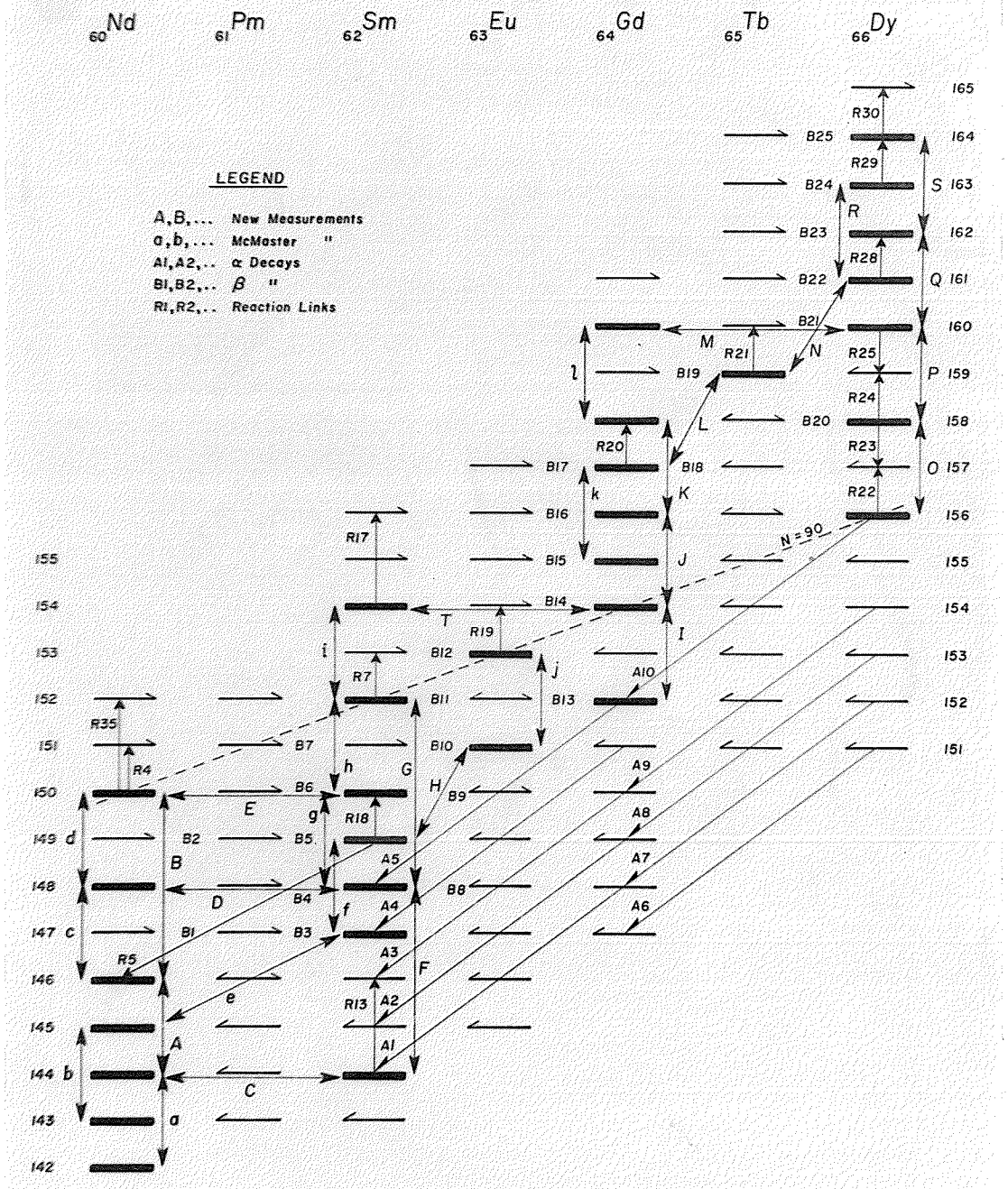
60 Nd
61 Pm
62 Sm
63 Eu
64 Gd
65 Tb
66 Dy
LEGEND
A,B,... New Measurements
a,b,... McMaster "
A1,A2,.. α Decays
B1,B2,.. β "
R1,R2,.. Reaction Links
N = 90
165
164
163
162
161
160
159
158
157
156
155
154
153
152
151
150
149
148
147
146
145
144
143
142
R30
R29
R28
R25
R24
R23
R22
R21
R20
R17
R19
R7
R35
R4
R18
R5
R13
B25
B24
B23
B22
B21
B19
B20
B18
B17
B16
B15
B14
B12
B11
B13
B10
B7
B6
B2
B5
B4
B1
B3
B9
B8
A10
A9
A8
A7
A6
A5
A4
A3
A2
A1
S
R
Q
P
O
M
N
L
K
J
I
T
H
G
F
E
D
C
B
A
l
k
j
i
h
g
f
e
d
c
b
a

TABLE 6

ADDITIONAL McMASTER DOUBLETS (μu)
(Z = 60 - 66) (Macdougall, 1966)

Code	Doublet	ΔM
a	$^{144}Nd^{35}Cl_2$-$^{142}Nd^{35}Cl^{37}Cl$	5 308.$^{3.}$
b	$^{145}Nd^{35}Cl_2$-$^{143}Nd^{35}Cl^{37}Cl$	5 703.$^{4.}$
c	$^{148}Nd^{35}Cl_2$-$^{146}Nd^{35}Cl^{37}Cl$	6 721.$^{4.}$
d	$^{150}Nd^{35}Cl_2$-$^{148}Nd^{35}Cl^{37}Cl$	6 939.$^{4.}$
e	$^{147}Sm^{35}Cl_2$-$^{145}Nd^{35}Cl^{37}Cl$	5 264.$^{4.}$
f	$^{149}Sm^{35}Cl_2$-$^{147}Sm^{35}Cl^{37}Cl$	5 231.$^{3.}$
g	$^{150}Sm^{35}Cl_2$-$^{148}Sm^{35}Cl^{37}Cl$	5 400.$^{4.}$
h	$^{152}Sm^{35}Cl_2$-$^{150}Sm^{35}Cl^{37}Cl$	5 396.$^{4.}$
i	$^{154}Sm^{35}Cl_2$-$^{152}Sm^{35}Cl^{37}Cl$	5 417.$^{4.}$
j	$^{153}Eu^{35}Cl_2$-$^{151}Eu^{35}Cl^{37}Cl$	4 329.$^{4.}$
k	$^{157}Gd^{35}Cl_2$-$^{155}Gd^{35}Cl^{37}Cl$	4 287.$^{3.}$
l	$^{160}Gd^{35}Cl_2$-$^{158}Gd^{35}Cl^{37}Cl$	5 899.$^{3.}$

TABLE 7

REACTION DATA

Code	Reaction	Q(keV)	Reference
R1	$^{142}Nd(d,p)^{143}Nd$	3 902.15.	Wiedner et al. (1967)
R2	$^{144}Nd(d,p)^{145}Nd$	3 521.15.	"
R3	$^{143}Nd(n,\gamma)^{144}Nd$	7 817. 5.	Hughes et al. (1966)
R4	$^{150}Nd(d,p)^{151}Nd$	3 084.15.	Nealy and Sheline (1967)
R5	$^{149}Sm(n,\alpha)^{146}Nd$	9 428. 5.	Beg and Macfarlane (1965)
R6	$^{148}Sm(d,p)^{149}Sm$	3 648.12.	Kenefick and Sheline (1965)
R7	$^{152}Sm(d,p)^{153}Sm$	3 645.12.	"
R8	$^{147}Sm(d,p)^{148}Sm$	5 920.10.	Kenefick and Sheline (1964)
R9	$^{149}Sm(d,p)^{150}Sm$	5 764.4.	"
R10	$^{148}Sm(d,p)^{149}Sm$	3 656.15.	Veje (1967)
R11	$^{148}Sm(d,t)^{147}Sm$	-1 890.15.	"
R12	$^{150}Sm(d,t)^{149}Sm$	-1 738.15.	"
R13	$^{144}Sm(t,p)^{146}Sm$	6 681.25.	Bjerregaard et al. (1966)
R14	$^{148}Sm(t,p)^{150}Sm$	5 372.25.	"
R15	$^{150}Sm(t,p)^{152}Sm$	5 376.25.	"
R16	$^{152}Sm(t,p)^{154}Sm$	5 361.25.	"
R17	$^{154}Sm(t,p)^{156}Sm$	4 556.25.	"
R18	$^{149}Sm(n,\gamma)^{150}Sm$	7 986.8 1.	Rasmussen et al. (1967)
R19	$^{153}Eu(n,\gamma)^{154}Eu$	6 415.9 1.	"
R20	$^{157}Gd(n,\gamma)^{158}Gd$	7 934.0 1.	"
R21	$^{159}Tb(n,\gamma)^{160}Tb$	6 420.6 1.	"
R22	$^{156}Dy(d,p)^{157}Dy$	4 748.10.	Bennett (1967, 1969)
R23	$^{158}Dy(d,t)^{157}Dy$	-2 804.10.	"
R24	$^{158}Dy(d,p)^{159}Dy$	4 608.10.	"
R25	$^{160}Dy(d,t)^{159}Dy$	-2 339.10.	"
R26	$^{160}Dy(d,p)^{161}Dy$	4 231.10.	"
R27	$^{162}Dy(d,t)^{161}Dy$	-1 943.10.	"
R28	$^{161}Dy(n,\gamma)^{162}Dy$	8 192.8 3.	Hafemeister and Shera (1966)
R29	$^{163}Dy(n,\gamma)^{164}Dy$	7 653.9 3.	"
R30	$^{164}Dy(n,\gamma)^{165}Dy$	5 716.3 3.	"
R31	$^{163}Dy(d,p)^{164}Dy$	5 434. 5.	Shelton and Watson (1966)
R32	$^{164}Dy(d,t)^{163}Dy$	-1 394. 5.	Schult et al. (1967)
R33	$^{162}Dy(d,p)^{163}Dy$	4 049. 5.	"
R34	$^{162}Dy(n,\gamma)^{163}Dy$	6 270.2 3.	"
R35	$^{150}Nd(t,p)^{152}Nd$	-4 125.30.	McLatchie (1968)

TABLE 8

ALPHA DECAY DATA

Code	Decay	Q (keV)	Reference
A1	$^{148}Gd(a)^{144}Sm$	3 270.$^{10.}$	NDS (B2-4)
A2	$^{149}Gd(a)^{145}Sm$	3 116.$^{10.}$	Machunka et al. (1966)
A3	$^{150}Gd(a)^{146}Sm$	2 804.$^{10.}$	MT (1964)
A4	$^{151}Gd(a)^{147}Sm$	2 671.$^{30.}$	Siivola and Graeffe (1965)
A5	$^{152}Gd(a)^{148}Sm$	2 201.$^{11.}$	(Calculated, p.100)
A6	$^{151}Dy(a)^{147}Gd$	4 171.$^{20.}$	MT (1964)
A7	$^{152}Dy(a)^{148}Gd$	3 749.$^{20.}$	MT (1964)
A8	$^{153}Dy(a)^{149}Gd$	3 574.$^{8.}$	Adam et al. (1968)
A9	$^{154}Dy(a)^{150}Gd$	2 930.$^{50.}$	MT (1964)
A10	$^{156}Dy(a)^{152}Gd$	1 747.$^{6.}$	(Calculated, p.100)

TABLE 9

BETA DECAY DATA

Code	Decay	Q (keV)	References
B1	$^{147}Nd(b^-)^{147}Pm$	$894.5^{1.0}$	Canty and Connor (1967)
B2	$^{149}Nd(b^-)^{149}Pm$	1 $669.^{10.}$	MT (1964)
B3	$^{147}Pm(b^-)^{147}Sm$	$224.7^{0.6}$	NDS (B2-4)
B4	$^{148}Pm(b^-)^{148}Sm$	2 $465.^{10.}$	"
B5	$^{149}Pm(b^-)^{149}Sm$	1 $071.^{2.0}$	MT (1964)
B6	$^{150}Pm(b^-)^{150}Sm$	3 $430.^{60.}$	"
B7	$^{151}Pm(b^-)^{151}Sm$	1 $191.^{7.}$	"
B8	$^{148}Eu(b^+)^{148}Sm$	3 $101.^{30.}$	NDS (B2-4)
B9	$^{150}Eu(b^+)^{150}Sm$	2 $248.^{18.}$	MT (1964)
B10	$^{151}Sm(b^-)^{151}Eu$	$75.9^{0.6}$	"
B11	$^{152}Eu(b^+)^{152}Sm$	1 $856.8^{3.0}$	"
B12	$^{153}Sm(b^-)^{153}Eu$	$801.^{5.}$	"
B13	$^{152}Eu(b^-)^{152}Gd$	1 $821.^{6.}$	"
B14	$^{154}Eu(b^-)^{154}Gd$	1 $978.^{5.}$	"
B15	$^{155}Eu(b^-)^{155}Gd$	$247.6^{3.0}$	"
B16	$^{156}Eu(b^-)^{156}Gd$	2 $447.^{16.}$	"
B17	$^{157}Eu(b^-)^{157}Gd$	1 $270.^{50.}$	"
B18	$^{157}Tb(ec)^{157}Gd$	$66.^{6.}$	Naumann and Hopke (1967)
B19	$^{159}Gd(b^-)^{159}Tb$	$947.^{7.}$	MT (1964)
B20	$^{158}Tb(b^-)^{158}Dy$	$946.^{10.}$	"
B21	$^{160}Tb(b^-)^{160}Dy$	1 $788.^{4.}$	(Calculated, p.101)
B22	$^{161}Tb(b^-)^{161}Dy$	$584.^{6.}$	MT (1964)
B23	$^{162}Tb(b^-)^{162}Dy$	2 $520.^{55.}$	Shima (1966)
B24	$^{163}Tb(b^-)^{163}Dy$	1 $680.^{50.}$	MT (1964)
B25	$^{164}Tb(b^-)^{164}Dy$	3 $100.^{100.}$	Monnand and Moussa (1968)
		3 $400.^{200.}$	Martin (1967)

$$1\ \mu u = 0.931\ 478^{15}\ \text{keV}$$

$$^{1}n = 1\ 008\ 665.2^{0.1}\ \mu u$$

$$2n - (^{37}Cl - ^{35}Cl) = 20\ 281.1^{0.5}\ \mu u$$

$$^{4}He = 4\ 002\ 603.1^{0.4}\ \mu u$$

$$S_n(^{2}H) = 2\ 224.5^{0.1}\ \text{keV}$$

$$S_n(^{3}H) = 6\ 257.4^{0.1}\ \text{keV}$$

$$S_{2n}(^{3}H) = 8\ 481.9^{0.2}\ \text{keV}$$

The mass - energy conversion factor is taken from Cohen and DuMond (1963) and the other values are from the Mass Table (1964).

Closed Loops

Six closed loops involving the new measurements and other data can be formed in Figure 24. In the first three of these the chlorine mass difference cancels out and hence contributes no error. In the fourth and fifth loops the mass of the neutron also cancels. These fives loops are:

$$A + B - E - g - F - C = 3.0^{5.2}\ \mu u$$

$$A + c - D - F - C = -3.3^{7.1}\ \mu u$$

$$D + d - E - g = -2.8^{7.6}\ \mu u$$

$$-R28 + S + R29 - R = 3.1^{4.8}\ \mu u$$

$$-R20 + 1 - M + Q + R28 - N - L = 7.8^{4.9}\ \mu u$$

The sixth loop does involve some of the data tabulated in the last section:

$$B + 2(^{37}Cl - ^{35}Cl) - E - [\cancel{^{1}n} - R18] - [^{4}He - \cancel{^{1}n} + R5] = 1.^{6.}\ \mu u$$

These results provide strong evidence for the accuracy both of the measurements made in our laboratory and

at McMaster, and of the various reaction Q values which are involved. It is a very satisfying state of affairs.

Calculation of Some Decay Energies

Several total decay energies can be calculated from the data represented in Figure 24. As in the previous section the chlorine mass difference and the mass of the neutron often enter but cancel out in the actual calculation. The first decay considered here is the alpha decay of ^{156}Dy (A10). The Mass Table (1964) gives $Q_\alpha = 1430.^{170.}$ keV.

$$Q_\alpha(^{156}\text{Dy}) = I + J + K + 1 - M - P - O + 2(^{37}\text{Cl}-^{35}\text{Cl}) - {}^{4}\text{He}$$

$$= 1\ 747.^{6.}\ \text{keV}$$

The alpha decay of ^{152}Gd (A5) can also be determined from mass spectroscopic measurements. The Mass Table (1964) gives $Q_\alpha = 2\ 236.^{9.}$ keV

$$Q_\alpha(^{152}\text{Gd}) = G + i - T - I + 2\,(^{37}\text{Cl}-^{35}\text{Cl}) - {}^{4}\text{He}$$

$$= 2\ 201.^{11.}\ \text{keV}$$

The alpha decay of ^{148}Sm can also be calculated. The Mass Table (1964) gives 2 001.$^{5.}$ keV and Macdougall (1966) gives a calculated value of 1 965.$^{8.}$ keV for this decay.

$$Q_\alpha(^{148}\text{Sm}) = A + c - D + 2(^{37}\text{Cl}-^{35}\text{Cl}) - {}^{4}\text{He}$$

$$= 1\ 977.^{6.}\ \text{keV}$$

According to the Mass Table (1964) the electron capture decay of ^{151}Gd has $Q = 400.^{1000.}$ keV.

A much better value can be calculated here

$$Q_{EC}(^{151}\text{Gd}) = A4 + {}^{4}\text{He} - f - H - 2(^{37}\text{Cl}-^{35}\text{Cl})$$

$$= 493.^{31.}\ \text{keV}$$

The energy available for the negatron decay of ^{153}Sm (B12) is well known (Mass Table: $801.^{5.}$ keV, Nuclear Data Sheets (Nov. '63): $804.^{5.}$ keV). An independent value can be obtained here by using three mass doublets and two reaction Q values.

$$Q_\beta(^{153}Sm) = -R18 + h - R7 - H - j + 2\ ^1n - (^{37}Cl - ^{35}Cl)$$
$$= 801.^{15.}\ keV$$

The Mass Table (1964) and the Nuclear Data Sheets (April 1964) give $1810.^{20.}$ keV for the negatron decay of ^{160}Tb (B21). An improved value is available here.

$$Q_\beta(^{160}Tb) = -R21 - [N - (Q + R28)]$$
$$= 1788.^{4.}\ keV$$

The energy obtained above for the negatron decay of ^{160}Tb can be combined with doublet M to calculate the energy available for the electron capture decay of this nuclide. The Mass Table (1964) gives $29.^{28.}$ keV for this quantity.

$$Q_{EC}(^{160}Tb) = B21 - M$$
$$= 61.^{4.}\ keV$$

Calculation of Double Neutron Separation Energies

The majority of the mass spectrometric doublets reported here together with the McMaster work (Table 6) are of the form $^{A}X\ ^{35}Cl - ^{A-2}X\ ^{37}Cl = \Delta m$. Since the chlorine mass difference and the mass of the neutron are well known, such doublets directly give double neutron separation energies.

$$S_{2n} = 2n - (^{A+2}X - ^{A}X)$$
$$= 2n - (^{37}Cl - ^{35}Cl) - \Delta m \qquad (6\text{-}1)$$

Double neutron separation energies are recorded in Table 10. Where mass doublets are available the S_{2n} values

TABLE 10

DOUBLE NEUTRON SEPARATION ENERGIES (keV)

Z	A	N	S_{2n}(New)		MT-New		Reaction-New	
$_{60}$Nd	143	83	15 936. 9.	NDS	- 27. 24.			
	144	84	13 947. 3.		- 17. 7.		- 3. 19.	R1,R3
	145	85	13 579. 4.		- 6. 9.		- 16. 20.	R2,R3
	146	86	13 319.9 1.1		- 15. 5.			
	147	87	12 853. 5.		- 4. 16.			
	148	88	12 631. 4.		- 12. 8.			
	149	89	12 399. 11.		- 26. 26.			
	150	90	12 428. 4.		- 54. 9.			
	151	91	12 670. 20.		70. 120.			
	152	92	12 607. 30.					
$_{61}$Pm	144	83	16 390. 110.	NDS				
	145	84	14 518. 15.	"				
	146	85	14 207. 48.	"				
	147	86	13 902.4 3.6	"	- 10. 14.			
	148	87	13 587. 25.	"	- 42. 56.			
	149	88	13 173. 4.		- 31. 10.			
	150	89	12 896. 60.		- 46. 120.			
	151	90	13 468. 10.		3. 27.			
$_{62}$Sm	144	82	19 040. 120.	NDS				
	145	83	17 379. 36.	"	- 159. 116.			
	146	84	15 163. 25.		46. 42.			
	147	85	14 783. 9.	NDS	- 12. 20.			
	148	86	14 498. 25.		- 31. 43.			
	149	87	14 019. 3.		- 31. 8.		- 2. 19.	R6,R8
							9. 24.	R10,R11
	150	88	13 861. 4.		- 33. 9.		0. 17.	R6,R9
							15. 25.	R10,R12
							- 7. 29.	R14
	151	89	13 588. 7.		3. 22.			

TABLE 10 (continued)

Z	A	N	S_{2n}(New)		MT-New		Reaction-New
	152	90	13 865.	4.	- 32.	10.	- 7. 29. R15
	153	91	14 134.	7.	- 25.	26.	
	154	92	13 846.	4.	- 56.	10.	- 3. 29. R16
	155	93	13 795.	17.	- 72.	33.	
	156	94	13 038.	25.	43.	52.	
$_{63}$Eu	146	83	17 693.	36. NDS			
	147	84	15 736.	24. "			
	148	85	15 287.	35. "	- 47.	95.	
	149	86					
	150	87	14 714.	35.	- 44.	85.	
	151	88					
	152	89	14 256.	19.	- 32.	38.	
	153	90	14 859.	4.	- 25.	23.	
	154	91	14 970.	20.	- 41.	38.	
	155	92	14 596.	8.	- 25.	27.	
	156	93	14 507.	17.	7.	35.	
	157	94	13 875.	50.	- 25.	100.	
$_{64}$Gd	149	85	15 926.	43.			
	150	86	15 629.	29.	45.	50.	
	151	87	15 228.	33.			
	152	88	15 101.	29.	- 66.	49.	
	153	89	15 094.	35.			
	154	90	15 148.3	2.1	- 62.	20.	
	155	91	15 117.	14.	- 55.	33.	
	156	92	14 975.7	1.5	7.	8.	
	157	93	14 898.	3.	- 24.	8.	
	158	94	14 303.9	1.4	- 27.	6.	
	159	95	13 909.	7.	52.	34.	
	160	96	13 397.	3.	10.	10.	
	161	97	13 020.	70. MT			

TABLE 10 (continued)

Z	A	N	S_{2n}(New)	MT-New	Reaction-New
$_{65}$Tb	159	94	14 922. 6.	46. 34.	
	160	95	14 574. 11.	3. 39.	
	161	96	14 084. 6.	- 10. 31.	
	162	97	13 920. 55.		
	163	98	13 377. 50.	- 17. 100.	
	164	99	13 050. 210.		
$_{66}$Dy	153	87	16 523. 56.		
	154	88	16 490. 60. MT		
	155	89			
	156	90	16 284. 58.	246. 228.	
	157	91			
	158	92	16 021.9 3.4	- 362. 173.	12. 17. R22,R23
	159	93	15 894. 28.		
	160	94	15 416.1 2.4	25. 32.	13. 16. R24,R25
	161	95	15 055. 20.	- 17. 52.	
	162	96	14 652.2 1.1	0. 9.	4. 15. R26,R27
					- 3. 11. R26,R28
	163	97	14 472.9 1.2	- 16. 6.	- 6. 7. R28,R33
					- 10. 5. R28,R34
	164	98	13 931.1 1.0	- 21. 8.	- 3. 7. R33,R29
					2. 8. R33,R31
					- 6. 8. R33,R32
					- 7. 5. R34,R29
					- 2. 7. R34,R31
					- 10. 7. R34,R32
	165	99	13 367. 5.	- 75. 16.	
	166	100	12 864. 33.	- 81. 66.	

are calculated directly according to the above equation. The region from A = 142 to 148 was recently covered by the Nuclear Data Sheets (NDS: B2-1, B2-4, 1967) and, as indicated, many of the S_{2n} values are taken directly from this source.

Several of the values in Table 10 have been calculated from various combinations of the data indicated in Figure 24. In the case of overdetermined values the one having the smallest possible error was usually selected while, when possible, tempering this choice with the reliability of the input data.

The best method of calculating the positions of the nuclides in Figure 24 involves a least squares analysis as was performed for the Mass Table (1964). Such an adjustment requires considerable time and insight in order properly to evaluate the reliability of the input data, not to mention the rather elaborate computer program required to perform the adjustment. In spite of these precautions and work, such adjustments can contain significant errors over large regions due to the presence of a few erroneous input values. A case in point is the 1964 Mass Table which contains the 1963 work of Demirkhonov et al. (Table 5) and some of the early McMaster work in the rare earth region (Barber et al., 1964).

Thus although the procedure used here is considerably simpler than a least squares adjustment, it should be relatively free of errors which propagate over a large region. Also, considering the quality of much of the input data, the values given in Table 10 represent a major improvement over the 1964 Mass Table.

The column labeled "MT - NEW" in Table 10 is a comparison with the 1964 Mass Table values. The agreement is quite poor in several instances. The absence of a comparison simply means that the Mass Table value either has a stated error greater than 300.keV or was used in the preceeding column (in two instances). The last column is a comparison of recent reaction data with S_{2n} values calculated directly from either this work or the latest McMaster work. The agreement is excellent.

Although it is not practicable to give here the details of all the calculations used to arrive at the values in Table 10, the calculation of S_{2n} for ^{156}Dy is outlined below as an example. This value is of particular interest since it occurs at N = 90 and the value obtained is about 250.keV lower than the Mass Table value.

S_{2n} for ^{156}Dy can be calculated from that of ^{148}Sm and four alpha decays (see Figure 24). S_{2n} for ^{148}Sm is available from three sources:

(i) Nuclear Data Sheets (B2-4, Dec. '67). This value when added to the NDS value for ^{146}Sm is 42. keV higher than that calculated from our doublet F. This discrepancy was traced to the failure of the compilers to recognize an incorrect McMaster value for the doublet ^{144}Sm - ^{144}Nd which is 37. keV higher than our doublet C. (The compilers did recognize this bad value in an earlier issue (B2-1, July '67)). Hence the Nuclear Data Sheet value for S_{2n} of ^{148}Sm is dubious.

(ii) Mass Table (1964). The sum of S_{2n} (^{148}Sm) and S_{2n} (^{146}Sm) is in reasonable agreement with our value F; however, the value for ^{146}Sm differs by nearly 50. keV from that calculated from the (t,p) reaction R13. This discrepancy combined with the presence of several bad mass doublets in the input of the Mass Table (as mentioned above) ruled out using the Mass Table value for S_{2n} (^{148}Sm).

(iii) Our doublet F and the reaction R13 also give a value for S_{2n} (^{148}Sm). This value was selected for Table 10.

The pertinent alpha decays are A3, A9, A5 and A10 (see Table 8). A3 is reasonably well known but A9 is uncertain by 50.keV; however, no other values are available. Values for A5 and A10 were calculated in the previous section. Thus $S_{2n}(^{156}Dy)$ can be calculated. Note that among the input data are nine Manitoba doublets, two McMaster doublets and a (t,p) reaction.

Calculation of Single Neutron Separation Energies and Neutron Pairing Energies

The binding energy of the last neutron in a nucleus is defined as

$$S_n = n - (^{A+1}X - ^{A}X) \qquad (6\text{-}2)$$

S_n values for the various nuclides from neodymium to dysprosium are listed in Table 11. As in Table 10, several values are taken directly from the 1964 Mass Table or the 1967 Nuclear Data Sheets. The remainder have been calculated from various combinations of the data indicated in Figure 24 in a manner

TABLE 11

SINGLE NEUTRON SEPARATION ENERGIES (keV)

Z	A	N	S_n(New)		MT-New		Reaction-New	
$_{60}$Nd	142	82	9 809.	9. NDS	0.	23.		
	143	83	6 127.4	2.0 "	- 27.	9.	0. 17.	R1
	144	84	7 817.2	1.8 "	13.	8.	0. 7.	R3
	145	85	5 760.4	1.9 "	- 16.	8.	- 14. 17.	R2
	146	86	7 559.5	2.2	1.	8.		
	147	87	5 293.2	4.0 NDS	- 5.	16.		
	148	88	7 333.7	4.8 "	- 3.	17.		
	149	89	5 067.	12.	- 25.	24.		
	150	90	7 361.	13.	- 29.	24.		
	151	91	5 309.	15.	101.	115.		
	152	92	7 298.	34.				
$_{61}$Pm	143	82	9 870.	100. NDS				
	144	83	6 529.	45. "				
	145	84	7 990.	43. "				
	146	85	6 219.	23. "	44.	48.		
	147	86	7 684.	23. "	- 56.	46.		
	148	87	5 904.	11. "	13.	32.		
	149	88	7 268.	11.	- 43.	32.		
	150	89	5 628.	60.	- 8.	120.		
	151	90	7 850.	60. MT				
$_{62}$Sm	143	81	8 430.	130. NDS				
	144	82	10 616.	36. "	- 156.	116.		
	145	83	6 763.	11. "	0.	21.		
	146	84	8 411.	19. "	35.	39.		
	147	85	6 354.	26.	- 29.	44.		
	148	86	8 144.0	4.8 NDS	- 2.	10.	1. 15.	R8
							3. 20.	R11
	149	87	5 874.	4.	- 28.	9.	- 1. 16.	R6
							7. 19.	R10

TABLE 11 (continued)

Z	A	N	S_n (New)	MT-New	Reaction-New
$_{62}$Sm	150	88	7 986.8 1.0	- 5. 4.	2. 5. R9
					8. 16. R12
	151	89	5 601. 7.	8. 22.	
	152	90	8 264. 8.	- 40. 24.	
	153	91	5 870. 12.	16. 22.	
	154	92	7 976. 13.	- 72. 25.	
	155	93	5 819. 11. MT		
	156	94	7 262. 26. "		
$_{63}$Eu	145	82	10 421. 38. NDS		
	146	83	7 259. 29. "	111. 89.	
	147	84	8 476. 22. "		
	148	85	6 810. 32. "		
	149	86			
	150	87			
	151	88	7 925. 19.	8. 42.	
	152	89	6 331. 9.	- 40. 25.	
	153	90	8 528. 10.	16. 22.	
	154	91	6 415.9 1.0	- 31. 21.	
	155	92	8 180. 8.	6. 19.	
	156	93	6 328. 17. MT		
	157	94	7 520. 50. "		
$_{64}$Gd	148	84	9 020. 21. NDS		
	149	85	6 906. 38.	44. 188.	
	150	86	8 723. 24.	- 3. 174.	
	151	87	6 505. 41.		
	152	88	8 614. 32.		
	153	89	6 480. 13. MT		
	154	90	8 668. 13.	- 62. 33.	
	155	91	6 449. 5.	7. 14.	
	156	92	8 527. 5. MT		
	157	93	6 369.9 1.7	- 23. 7.	
	158	94	7 934.0 1.0	- 5. 5.	

TABLE 11 (continued)

Z	A	N	S_n (New)	MT-New	Reaction-New
$_{64}$Gd	159	95	5 975. 7.	56. 34.	
	160	96	7 422. 8.	- 46. 36.	
	161	97	5 650. 70. MT		
$_{65}$Tb	158	93	6 769. 13.	22. 40.	
	159	94	8 153. 11.	24. 36.	
	160	95	6 420.6 1.0	- 21. 19.	
	161	96	7 663. 6.	11. 28.	
	162	97	6 257. 55.		
	163	98	7 120. 74.		
	164	99	[6 230. 130. [5 930. 220.		
$_{66}$Dy	152	86	9 442. 35.		
	153	87	7 081. 44.	49. 194.	
	154	88	9 409. 75.	- 39. 235.	
	155	89			
	156	90			
	157	91	6 973. 10.		
	158	92	9 061. 10.		
	159	93	6 833. 10.	18. 44.	
	160	94	8 596. 10.	- 6. 40.	
	161	95	6 459.4 3.2	- 11. 15.	- 3. 13. R26
	162	96	8 192.8 3.0	11. 12.	7. 13. R27
	163	97	6 280.1 3.2	- 27. 11.	- 6. 8. R33
					- 10. 6. R34
	164	98	7 651.1 3.4	6. 8.	3. 6. R29
					8. 8. R31
					0. 8. R32
	165	99	5 716. 3.	- 81. 13.	
	166	100	7 148. 33. MT		

similar to that described in the previous section for double neutron separation energies. Many values can be calculated directly from (d,p), (d,t) and (n,γ) reaction Q values.

As in Table 10 Mass Table values with possible errors in excess of 300. keV are not considered in the "MT - NEW" column. In several cases the agreement with the Mass Table is poor; however, where comparisons are available, the agreement with other reaction data is very good.

Two values are recorded for S_n (^{164}Tb). Among the input data for this calculation is the decay energy for this nuclide (B25, Table 9). Although the measurement by Monnand and Moussa has a smaller possible error, regularities amongst the S_n values (see Chapter 7) suggest that Martin's value is more accurate. Thus the latter value was used in evaluating both S_{2n} (^{164}Tb) and the neutron pairing energy of ^{163}Tb.

Neutron pairing energy, as the term implies, refers to the extra binding that results from the completion of a neutron pair. One definition that has been used (Johnson and Nier, 1957), (Benson and Johnson, 1966) (Macdougall, 1966) (Whineray, 1966) is

$$P_n(Z,N) = S_n(Z,N) - S_n(Z,N-1) \qquad (6\text{-}3)$$

(N even)

However, this definition does not take into account the variation of S_n with N for a given element.

A definition which, to a good approximation, allows for this variation has been given by Nilsson and Prior (1961).

$$P_n(Z,N) = (-1)^N \frac{1}{2}\left\{S_n(Z,N) - \frac{1}{2}\left[S_n(Z,N+1) + S_n(Z,N-1)\right]\right\} \qquad (6\text{-}4)$$

They call P_n the "odd - even mass difference parameter". The factor of 1/2 effectively changes P_n to the pairing energy per neutron. Also this definition is not restricted to even N. In the case of odd N, P_n can be interpreted as a "missing" pairing energy per neutron. P_n will be further discussed in the next Chapter where its variation with neutron number is examined.

Equation (6-4) has been used with the data of Table 11 to calculate the values in Table 12.

TABLE 12

NEUTRON PAIRING ENERGIES

Z	A	N	P_n (keV)
$_{60}Nd$	144	84	$936.7^{1.2}$
	145	85	$964.0^{1.2}$
	146	86	$1\,016.4^{1.6}$
	147	87	$1\,076.7^{2.4}$
	148	88	$1\,077.^{4.}$
	149	89	$1\,140.^{7.}$
	150	90	$1\,087.^{8.}$
	151	91	$1\,010.^{12.}$
$_{61}Pm$	145	84	$808.^{25.}$
	146	85	$809.^{17.}$
	147	86	$812.^{13.}$
	148	87	$786.^{9.}$
	149	88	$751.^{16.}$
	150	89	$965.^{34.}$
$_{62}Sm$	146	84	$927.^{12.}$
	147	85	$962.^{14.}$
	148	86	$1\,015.^{7.}$
	149	87	$1\,096.^{3.}$
	150	88	$1\,125.^{2.}$
	151	89	$1\,262.^{4.}$
	152	90	$1\,265.^{6.}$
	153	91	$1\,125.^{7.}$
	154	92	$1\,066.^{8.}$
	155	93	$900.^{10.}$

TABLE 12 (continued)

Z	A	N	P_n (keV)
$_{63}Eu$	147	84	721.$^{16.}$
	152	89	948.$^{7.}$
	153	90	1 077.$^{6.}$
	154	91	969.$^{3.}$
	155	92	904.$^{6.}$
	156	93	761.$^{15.}$
$_{64}Gd$	149	85	983.$^{21.}$
	150	86	1 009.$^{22.}$
	151	87	1 082.$^{23.}$
	152	88	1 061.$^{20.}$
	153	89	1 081.$^{11.}$
	154	90	1 102.$^{8.}$
	155	91	1 075.$^{5.}$
	156	92	1 059.$^{3.}$
	157	93	930.$^{2.}$
	158	94	881.$^{2.}$
	159	95	852.$^{4.}$
	160	96	805.$^{18.}$
$_{65}Tb$	159	94	779.$^{7.}$
	160	95	744.$^{3.}$
	161	96	662.$^{14.}$
	162	97	568.$^{33.}$
	163	98	513.$^{70.}$

TABLE 12 (continued)

Z	A	N	P_n (keV)
$_{66}Dy$	153	87	$1\,173.^{30.}$
	158	92	$1\,079.^{6.}$
	159	93	$998.^{6.}$
	160	94	$975.^{6.}$
	161	95	$968.^{3.}$
	162	96	$911.6^{1.9}$
	163	97	$820.9^{2.0}$
	164	98	$826.5^{2.1}$
	165	99	$841.^{9.}$

CHAPTER 7

NEUTRON SEPARATION ENERGY SYSTEMATICS

Introduction

A study of the variation of neutron separation energies with neutron number is a convenient and sensitive method for investigating nuclear shell and subshell effects and collective nucleon behavior. (Johnson and Nier, 1957) (Barber et al., 1963a) (Barber et al., 1963b) (Bishop et al., 1963) (McLatchie et al., 1964a) (Barber et al., 1964) (Benson and Johnson, 1966). Although nuclei near N = 90 have been previously examined in this fashion, the data presented in Chapter 6 provide the most accurate and detailed picture of this region yet available.

Double Neutron Separation Energies

The data presented in Table 10 are plotted in Figure 25. The lines connect nuclides of constant Z. Although odd N points lie close to the corresponding curves, the restriction to even N removes fluctuations due to the different nature of odd N nuclei. For such nuclei the two neutrons concerned are not paired, although S_{2n} is the energy required to remove two neutrons and to break a neutron pair.

In the absence of shell, subshell, and collective effects, double neutron separation energy curves, for various elements display a remarkable regularity (Barber et al., 1963b) (Bishop et al., 1963). The curves display negative slopes, are nearly straight, and are virtually parallel from one

FIGURE 25

Double Neutron Separation Energies (even N)

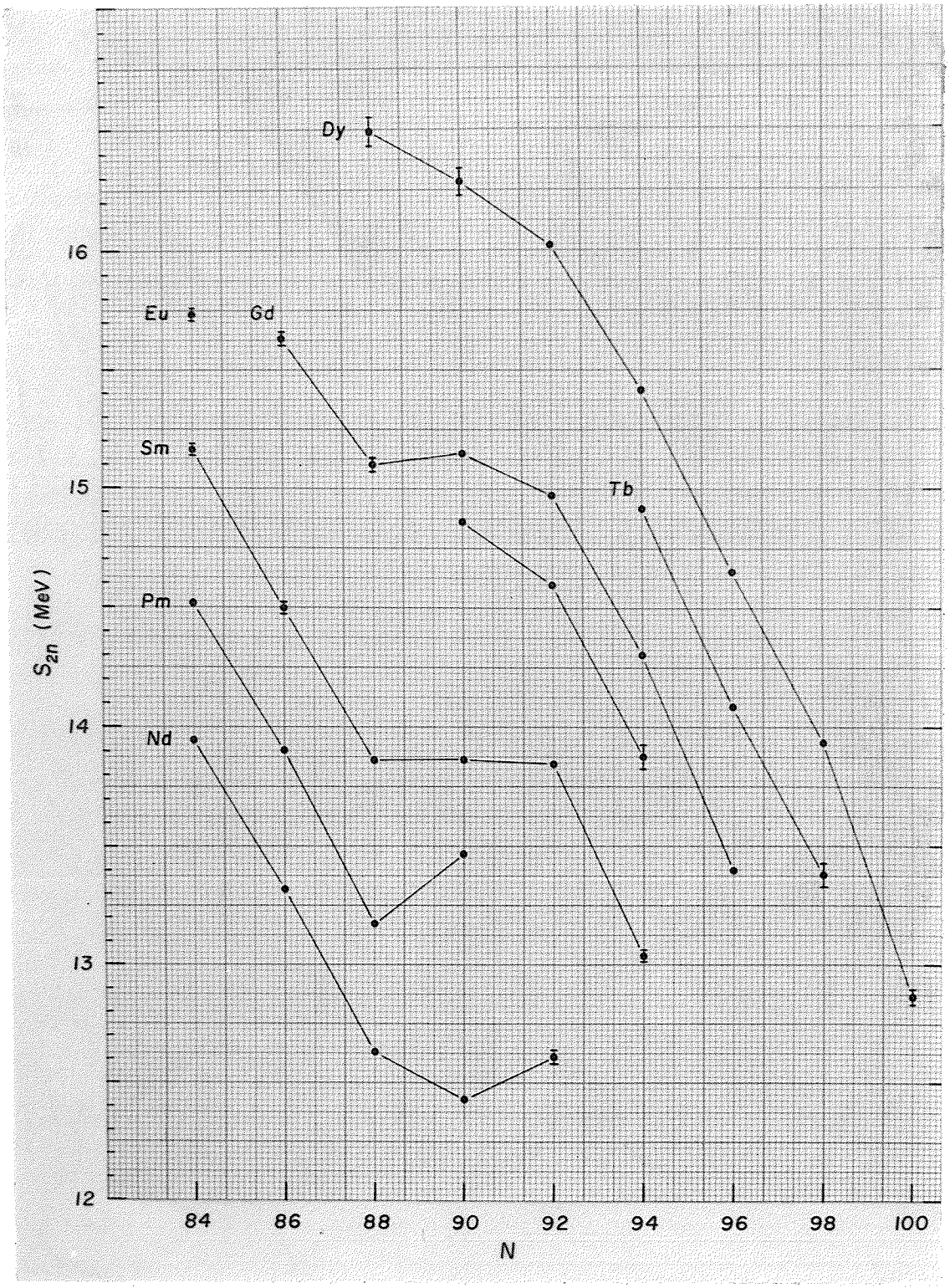
Dy
Eu
Gd
Sm
Tb
Pm
Nd
16
15
14
13
12
S_{2n} (MeV)
84
86
88
90
92
94
96
98
100
N

element to the next. The negative slope is due chiefly to the increasing neutron excess, an effect which forms the basis for the asymmetry term in the semiempirical mass formula. This term also accounts for the increase of S_{2n} as Z increases for constant N.

The curves in Figure 25 display the features discussed above; however, in the region from N = 88 to N = 92 there is a striking change corresponding to the onset of nuclear deformation. The appearance of collective motion of certain of the nucleons implies the existence of an additional bond between these particles, in agreement with the upward break displayed here. Several features in Figure 25 are worth special comment.

(i) The curves demonstrate the suddenness with which nuclear deformation occurs as N exceeds 88.

(ii) The curves suggest that nuclear deformation associated with neutrons does not increase appreciably beyond N = 92.

(iii) Because S_{2n} curves are so regular in the absence of shell, subshell and collective effects, the extrapolation of the "normal" curves in Figure 25 beyond N = 88 provides a method of estimating the energy of deformation and of predicting the location of possible low-lying spherical excited states at N = 90 (Whineray, 1966) (McLatchie, 1966).

(iv) The deformation varies with Z, being least for dysprosium and rather large for gadolinium and samarium. For neodymium the onset of deformation is

less rapid; however, the point at N = 92 suggests that this element also undergoes a large distortion. Although data are less plentiful for the odd Z nuclei, the curves for promethium and europium suggest that these nuclei may have the largest deformations.

A few years ago techniques developed in the BCS theory of superconductivity were applied to the nucleus by Belyaev (1959) and Soloviev (1959) on the suggestion of Bohr et al. (1958). More recently this theory has been applied to rare earth nuclei (Kumar and Baranger, 1968). In addition to accounting qualitatively for certain features of the excited states of even-even nuclei and of nuclear moments of inertia, Belyaev's theory indicates that the equilibrium shape of a nucleus is determined by a competition between two interactions among the nucleons: a pairing interaction which favors sphericity, and a quadrupole interaction which tends to produce distortion. When the latter interaction emerges as the dominant one, Belyaev predicts that the transition from spherical to deformed nuclei is rather sharp. This is consistent with (i) above. The large deformation indicated for odd Z nuclei (iv) is also in accord with this theory since these nuclei lack the stabilizing influence of an even number of protons.

Single Neutron Separation Energies

The data presented in Table 11 are plotted in Figure 26. The lines connect nuclides of constant Z for either even or odd N.

FIGURE 26

Single Neutron Separation Energies

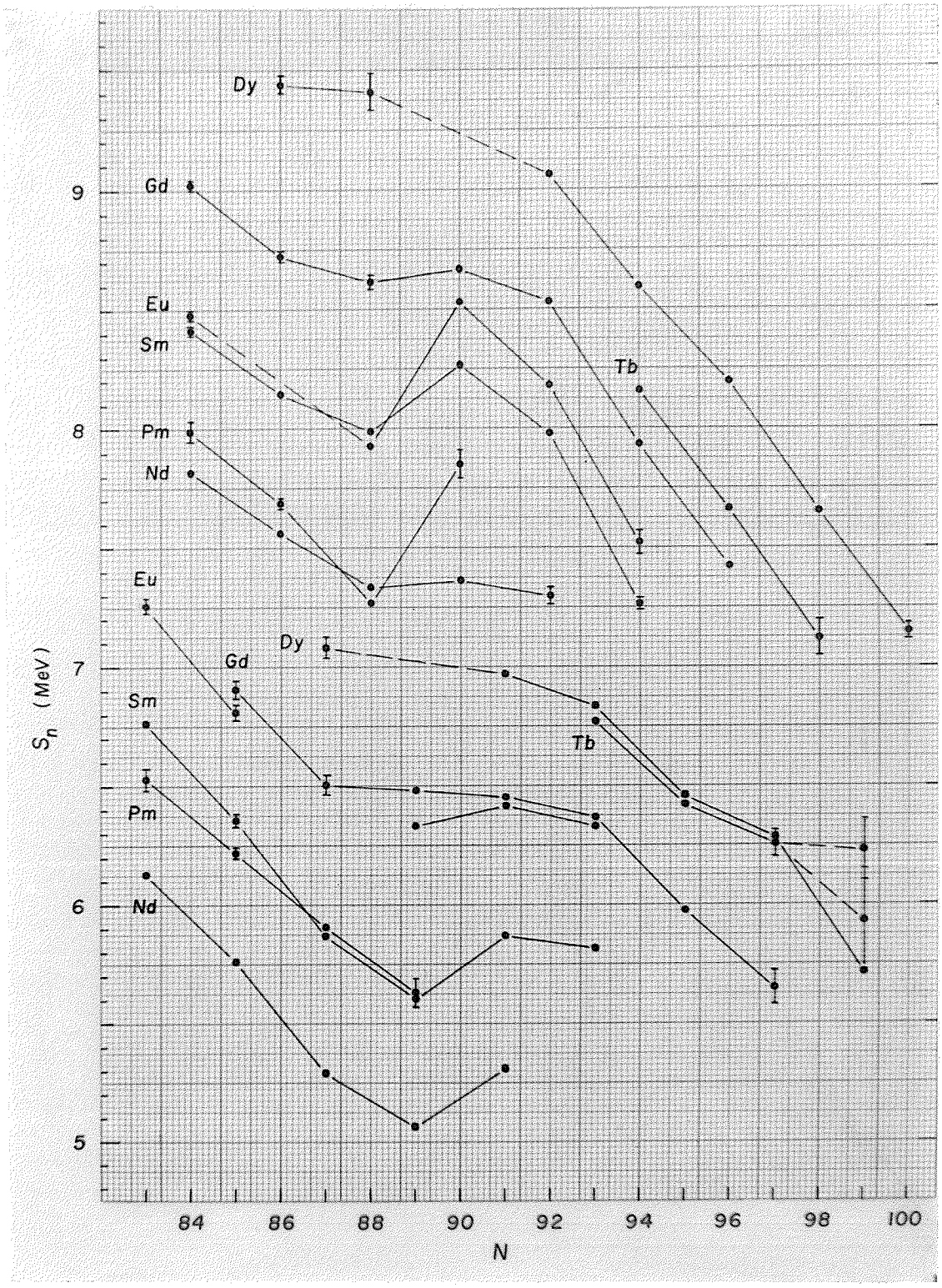
Dy
Gd
Eu
Sm
Pm
Nd
Tb
Eu
Dy
Gd
Sm
Tb
Pm
Nd
9
8
7
6
5
S_n (MeV)
84
86
88
90
92
94
96
98
100
N

As in the S_{2n} case, the curves are quite regular up to N = 88, while from N = 88 to N = 92 there is strong evidence for a rapid increase in nuclear distortion. Again this effect is least for dysprosium and is strongest among the odd Z elements indicating that nuclei containing an odd number of protons deform more readily than their even-even neighbours.

The stabilizing effect of an even number of similar nucleons is also apparent in the case of neutrons if the even N curves are compared with the odd N curves. The former return more rapidly towards the extrapolated curves for spherical nuclei than do the odd N curves. Additional evidence for this even-odd neutron effect is found in electric quadrupole moment data (Myers and Swiatecki, 1966). In the rare earth region there is a distinct tendency for odd N isotopes to have larger quadrupole moments than their even N neighbours, which suggests that odd N nuclei are often more deformed than adjacent even N nuclei.

Another interesting feature of the S_n curves is the tendency of the odd Z points to lie near neighbouring even Z points. In the case of the odd N curves, those of odd Z are displaced upward indicating an increased binding of the odd neutron in the presence of the odd proton. For the even N curves the displacement is in the opposite sense which suggests that the even neutron is less tightly bound in the presence of the odd proton. This grouping trend diminishes near N = 90 where nuclear deformation is being established. This effect has also been noted by Benson and Johnson (1966) in the region $76 \leq N \leq 90$. They attribute it to an odd proton-neutron interaction. (Saxena, 1961)

The two values plotted for terbium at N = 99 were discussed in the last section of Chapter 6. The regularities exhibited by the S_n curves strongly suggest that the larger of the two is in error.

Neutron Pairing Energies

The data presented in Table 12 are plotted in Figure 27 for even Z only. The lines connect nuclides of constant Z for either even or odd N. As indicated the odd N points have been displaced downward by 0.3 MeV for clarity. The P_n values for odd Z nuclei are about 0.2 MeV lower than those for even Z due to the odd proton-neutron interaction mentioned above; however, since these data are not plentiful P_n has been plotted for even Z nuclei only.

As defined in equation (6-4) each $P_n(Z,N)$ value represents one half of the vertical distance between the appropriate even N and odd N S_n curves of Figure 26. Nilsson and Prior (1961), who introduced this definition, note that the fluctuations of the P_n versus N curves are smaller than those of curves based on the simpler definition given in equation (6-3). This more regular behavior is evident here if one compares the even-even curves with those plotted by Macdougall (1966).

The chief feature of the P_n curves is the peak at N = 89 and 90. Nilsson and Prior also found this feature; however, the data used here are much more accurate than those available in 1961. The large increase in pairing energy near N = 90 is in accord with the evidence displayed by the S_n and S_{2n} curves for nuclear deformation in this region.

FIGURE 27

Neutron Pairing Energies (even Z)
(Odd N points have been decreased
by 300 keV for clarity.)

Note: Estimated uncertainties of ± 20 keV were originally assigned to reactions R22 to R27 inclusive; however, in a recent communication Bennett gives ± 10 keV for these reactions. Because of this change the error bars shown in Figure 27 for Dy at N = 92, 93, 94 and 95 should be reduced by about 50%. (Although these changes were received too late to be included in Figure 27, they have been included in Tables 7, 10, 11 and 12).

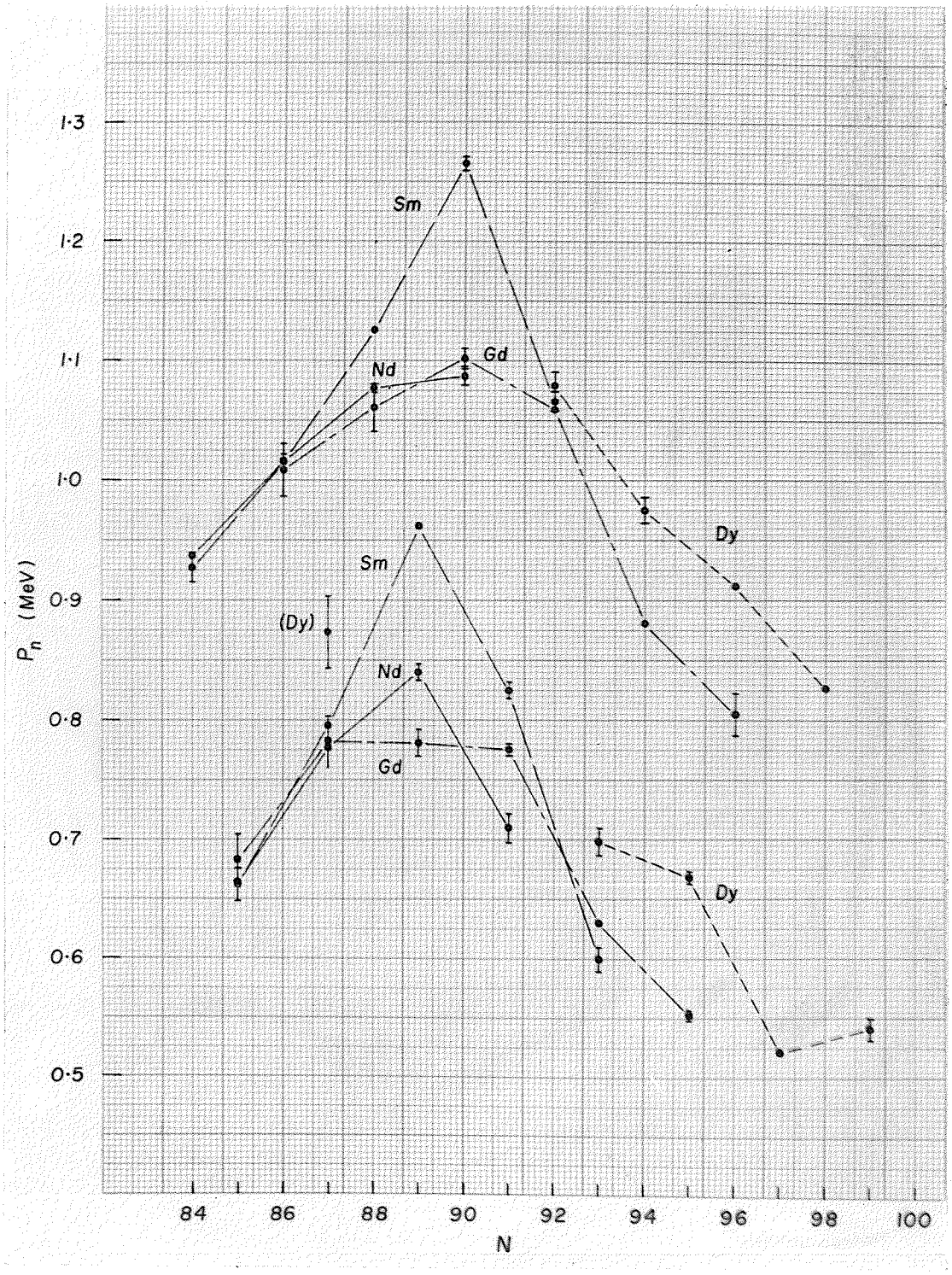
1·3
1·2
1·1
1·0
0·9
0·8
0·7
0·6
0·5
P_n (MeV)
Sm
Nd
Gd
Dy
Sm
(Dy)
Nd
Gd
Dy
84
86
88
90
92
94
96
98
100
N

SUMMARY

A high precision voltage supply and potentiometer circuit has been constructed to supply and measure the voltage ratio required by the new Manitoba second order mass spectrometer. The potentiometer is capable of matching a spectrometer precision of at least one part in one billion for mass doublets as wide as one part in 5,000, and may do nearly as well for doublets as wide as one part in 100. To date the precision of the spectrometer has been somewhat lower with the result that the potentiometer has contributed negligible uncertainty to the mass measurements reported here.

The new second order spectrometer has been completed and used to measure some twenty close doublets among the rare earths between Z = 60 and Z = 66. Together with twelve McMaster measurements these data provide for the first time connections accurate to a few keV between all of the stable isotopes in this region. The mass measurements are internally consistent, agree well with all available precise external data, and permit the calculation of some decay energies with improved precision.

The new measurements have been combined with other data in order to calculate neutron separation and pairing energies. The neutron separation energy systematics confirm in greater detail the well established onset of nuclear deformation near N = 90 but indicate that the effect is not as strong in the case of dysprosium as for the other elements in this region.

REFERENCES

ADAM, TOTH and ROCHE (1968) Nuc. Phys. A121, 304.

ASTON (1922) Isotopes (Edward Arnold and Co.)

AUGUSTYNEK (1968) Am. Jor. Phys. 36, 126.

BAINBRIDGE (1933) Phys. Rev. 44, 123.

BAINBRIDGE and COLLINS (1957) Nuclear Masses and Their Determination (Pergamon Press) p. 213.

BAINBRIDGE and DEWDNEY (1967) Proc. 3rd Int. Conf. on Atomic Masses (U. of Manitoba Press) p. 758.

BARBER (1962) Thesis, McMaster University.

BARBER, BISHOP, McLATCHIE, VAN ROOKHUYZEN and DUCKWORTH (1963a) Can. J. Phys. 41, 696.

BARBER, McLATCHIE, BISHOP, VAN ROOKHUYZEN and DUCKWORTH (1963b) Can. J. Phys. 41, 1482.

BARBER, DUCKWORTH, HOGG, MACDOUGALL, McLATCHIE and VAN ROOKHUYZEN (1964) Phys. Rev. Lett. 12, 597.

BARBER (1965) Can. J. Phys. 43, 716.

BARBER, MEREDITH, BISHOP, DUCKWORTH, KETTNER and VAN ROOKHUYZEN (1967) Proc. 3rd Int. Conf. on Atomic Masses (U. of Manitoba Press) p. 717.

BEG and MacFARLANE (1965) Bull. Am. Phys. Soc. 10, 6, 724.

BELYAEV (1959) Mat. Fys. Medd. Dan. Vid. Selsk. 31, No. 11

BENNETT (1967) Thesis, Florida State University (NSA 22, 18305)

BENNETT (1969) Private Communication

BENSON and JOHNSON (1964) Phys. Rev. Lett. 13, 24, 274.

BENSON and JOHNSON (1966) Phys. Rev. 141, 1112.

BHANOT, JOHNSON and NIER (1960) Phys. Rev. 120, 235.

BISHOP, BARBER, McLATCHIE, MACDOUGALL, VAN ROOKHUYZEN and DUCKWORTH (1963) Can. J. Phys. 41, 1532.

BJERREGAARD, HANSEN and NATHAN (1966) Nuc. Phys. 86, 145.

BLEAKNEY (1936) Am. Phys. Teacher 4, 12.

BOHR, MOTTELSON AND PINES (1958) Phys. Rev. 110, 936.

CANTY and CONNOR (1967) Nuc. Phys. A104, 35.

COHEN and DuMOND(1963) Proc. 2nd Int. Conf. on Nuclidic Masses (Springer Verlag, 1964) p. 181

COHEN and DuMOND (1965) Rev. Mod. Phys. 37, 537.

DAMEROW, RIES and JOHNSON (1963) Phys. Rev. 132, 1673.

DEMIRKHANOV, DOROKHOV and DZKUYA (1963) Proc. 2nd Int. Conf. on Nuclidic Masses (Springer Verlag, 1964) p. 430

DEMIRKHANOV, DOROKHOV and DZKUYA (1965) Izv. AN. SSSR, ser. fiz. 29, N5, 857.

DEMIRKHANOV, DOROKHOV and DZKUYA (1967) Proc. 3rd Int. Conf. on Atomic Masses (U. of Manitoba Press) p. 864.

DEWDNEY and BAINBRIDGE (1965) Phys. Rev. 138, B540.

DICKE (1967) Phys. Today 20, 1, 55.

DUCKWORTH (1958) Mass Spectroscopy (Cambridge U. Press).

DUCKWORTH, BARBER, BISHOP, CAMBEY, MACDOUGALL, McLATCHIE, ORMROD and VAN ROOKHUYZEN (1963) Proc. 2nd Int. Conf. on Nuclidic Masses (Springer Verlag, 1964) p. 393.

FEYNMAN (1965) Symmetries in Elementary Particle Physics (Academic Press) p. 400

HAFEMEISTER and SHERA (1966) Phys. Rev. 152, 1084.

HEATH (1967) Proc. 3rd Int. Conf. on Atomic Masses (U. of Manitoba Press) p. 251.

HERZOG (1934) Z. Phys. 89, 447.

HERZOG (1935) Z. Phys. 97, 596.

HINTENBERGER and KÖNIG (1957) Z. Naturf. 12a, 773.

HINTENBERGER and KÖNIG (1959) Advances in Mass Spectrometry (Pergamon Press, London) p. 16-35.

HINTENBERGER, MATTAUCH, MÜLLER-WARMUTH, VOSHAGE and WENDE (1960) Proc. Int. Conf. on Nuclidic Masses (U. of Toronto Press) p. 387.

HOGG and DUCKWORTH (1954) Can. J. Phys. 32, 65.

HUGHES, KENNETT, PRESTWICH and WALL (1966) Can. J. Phys. 44, 919.

JOHNSON and NIER (1957) Phys. Rev. 105, 1014.

JOHNSON, HUDSON, BRITTEN and KAYSER (1967) Proc. 3rd Int. Conf. on Atomic Masses (U. of Manitoba Press) p. 673.

KENEFICK and SHELINE (1964) Phys. Rev. 133, B25.

KENEFICK and SHELINE (1965) Phys. Rev. 139, B1479.

KUMAR and BARANGER (1968) Nuc. Phys. A110, 529.

MACDOUGALL (1966) Thesis, McMaster University.

MACDOUGALL, McLATCHIE, WHINERAY and DUCKWORTH (1966) Zeits. f. Naturf. 21a, 63.

MACFARLANE and CERNY (1967) Proc. 3rd Int. Conf. on Atomic Masses (U. of Manitoba Press) p. 327.

McLATCHIE, BARBER, BISHOP, DUCKWORTH, HOGG, MACDOUGALL and VAN ROOKHUYZEN (1964a) Can. J. Phys. 42, 926.

McLATCHIE, BARBER, DUCKWORTH and VAN ROOKHUYZEN (1964b) Phys. Lett. 10, 330.

McLATCHIE (1966) Thesis, McMaster University.

McLATCHIE (1968) Private Communication.

MAHUNKA, MAHUNKA and FENYES (1966) Sov. J. Nuc. Phys. 2, 143.

MARTIN (1967) Thesis, University of Arkansas (NSA 22, 11974).

Mass Table (1964) MATTAUCH et al. Nuc. Phys. 67, 1, 1965.

MATSUDA, FUKUMOTO and MATSUO (1967) Proc. 3rd Int. Conf. on Atomic Masses (U. of Manitoba Press) p. 733.

MATTAUCH (1960) Proc. Int. Conf. Nuclidic Masses (U. of Toronto Press) p. 459.

MEREDITH (1969) Thesis, University of Manitoba.

MONNAND and MOUSSA (1968) J. Phys. (Paris) 29, 545.

MYERS and SWIATECKI (1966) Nuc. Phys. 81, 1.

NAUMANN and HOPKE (1967) Phys. Rev. 160, 1035.

NEALY and SHELINE (1967) Phys. Rev. 164, 1503.

NIER and ROBERTS (1951) Phys. Rev. 81, 507.

NILSSON and PRIOR (1961) Mat. fys. Medd. Dan. Vid. Selsk. 32, No. 16.

Nuclear Data Sheets (Academic Press)

OGATA, MATSUMOTO, NAKABUSHI and KATAKUSE (1967) Proc. 3rd Int. Conf. on Atomic Masses (U. of Manitoba Press) p. 748

QUISENBERRY, SCOLMAN and NIER (1956) Phys. Rev. 102, 1071.

RASMUSSEN, ORPHAN and HUKAI (1967) Proc. 3rd Int. Conf. on Atomic Masses (U. of Manitoba Press) p. 278.

ROLL, KROTKOV and DICKE (1964) Ann. Phys. 26, 442.

SAXENA (1961) Phys. Rev. 121, 595.

SCHIFF (1955) Quantum Mechanics, 2nd ed. (McGraw-Hill)

SCHIMA (1966) Phys. Rev. 151, 950.

SCHULT, BUNKER, HAFEMEISTER, SHERA, JURNEY, STARNER, BÄCKLIN, FOGELBERG, GRUBER, MAIER, KOCH, SHELTON, MINOR and SHELINE (1967) Phys. Rev. 154, 1146.

SHELTON and WATSON (1966) Phys. Lett. 22, 648.

SIIVOLA and GRAEFFE (1965) Nuc. Phys. 64, 161.

SMITH and DAMM (1953) Phys. Rev. 90, 324.

SMITH and DAMM (1956) Rev. Sci. Instr. 27, 638.

SMITH (1967) Proc. 3rd Int. Conf. on Atomic Masses (U. of Manitoba Press) p. 811

SOLOVIEV (1959) Nuc. Phys. 9, 655.

STAUB (1967) Proc. 3rd Int. Conf. on Atomic Masses (U. of Manitoba Press) p. 495.

STEVENS and MORELAND (1967) Proc. 3rd Int. Conf. on Atomic Masses (U. of Manitoba Press) p. 673.

SWANN (1931) Jor. Franklin Inst. 212, 439.

VEJE (1967) Nuc. Phys. A103, 188.

VON ARDENNE (1962) Tabellen zur angewandten Physik, Band 1 (Veb Deutscher Verlag der Wissenshaften, Berlin).

WAPSTRA (1964) Nucl. Phys. 57, 48.

WAPSTRA (1967) Proc. 3rd Int. Conf. on Atomic Masses (U. of Manitoba Press) p. 833.

WHINERAY (1966) Thesis, McMaster University.

WICHERS (1962) Nature 194, 621.

WIDNER, HENSLER, SOLF and WURM (1967) Nuc. Phys. A103, 433.